Review Article

Biomass Pyrolysis: A Comprehensive Review of Production Methods, Derived Products, and Sustainable Applications in Advanced Materials

Joko Waluyo*, Ibnu Tryansar Purba, Zhufara Adhil Linanggeng and Muhammad Luthfi Maulana
Chemical Engineering Department, Faculty of Engineering, Universitas Sebelas Maret, Surakarta, Indonesia

Ekkachai Kanchanatip
Department of Civil and Environmental Engineering, Faculty of Science and Engineering, Kasetsart University Chalermphrakiat Sakon Nakhon Province Campus, Sakon Nakhon, Thailand

Mi Yan
Institute of Energy and Power Engineering, College of Mechanical Engineering, Zhejiang University of Technology, Hangzhou, China

Dwi Hantoko
Interdiscipilinary Research Center for Refining & Advanced Chemicals, King Fahd University of Petroleum & Minerals, Dhahran, Saudi Arabia

* Corresponding author. E-mail: jokowaluyo@staff.uns.ac.id DOI: 10.14416/j.asep.2024.11.009
Received: 29 July 2024; Revised: 22 September 2024; Accepted: 28 October 2024; Published online: 21 November 2024

Abstract
Pyrolysis is an effective method of turning complex materials, like waste, into valuable commodities. This process stands out because it can be easily adjusted to change different parameters and improve the quality of the final products. Biomass, abundant in carbonaceous constituents, emerges as a primary candidate for pyrolysis, presenting the opportunity to generate a diverse array of carbon-based products with broad applicability and desirability, including activated carbon (AC), magnetic activated carbon (MAC), graphene, and carbon nanotubes (CNT). The study explores various methodologies of biomass pyrolysis, highlighting the factors that influence product characteristics and examining the potential applications of pyrolysis-derived products. These processes demonstrate the capability of pyrolysis technology to convert biomass into valuable carbon-based materials, which are highly sought after in applications ranging from environmental remediation and other relevant applications. AC and MAC can be synthesized from biomass through pyrolysis. At the same time, graphene and CNT can be derived from the hydrocarbon fraction of pyrolyzed biomass or through *in situ* exfoliation and oxidation-reduction reactions of graphite. A comprehensive examination of these facets establishes a framework for grasping the potential of pyrolysis in biomass conversion and the possibilities for commercializing the end-products. The global warming potential of graphene production is higher compared to other materials (reaching 10^6 kg CO_2/kg), making it the most expensive material (US$ 857/cm^2). The predicted global market size for the commercial viability of AC, graphene, and CNT has a steady incline, indicating a robust rising trend in demand. This increasing demand makes the production of these materials attractive and significant economically.

Keywords: Activated carbon, Carbon nanotube, Global warming potential impact, Graphene, Magnetic activated carbon, Market Size

1 Introduction

Biomass is one of the potential resources in the world, with its abundance of global availability reaching 146.7 million per year. It can be obtained from crops, trees, agricultural waste, forest waste, and organic components from industry and households, which are used as foodstuffs, animal feed, vegetable oils, building materials, and energy sources. By 2020, biomass waste generated worldwide was estimated at 53.7 million tons [1], [2].

The energy source of biomass has the advantage of being renewable, so it is considered sustainable energy. Biomass is also known as an environmentally-friendly energy source associated with less harmful gas emissions, as it contains lower nitrogen (N) and sulfur (S) components compared to fossil fuel energy sources [3]. Char or charcoal is a typical carbon-rich material, obtained from pyrolysis [4]. Char produced from the pyrolysis process depends on the temperature variation used, at pyrolysis temperatures of 300–700 °C, the yield obtained is around 30–50 wt% [5]. It has been used as an adsorbent, chemical catalyst, electron conductor (on anaerobic digestion), and carbon sink [6].

Aside from pyrolysis, other biomass conversion processes, such as gasification and torrefaction, also play significant roles in transforming biomass into valuable products [7]. Regarding end products, gasification yields gas fuels and chemicals, rapid pyrolysis yields liquid fuels and chemicals, and torrefaction yields solid fuels [8]. Gasification operates at high temperatures (800–1200 °C) in the presence of limited air, oxygen, steam, carbon dioxide, or a mixture of these as gasifier agents, producing syngas (mainly, a mixture of carbon monoxide, hydrogen, and methane) [9]. Although gasification is efficient for energy generation, it produces fewer solid carbon materials. The syngas produced are typically geared towards energy and chemical production, with minimal char yield [10].

Torrefaction is a mild thermal treatment process that heats biomass in the temperature range of 200–300 °C under inert or limited oxygen conditions to produce a solid char-like material called biochar (77%), with smaller quantities of gases (23%) and liquids (0–5%) [11]. The biomass undergoes torrefaction, which increases its energy density and hydrophobic qualities and enhances its suitability as a fuel. Torrefaction, on the other hand, produces a lower carbon content (6–9 wt%) than pyrolysis (76–85 wt%), making it less appropriate for applications requiring advanced materials [12].

Overall, pyrolysis offers significant advantages over gasification and torrefaction, particularly in terms of char production and its potential for creating high-value carbon-based materials. Unlike torrefaction, which primarily enhances the energy density of biomass, pyrolysis enables the production of activated carbon, magnetic activated carbon, carbon nanotubes, and graphene. The higher operational temperatures in pyrolysis facilitate the breakdown of lignocellulosic structures, resulting in chars with much larger surface areas and porosities, ideal for adsorption applications and energy storage devices [13]. In addition to solid products, pyrolysis generates substantial quantities of bio-oil and non-condensable gases. These liquid and gas byproducts can serve as secondary energy sources, with the potential for upgrading into biofuels or chemicals. Likewise, the liquid fraction often requires further processing to enhance its fuel properties [14], the versatility of pyrolysis in producing both solid materials and energy-rich byproducts makes it a more attractive process when aiming for a wide range of applications.

The use of catalysts in the pyrolysis process significantly enhances the efficiency and selectivity of product formation from biomass feedstocks [15], [16]. Catalysts facilitate the breakdown of complex organic materials, promoting the conversion of biomass into valuable bio-oils, gases, and char [16], [17]. This catalytic effect can lead to higher yields of desirable products, reduced reaction temperatures, and minimized by-product formation [18], ultimately contributing to the sustainability and economic viability of biomass pyrolysis. As the demand for cleaner energy sources increases, understanding the role of catalysts in optimizing pyrolysis processes becomes crucial for advancing sustainable material applications.

Char generated through pyrolysis has a wide surface area, so it is potentially activated into AC for use as an adsorbent or a catalyst because of its adsorption capability [4]. AC is an adsorbent material and a catalyst buffer that is widely developed because it is a porous material that has a large surface area (500–3000 m^2/g) [19]. It would have a massive adsorption capacity if it was impregnated by precursor and alkali solution to form MAC. While CNT has high electrical conductivity and robust mechanical strength. Therefore, it has a wide range of applications such as adsorbents, catalysts, composite materials, electronic devices, reactor coatings, dyes, lubricants,

sensors, and fuel cells [20], [21]. CNT might be produced based on various sources, such as carbon sources derived from cellulose [22], CO, and CH_4 gases from pyrolysis or biomass gasification [23]. However, graphene is a one-atom-thick planar sheet carbon atom with a bond of sp^2 [24]. Its application is huge such as on nanoelectronics components (transistors), lithium battery ions, supercapacitors [25], catalysts [26], electrocatalysts [27], and heterogeneous activation on chemical production [28]. Biomass is an alternative material used for producing graphene with high porosity characteristics [28].

This review provides a comprehensive overview of the potential of biomass to be transformed into valuable products, such as AC, MAC, graphene, and CNT through pyrolysis processes. It also explores the correlations between material properties, pyrolysis conditions, and the catalysts used in the production of these derived products and their end applications.

2 Biomass Characteristics

Biomass is a highly abundant resource, with an estimated global availability of approximately 146.7 million tons annually. It may come from crops, trees, agricultural waste, forest waste, and organic components from industry and households, which are used as foodstuffs, animal feed, vegetable oils, building materials, and energy sources. By 2020, biomass waste is generated worldwide, estimated at 53.7 million tons. Biomass analysis consists of proximate analysis, ultimate analysis and lignocellulosic components (including cellulose, hemicellulose, and lignin) [2].

Rice is one of the most important staple crops, particularly in the Asia region, but its cultivation faces numerous challenges, including soil nutrient depletion, high water consumption, and the environmental impacts of rice residue management. Rice farming often generates large quantities of biomass waste, primarily rice husks and straw, which are frequently burned in the field, contributing to air pollution and carbon emissions [29]. Managing this biomass in a more sustainable way can directly impact the productivity and environmental footprint of rice cultivation.

As shown in Table S1, the results of proximate analysis on various biomass show that volatile matter is the dominant product. High volatile matter values in biomass will form more bio-oils with high volatility and reactivity. Pyrolysis products with a high char content can be obtained by using biomass, which has a high fixed carbon content [30]. Meanwhile, the high ash content contributes to the formation of char and non-condensable gas and decreases bio-oil yield [31]. Each biomass has its specific characteristics, particularly on the volatile matter (VM) at the range of 15.13–82.58 wt% (Table S1). The value of volatile matter will affect the yield of pyrolysis products, which tend to produce bio-oil as the most common product. It is obtained from high volatile matter biomass, such as corn stover, sugarcane bagasse, coffee hulls, bamboo leaves, etc. Fixed carbon (FC) is just as crucial as VM, several biomasses contain at range of 7.6–23.53 wt% that affects the char generation (Table S1). The ash might shrink the char, bio-oil, and non-condensable gas yield content. The ash content of biomass varies depending on each characteristic. The common biomass has around 0.7–21.41 wt%. Lower ash content and higher FC are the most preferable biomass characteristics for optimal pyrolysis [32].

The component ratio obtained from the ultimate analysis can be determined as the heat value of the material [3]. Table S1 shows the biomass component ratio of C 31.46–49.38 wt%, O 33.63–54.62 wt%, H 3.94–7.16 wt%, N 0.1–2.7 wt%, and S 0–0.3 wt%. Biomass with a high content of carbon and hydrogen is more easily converted into hydrocarbon fuels because these elements are the primary building blocks of hydrocarbons. Their abundance in biomass facilitates reliable conversion processes, leading to higher yields of liquid fuels. Meanwhile, biomass with a high O content can reduce the heat value [33]. Biomass with low N and S content will produce more environmentally friendly gas emissions than fossil energy [3].

To achieve the optimal biochar production, the biomass should contain less than 84.2% volatile matter [34]. Additionally, when the biomass has a fixed carbon content of 12.0% or less and a hydrogen content exceeding 5.3%, there is a strong potential for attaining a high bio-oil yield with considerable precision and the most important parameters for syngas generation are a high temperature of >912 K, a minimal particle size of <6.5 mm, and a biomass H concentration of >5.8% [34]. Therefore, the entire biomass shown in Table S1 is appropriate for high biochar yield, while paper waste and corn stalks are suitable for high bio-oil yield, and several biomasses such as cassava pulp, oil palm empty fruit bunch, and palm kernel shell are sufficient for high syngas

production. Nonetheless, it is also important to note that biomass availability is also a benchmark for a more stable production process.

Hemicellulose and cellulose in biomass are easily decomposed during pyrolysis, whereas lignin is more difficult to decompose [35]. Lignin has a lower activation energy compared to cellulose and hemicellulose. However, it decomposes at a higher temperature of 797 K, whereas hemicellulose and cellulose decompose at lower temperatures of 590 K and 620 K, respectively. This suggests that hemicellulose and cellulose exhibit higher reactivity than lignin [36]. The primary outcome of cellulose pyrolysis yields anhydrosugars, which can undergo further transformation into light oxygenates such as furans, aldehydes, ketones, acids, etc. at elevated temperatures [37], [38]. In contrast to cellulose components, hemicellulose exhibits a more intricate structure with abundant branched chains and various substituents. It is predominantly composed of xylans, mannans, xyloglucans, and β-1,3;1,4-glucans, with the latter displaying similar pyrolysis properties to anhydrosugars [39]. During the pyrolysis of lignin, higher temperatures are necessary for cleaving linkages, resulting in the production of significant quantities of phenolic compounds along with minor amounts of acids, alcohols, and light aromatic hydrocarbons [40]. The cracking process of the component will determine the product of pyrolysis. In addition to the influence of the source of lignocellulose, the other parameters such as heating rate and temperature will also affect the pyrolysis products [41], [42]. Figure 1 represents biomass with higher content of cellulose and hemicellulose than lignin, among various biomasses. The content of the cellulose and hemicellulose in the materials above are 13–85 wt%. Several biomasses tend to produce more bio-oil and syngas than biochar due to they have dominant content of cellulose and hemicellulose. Conversely, most biomass contains relatively high levels of lignin, which contributes to char generation during the process. Biomass such as bean skins, bamboo leaves, palm kernel shells, oleaster fruit, and cocoa peels have a higher lignin content, around 16.83–60.67 wt%. In addition to cellulose, hemicellulose, and lignin, lignocellulosic biomass can contain extractives, ash, protein, tannins, and soluble sugars in certain compositions (Figure 1).

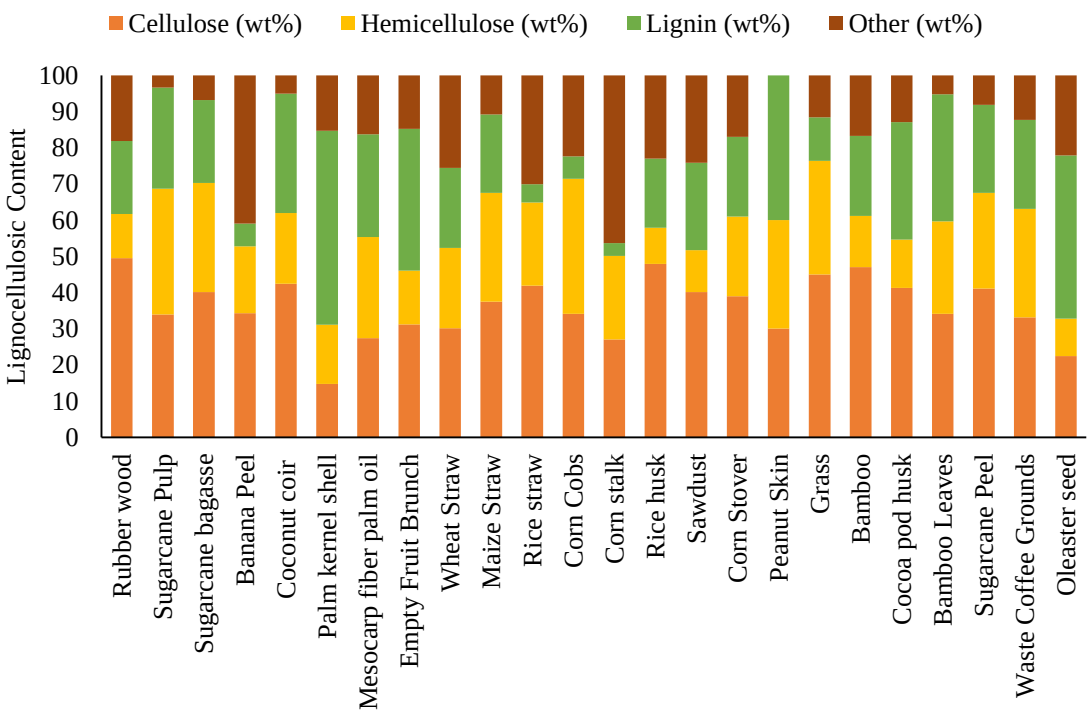

Figure 1: Cellulose, hemicellulose, and lignin content in various types of biomass. Data adapted from [43]–[53].

3 Biomass Pyrolysis

Pyrolysis is thermochemical decomposition without involving oxygen in its reaction, to decompose a complex compound, such as polymers and biomass that have long-chain molecules to be smaller [54], [55], [56]. The three main products in pyrolysis are charcoal (char), oil, and gas, which are derived into useful and valuable products [57]. Pyrolysis is one of the thermal decomposition methods. It is often used because it is considered effective and flexible. The parameter process of pyrolysis can be manipulated according to the characteristics of the desired product. In addition, pyrolysis is categorized as green technology because it is considered to be environmentally friendly since it does not cause water contamination and its gas phase products have a high heat value that can be recycled for the pyrolysis process [56], [58]. According to existing studies, pyrolysis has several advantages including shorter reaction time, better conversion results than biochemical, higher charcoal yield results, the possibility to be operated at atmospheric and low temperatures which shrink the production cost [3]. Pyrolysis conditions can be optimized to produce char, gas, and oil products with high energy densities [54], [59].

Pyrolysis is similar to the processes of cracking, devolatilization, carbonization, dry distillation, destruct distillation, and thermolysis. However, its process is different compared to gasification. On gasification, biomass would react to a gasifying agent [60]. It is carried out at 800–1000 °C and pyrolysis is generally carried out at temperatures between 300–650 °C [61]. The temperature and heating rate used in the pyrolysis process significantly impact the yield and composition of the resulting products. Low temperatures and slow heating rates tend to favor the production of charcoal, as these conditions are less conducive to the thermal breakdown of biomass. Under such conditions, the biomass undergoes slow pyrolysis, which primarily yields solid biochar. In contrast, higher temperatures and faster heating rates shift the yield towards bio-oil and syngas products. This occurs because rapid heating and elevated temperatures facilitate the secondary decomposition reactions of pyrolysis vapors, leading to the swift depolymerization of solids into primary volatile compounds. As temperatures increase, the biochar undergoes further decomposition, producing gases that are non-condensable and contributing to a higher yield of gaseous products. Consequently, while the production of bio-oil and syngas increases at higher temperatures and heating rates, the yield of biochar decreases due to these secondary reactions. Understanding these dynamics is crucial for optimizing pyrolysis conditions to achieve desired product distributions, whether for maximizing biochar, bio-oil, or gaseous outputs [57], [62]–[68], and will affect the quality of bio-oil [69].

4 Pyrolysis Classification

According to the rate of heating, pyrolysis can be classified into four types, i.e., slow, intermediate, fast, and flash pyrolysis [57], [67], [70]. Slow pyrolysis is purposed to yield maximum char product [71], fast pyrolysis is projected to yield maximum oil (tar) product [72], while intermediate pyrolysis is an alternative to those of difficult-to-manage references such as size equalization, reactor movement and residence time [73].

4.1 *Slow pyrolysis*

Slow pyrolysis is carried out at 300–500 °C at a very slow heating rate (HR) or below 1 °C/s and with a stay of solids in the reactor for up to several hours by passing inert gas with a certain flow rate (FR). The time to equalize the heat of biomass to the process temperature is longer than the reaction time of pyrolysis [71]. Slow pyrolysis has been investigated by several researchers. They found biochar products have higher yields compared to bio-oil and gas. In grass pyrolysis at 400 °C, the optimum yield of char reaches 48 wt%, while the bio-oil and syngas yields are lower, which is 22 wt% and 8 wt%. This finding is supported by a relevant study at relative conditions, which shows slow pyrolysis at 400 °C produces around 30% oil yield and 35% char yield, with the majority yield being char [14]. This happened due to bio-oil and syngas production depend on the decomposition of volatile matter [74]. At lower temperatures, like 400 °C, the thermal degradation of biomass does not fully promote the release of volatiles required for producing bio-oil and gas. At 500 °C biochar yields decrease to 42 wt% while that of bio-oil and syngas expand to 28 wt% and 9 wt%. At 600 °C, bio-oil and syngas yields rise significantly to 37 wt% and 26 wt% while biochar yields drop to 25 wt% [75]. Similar to bamboo pyrolysis, at 300 °C the yield of biochar is 80 wt% while that of bio-oil and syngas is still low at 5 wt% and 15 wt%. When the temperature

is raised to 600 °C, the yield of bio-oil and syngas rises, while the biochar shrinks [76].

A study demonstrated that pyrolyzed poplar wood with various temperatures and heating rates produced a high bio-oil yield at the temperature process [77]. According to Figure 2, using temperatures of 400–500 °C with heating rates of 10, 30, and 50°C/min results in the yield of bio-oil, which is between 37.62–41.53 wt%, 40.82–42.16 wt%, and 41.83–43.54 wt% respectively. However, increasing temperatures of up to 600 °C result in bio-oil yields decreasing to 39.25 wt%, 39.31 wt%, and 41.67 wt% respectively. Therefore, the optimal temperature to achieve bio-oil is 500 °C because the higher temperature in pyrolysis leads to secondary cracking in volatile components. Meanwhile, escalating the temperature and heating rate reduces the biochar, in the range of 400–600 °C at the same heating rates, each biochar yields from 34.83 wt% to 28 wt%, from 32.8 wt% to 27.2 wt%, and from 31.95 wt% to 26.9 wt% respectively. However, the syngas yields increase in tune with the process temperature, but they are not significantly affected by the heating rate. At 400–600 °C on the same heating rates the syngas yields from 27.55 wt% to 33.2 wt%, from 26.38 wt% to 33.4 wt%, and from 26.22 wt% to 31.1 wt%, respectively (Figure 2). It is due to secondary decomposition in charcoal and bio-oil, which forms non-condensable gases [77].

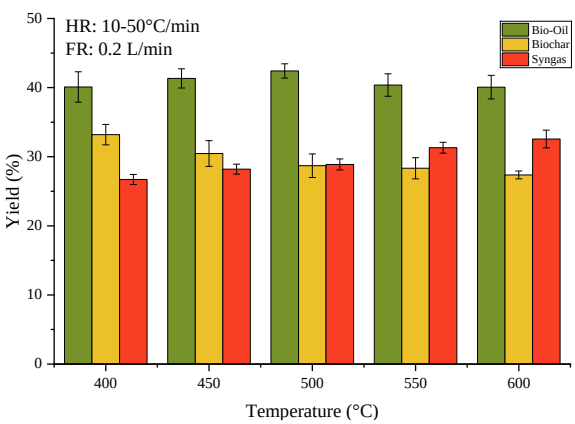

Figure 2: Yield of slow pyrolysis on poplar wood. Data adapted from [77].

Increasing the temperature and heating rate in the pyrolysis process will increase the yield of bio-oil and syngas but it will lower the yield of biochar due to the secondary decomposition process. In contrast, a low heating rate will prevent secondary decomposition so the biochar yield can be optimal [71]. This outline is supported by a previous study that said the increase in temperature and heating rate in pyrolysis leads to a decrease in biochar yields [67]. The yield of biochar results in slow pyrolysis is more than that in fast pyrolysis so it can be utilized to improve soil quality and adsorb carbon [78].

It can be concluded that temperature and heating rate are factors that significantly affect the yield of pyrolysis results. Increasing temperature and heating rate causes secondary decomposition in biochar that produces primary volatiles and unconsolidated gases so that bio-oil and syngas yields increase while that of bio-char decreases.

4.2 *Fast pyrolysis*

Fast Pyrolysis is run at temperatures up to 500 °C with a heating rate (HR) of >10 °C/s and a fast solid residence time of about 1 second on set-point of gas flow rate (FR) and temperature (T) [71]. Figure 3 shows the relative effect of fast pyrolysis of different types of biomasses on pyrolysis yields. Previous research also conducted the pyrolysis of rice straw and sawdust at 500 °C, 750 °C, and 850 °C. As the heating rate increases, bio-oil and biochar yield generally decrease, with a corresponding increase in syngas generation. Pyrolysis gas products from rice straw and sawdust are optimal at 850 °C, with the highest syngas yields of 40.6 wt% and 46.5 wt%, respectively. Bio-oil and biochar products obtained from pyrolysis of rice straw were 19.4 wt% and 26 wt%, respectively, while in sawdust were 15.5 wt% and 21 wt% [79]. It is important to note that the use of higher heating rates in this case affects each feedstock differently due to variations in their specific characteristic and composition. Each feedstock may perform better for certain products based on their unique characteristics and the process conditions.

In pyrolysis, waste wood with a temperature of 800 °C and heating rates of 90 and 350 °C/min obtains syngas yield from 17.5 wt% to 52.9 wt%. Bio-oil and biochar yields are obtained from 57.4 wt% to 27.5 wt% and from 20.8 wt% to 15.7 wt%. It also occurs in the pyrolysis of cellulose, xylan, and lignin where syngas product yields increase, however, biochar and bio-oil products decrease by increasing the heating rate. Increasing of heating rate can promote secondary cracking on volatile components so that syngas products increase, form more aromatic bio-oil, and produce biochar with a high surface area due to rapid devolatilization leading to highly porous biochar [80]. The secondary decomposition of solid materials produces more non-condensable gases than condensable gases, resulting in higher yields of syngas than bio-oil [72]. Decomposition of biomass compounds increases with a high heating rate in fast pyrolysis resulting in more bio-oil and gases [71]. The same findings are also conveyed by Al-Arni [81] that the optimal production of tar/oil can be obtained by regulating short residence times and high temperatures. However, an increase in temperature can lead to a decrease in tar production so that the resulting syngas products become more numerous. Fast pyrolysis is often used to obtain syngas products, which are economically more profitable [78]. It can be concluded that the use of high temperatures and heating rates in fast pyrolysis leads to faster secondary decomposition in biomass tar/bio-oil and syngas production more than slow pyrolysis does. As a result, fast pyrolysis can be used to maximize liquid/bio-oil products and gases.

4.3 *Intermediate pyrolysis*

Intermediate pyrolysis is used as an alternative to fast and slow pyrolysis, which is too challenging to control on biomass pyrolysis, such as size equalization, movement into reactors, and residence time [83]. Intermediate pyrolysis is approximately produced 40 wt% of bio-oil and 40% of bio-char. Figure 4 shows the impact of intermediate pyrolysis of different types of biomasses on pyrolysis yields, which operate at 500±10 °C.

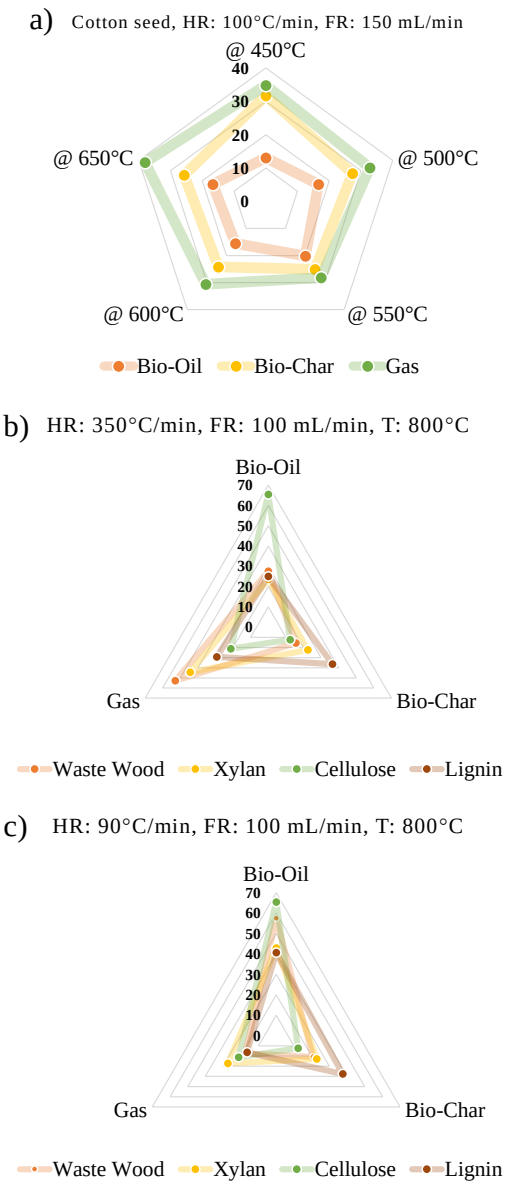

Figure 3: Fast pyrolysis product, a) fast pyrolysis yield (wt%) from cotton seed at various temperatures. Adapted from [82]. b) fast pyrolysis yield (wt%) of several types of biomasses at HR = 350 °C/min and c) HR = 90 °C/min. Adapted from [79], [80].

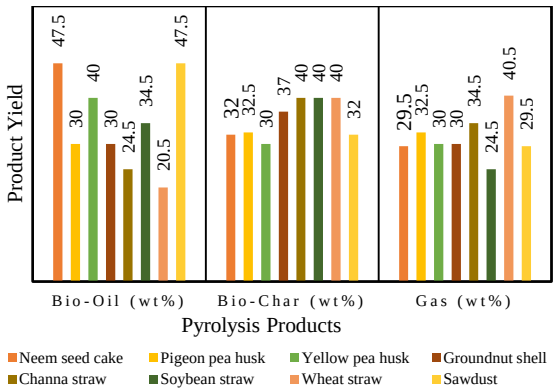

Figure 4: Intermediate pyrolysis yield from several types of biomasses [73].

Intermediate pyrolysis is pyrolysis performing parameters between slow pyrolysis and fast pyrolysis. The yield produced in pyrolysis intermediates is in between the fast and slow pyrolysis. The residence time on intermediate pyrolysis is longer. As evidence, bio-oils with smaller molecular weights such as phenols and ketones are produced [84]. Intermediate pyrolysis is used to maximize biochar and syngas products so that bio-oil production is relatively lower [42]. Another study also stated that the residence time for intermediate pyrolysis is longer than fast pyrolysis, which causes secondary reactions such as fractionation and depolymerization, and produces more biochar and water-containing bio-oil [32]. The size of raw materials used is also larger so that it is easier to use them in the industry [84]. It can be concluded that intermediate pyrolysis has a longer residence time than fast pyrolysis, and produces more biochar and syngas than bio-oil. The bio-oil produced has a smaller molecular weight and contains a certain amount of water.

4.4 *Flash pyrolysis*

The key characteristics of flash pyrolysis are operating temperatures of around 1000 °C, vapor residence durations of less than 0.5 seconds, and a very fast heating rate of up to 2500 °C/s [85]. Pyrolyzed oil is the primary product of this method. One of the main differences between rapid pyrolysis and flash pyrolysis is the much greater heating rate used in the former [86]. As such, compared to rapid pyrolysis, flash pyrolysis usually yields a higher yield of pyrolysis oil [87].

The process of flash pyrolysis has been investigated using microalgae (*Chlorella vulgaris*) and palm kernel shells within an entrained-flow reactor. When subjected to a temperature of 800 °C, the pyrolysis of microalgae produced 21.36% biochar, 60.22% bio-oil, and 18.42% syngas. In contrast, the palm kernel shell, processed at a lower temperature of 600 °C, resulted in 20.89% biochar, 73.74% bio-oil, and 5.37% syngas [88].

A recent study compared flash pyrolysis (PF) and conventional pyrolysis (PC) of grape seed (GS) and chestnut shell (CS), particularly in syngas products. Using a heating rate of 25 °C/min and a nitrogen flow rate of 100 mL/min, the PC process was carried out. The temperature was raised to a maximum of 750 °C and held there for an hour. The temperature range at which the gas and liquid fractions were collected was 200 °C to 600 °C. When using the PF method, the sample was added right away when the furnace reached the specified temperature (750 °C and 850 °C) and it remained there for 10 minutes while nitrogen flowed at a rate of 100 mL/min. The bio-oils from the condenser were extracted using dichloromethane (CH_2Cl_2) [89].

The results indicate that PF produced a lower CO_2 fraction than PC, approximately 25% to 28%, under the same conditions. When the temperature was raised to 850 °C, the CO_2 levels decreased by about 1% to 3%. PF exhibited greater efficiency in producing CO gas, with the gas fraction reaching about 42% at 750 °C and 850°C, compared to PC, which only reached 35%. The results for H_2 gas fraction differ significantly. PC yields less than 1%, whereas PF produces up to 15% at 750 °C and increases to 22% at 850 °C. Additionally, PF has the potential to yield a CH_4 content of up to 20% at temperatures of 750 °C and 850 °C. In contrast, PC can only achieve a maximum of 7% CH_4 production at 750 °C [89].

5 Catalytic Pyrolysis

Biomass contents affect the yield of pyrolysis products in the form of biochar, bio-oil, and gas. In addition, temperature and heating rate are important factors that can affect pyrolysis products. The use of catalysts in the pyrolysis process may increase product yields and limit the formation of undesired products can improve the distribution of product phases by influencing the reaction pathways [69], [90]. Various sources of catalysts can be employed in the pyrolysis process, i.e., activated carbon, metal based, zeolite, etc. Each is designed to achieve specific outcomes depending on the desired product and reaction conditions.

5.1 *Activated carbon catalyst*

Activated carbon is a highly porous material with a large surface area, composed primarily of carbon. Its robust structure and extensive surface area make it effective for adsorbing gases and breaking down their components into smaller fragments. The conversion of biochar, a byproduct of biomass pyrolysis, into activated carbon can be achieved through both physical and chemical activation methods [18]. The use of activated carbon as a catalyst led to a reduction in bio-oil production and an increase in syngas yield, while the biochar yield remained relatively constant. This outcome is attributed to the reforming process that takes place during the degradation of the sample in the presence of the activated carbon catalyst, which promotes further cracking reactions [91].

Table 1 presents the results of an experiment on pyrolyzing Douglas fir sawdust pellets to produce activated carbon from sources such as bituminous coal, wood, and lignite coal. Without a catalyst, the bio-oil yield was 45.20 wt%, syngas production was 11.80 wt%, biochar yield was 43.00 wt%, and phenolic compounds accounted for 2.54 wt%. Upon introducing activated carbon, both bio-oil and biochar yields decreased, while syngas production rose. Notably, there was a significant increase in phenolic compounds, likely due to the breakdown of other components into smaller fragments, which predominantly converted into phenolic compounds [92].

Table 1 also shows that the use of a catalyst leads to a decrease in bio-oil production, while the yield of syngas increases, and the biochar yield remains relatively constant. Increasing the catalyst-to-biomass ratio further reduces bio-oil output and raises syngas production. Additionally, the quality of bio-oil is improved, and phenol production increases with the use of a catalyst and a higher catalyst-to-cellulose ratio. The author attributes the reduction in bio-oil yield to the reforming process, where the sample degrades, and volatile compounds passing through the activated carbon undergo additional cracking reactions [91].

Table 1: Effect of activated carbon on pyrolysis process.

Source	Catalyst	Products (wt%)			Ref.
		Biochar	Bio-oil	Syngas	
Douglas fir sawdust pellets	No catalyst	43.00	45.20	11.80	[92]
	GAC 830 PLUS (Bituminous)	24.40	31.00	44.60	
	DARCO 830 (Lignite)	23.50	28.97	47.53	
	DARCO MRX (Wood)	20.83	26.50	52.67	
	Catalyst/Source ratio				
Glucose	0.00	17.6	63.3	18.8	[91]
	0.28	24.0	52.8	18.7	
	0.40	256	49.5	18.9	
	0.70	29.1	45.8	18.8	
	1.13	29.6	44.6	18.7	

Activated carbon can promote the formation of hydrocarbons or aromatic compounds, with higher pH levels and increased heating values enhancing the quality of bio-oil. However, as the temperature rises, the decomposition of components into lower molecular weight compounds leads to a reduction in bio-oil yield [93], [94]. In contrast, an increase in the feedstock-to-catalyst ratio leads to greater bio-oil production and a reduction in syngas output. This shift also causes a decrease in aromatic compounds while boosting the proportion of aliphatic compounds [94].

5.2 *Metal based catalyst*

Metal catalysts may expand the formation of biochar in pyrolysis processes. Biochar products generated through catalytic pyrolysis using Ce, Mn, and Zn catalysts yield higher quantities compared to those produced through Ni and Cu catalysts. However, metal catalysts can significantly enhance syngas products. Nickel is an active catalyst for cracking indicated by the higher syngas and low bio-oil product [95]. A related study also found that increasing the Ni catalyst ratio may escalate hydrogen gas due to the active site tends to increase, thus accelerating devolatilization and steam reforming reactions. The increase in H_2 and CO gases is a result of the decomposition of tar and other macromolecules at higher temperatures. CO gas decreases as it reacts with carbon compounds emitting CO_2 gas [96]. Meanwhile, the wet reform between methane and water vapor produces H_2 and CO, lowering the methane gas. The use of Fe catalyst can improve syngas yield and decrease solid product. Bio-chars generated over Fe

catalyst pyrolysis gain rich in carbon compounds [97]. Metal catalyst stimulates increasing deoxygenation and dehydration reactions [69].

Precious metal catalysts such as Au, Ag, Pt, and Pd may diminish the oxygen content in bio-oil as they can increase hydrodeoxygenation and aromatization reactions. The excess of precious metal catalysts is resistant to corrosion, but the operation cost is expensive [69]. The use of metal oxide catalysts such as CoO, Cr_2O_3, CuO, Fe_2O_3, Mn_2O_3, NiO, TiO_2, V_2O_5 and CeO_2 is essential in increasing bio-oil and decreasing syngas yields and it inhibits further cracking in primary products [98]. Light bio-oils are produced from the addition of Ce, Cr, Cu and Fe catalysts, while heavy bio-oils result from the addition of V, Mn, Ti and Co-based catalysts [98]. The formation of furans, ketones, alcohols, acetic acid, and phenolic acids is obtained from the use of metal oxide catalysts, except Fe_2O_3. Fe-based catalysts form cellulose and hemicellulose derivatives, which among others are furan compounds, carboxylic acids, ethylene glycol, and aldehydes, such as acetaldehyde or hydroxyl acetaldehyde, and have no significant effect on the formation of hydroxyl acetone and esters. Coke with a high content emerged from the use of catalysts V, Mn, Cu, and Co. The lowest oxygen content in bio-oil is drawn from the use of CeO_2 catalysts [99]. Table S3 shows several findings regarding the effect of metal catalyst used and catalyst ratio variations on pyrolysis products.

5.3 *Zeolite catalyst*

Zeolite catalysts in biomass pyrolysis processes may maximize syngas yields as well as minimize bio-oil yields. Bio-oil products contain more aromatic hydrocarbon compounds, such as benzene, toluene, xylene, ethylene and propylene, and may degrade oxygenated compounds such as ketones and aldehydes [84]. In addition, these catalysts take part in dehydration reactions and long-chain hydrocarbon bending processes (C_{14}–C_{17}) that produce branched, cyclic or small molecule aromatic compounds. Zeolite is an optimal hydrocracking catalyst due to its high acidity, which enhances cracking efficiency, excellent thermal and hydrothermal stability, superior naphtha selectivity, strong resistance to nitrogen and sulfur contaminants, low coke formation, and ease of regeneration [100], [101]. Synthetic zeolites, such as H-ZSM-5, MCM-41, and HY, along with their modified versions, are commonly utilized in various industrial chemical processes. In contrast, naturally occurring zeolites, like chabazite and mordenite, are found in geological formations [18]. Among these, H-ZSM-5 has been extensively employed as a catalyst in the petroleum industry due to its shape-selective properties, optimal pore size with steric hindrance, thermal stability, and solid acidity [102]. The H-zeolites-socony-mobile#5 (H-ZSM-5) catalyst encourages the formation of volatile compounds due to their porous characteristics and has an acidic site that can absorb reactants to form positive carbon ions [69]. Moreover, the molecular structure and acid sites in the H-ZSM-5 catalyst partake in pyrolysis vapor bending, thereby adding more yields of bio-oil. The combination of H-ZSM-5 and metal catalyst leads to the presence of metal sites, which play a significant role in hydrogenation and dehydrogenation reactions. While the acid site is responsible for accelerating the isomerization process and triggering the bio-oil products with less moisture content and increasing hydrocarbon products [69].

MCM-41 is a mesoporous material characterized by its extensive surface area, which significantly improves both the yield of hydrocarbons and the quality of pyrolysis oil [103]. Previous study demonstrated that MCM-41 offers distinct advantages due to its larger pore size, facilitating macromolecular catalysis, adsorption, and separation by minimizing molecular diffusion resistance within the channels. Additionally, MCM-41's high specific surface area, approximately 1000 m^2/g, ensures ample surface sites for the adsorption and catalytic reactions of active components [104]. Although it produces bio-oil with a high hydrocarbon and tiny moisture, the yield of bio-oil produced is relatively lower compared to zeolite catalyst products [69].

Evidence from recent studies demonstrated that HY zeolite exhibits excellent catalytic performance due to its well-defined pore structure, stability, and reactivity [105]. Concurrently, during co-pyrolysis of LDPE HY significantly improves yields, with the production increasing from 23.5% to 80.4% as the HY to LDPE ratio escalates from 0 to 1:5. The optimal balance of oil production and quality is achieved with a HY to LDPE ratio of 1:10 [106].

Table 2 shows the catalytic performance of LDPE across various catalysts within the temperature range of 450 °C to 650 °C. The data reveal that the pyrolysis temperature markedly influences yield distribution. As the temperature increased, there was a substantial rise in the total yields of gas and oil, while

the solid yield significantly decreased. This change is likely attributable to the decomposition and secondary reactions of LDPE pyrolysis volatiles [107]. Higher temperatures deliver additional heat to the polymer, which weakens its chain structure and leads to greater polymer chain fragmentation [108]. This observation aligns with findings from similar studies on polymer pyrolysis [109], [110]. Specifically, Table 2 shows that the yield of the liquid phase was relatively low at 450 °C (31.3%) and 500 °C (55.6%). However, as the temperature increased, polymer conversion improved [108], resulting in a liquid yield of 82.0% at 550 °C. This phenomenon occurs because elevated temperatures further crack oligomers into smaller gaseous hydrocarbons, while the liquid yield remains relatively stable.

Table 2: Zeolite catalysts performance through pyrolysis process [101].

Catalysts	Temperature	Product yield (wt%)		
		Biochar	Bio-oil	Syngas
No catalyst	450 °C	64.6	31.3	4.1
	500 °C	38.1	55.6	6.3
	550 °C	10.1	82.0	7.9
	600 °C	6.0	85.0	9.0
	650 °C	2.7	88.1	9.2
ZSM-5	450 °C	15.7	54.6	29.7
	500 °C	1.8	59.9	38.3
	550 °C	1.5	50.1	48.4
	600 °C	1.3	44.9	53.8
	650 °C	0.7	37.9	61.4
HY	450 °C	10.1	59.5	30.5
	500 °C	4.5	60.9	34.6
	550 °C	3.7	55.1	41.6
	600 °C	3.0	38.9	58.1
	650 °C	2.7	30.2	67.1
MCM-41	450 °C	40.6	51.1	8.3
	500 °C	23.8	60.4	15.9
	550 °C	13.3	69.5	17.3
	600 °C	8.0	72.9	19.1
	650 °C	1.6	78.4	20.0

6 Biomass Pyrolysis Product

According to Figure 5, the pyrolysis process begins with the pretreatment of biomass, where feedstock undergoes size reduction, moisture control, or chemical adjustments to ensure optimal conditions for pyrolysis [111]. Once pretreated, the biomass enters a pyrolysis reactor, where it is exposed to a certain temperature in the absence of oxygen, preventing combustion and instead initiating thermal decomposition. Inside the reactor, the complex organic polymers, including cellulose, hemicellulose, and lignin, break down into three primary product streams: biochar, bio-oil, and syngas.

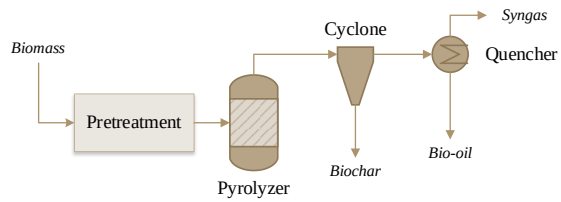

Figure 5: Pyrolysis overall process flow.

The solid fraction, biochar, forms through carbonization, retaining much of the structure of the original biomass while being transformed into a carbon-rich material with a highly porous surface. This char is prized for its versatility in applications such as soil amendment, carbon sequestration, and environmental remediation, especially for water purification. Alongside biochar, volatile organic compounds released during pyrolysis are condensed into bio-oil, a dark, viscous liquid rich in oxygenated hydrocarbons. Bio-oil is a renewable energy source with potential for upgrading into biofuels or chemicals, although its high oxygen content requires further refinement for commercial fuel use. Lastly, the non-condensable gases that do not liquefy under cooling form syngas, a mixture primarily composed of hydrogen, carbon monoxide, and small amounts of methane.

6.1 *Biochar*

Biochar is a solid product of biomass pyrolysis that can be used as a high-quality fuel, adsorbent, activated carbon raw material, catalyst buffer, and supercapacitor electrodes [71], [112]. The main constituent of biochar is carbon (up to 85%), but it also contains oxygen and hydrogen. Unlike fossil fuels, biomass has less organic ash content. The source of biomass and the operating conditions of pyrolysis will determine the characteristics of the resulting product [113]. The breaking of weaker bonds in the biochar structure leads to the loss of hydrogen and oxygen, resulting in biochar being highly carbonated and consequently, the heat value of biochar also increases at higher pyrolysis temperatures [65], [75].

According to existing research, rising temperature and heating rate can lead to an increase in ash, fixed carbon and carbon contents, but decrease the amounts of volatile matter, oxygen, hydrogen, and

nitrogen [77]. Biochar produced at high temperatures has more aromatic characteristics and contains high carbon so that it can be used as a fuel. In parallel with other investigations [68], [71], [114] convey that higher pyrolysis temperatures can increase the content of carbon elements, and HHV values, but decrease the H/C and O/C ratio. The HHV of biomass char is about 32 MJ/kg, which is greater than that of the initial biomass or liquid products of pyrolysis [115]. The adsorption capabilities of biochar can be seen from the surface area. Increased temperature and heating rate can increase the surface area and pore volume of the biochar. The reason is that the release of volatile components from the surface results in an open fiber structure that leads to the formation of cavities in biochar [77] and has a high heat value [80]. As presented in Table S2 and the ultimate analysis results, the composition of the components contained in the biochar is C (59.7–82.1 wt%), O (3.7–31.4 wt%), H (0.7–3.76 wt%), S (0–0.9 wt%), and N (0.53–1.77 wt%). In addition, the analysis of the most proximate content, i.e., fixed carbon, is followed by volatile matter and ash. Excess biochar with a high carbon content can be used as a storage medium, energy source, as well as pollutant absorption [76].

The application of biochar has shown significant potential to address several relative issues in agricultural cultivation as mentioned in *section 2*. Biochar can be used as a soil amendment to improve soil fertility, increase water retention, and enhance nutrient availability [116]–[118]. Studies have demonstrated that the incorporation of biochar into paddy fields can enhance rice yield with better water productivity due to their porous structure and controlled fertilizer release capacity. Biochar enhanced the water productivity up to 25.3% [119], in the other study, it sharply reduced the irrigation water usage by 28.8% [120]. Additionally, the fertilizer uptake and recovery were boosted by biochar up to 24.5%. Biochar accelerated the agronomic use efficiency and partial factor productivity of nitrogen up to 21%. It also profoundly enhanced the pH, the total carbon and nitrogen and the available nitrogen (NH_4^+ and NO_3^-) of the post-harvest soil [120]. Furthermore, biochar's porous structure promotes beneficial microbial activity, which can increase nutrient cycling and lead to improved crop yields [121].

6.2 *Bio-oil*

Bio-oil, referred to as pyrolysis oil, is the principal output derived from the fast pyrolysis of biomass. This substance is a dark and viscous liquid, consisting of numerous oxygenated organic compounds such as carboxylic acids, ketones, aldehydes, furans, sugars, and water [122]. From a chemical standpoint, bio-oil is a highly intricate blend formed through the depolymerization and fragmentation of cellulose, hemicellulose, and lignin during the pyrolysis process [123].

To achieve the maximum yield of bio-oil during pyrolysis, the ideal operating temperature is approximately 500 °C [14], [124]. Elevated temperatures tend to promote the formation of small aldehydes and acids while decreasing the presence of phenols, the precise composition of the products can vary depending on the feedstock type and additional variables [123]. Introducing a catalyst can further enhance bio-oil yield and quality by improving the conversion process and the characteristics of the final bio-oil [14], [124].

Table 3: Comparative properties of bio-oil and commercial fuel oils.

Properties	Bio-oil	Gasoline	LFO	HFO
Composition, wt%	54-58 for C, 5.5–7 for H, 0–0.2 for N, 35–40 for O	86 for C, 12.8 for H, 0.0 for N, 1.0 for S	86 for C, 11–14 for H, <3 for O, <0.3 for N, 0.2 for S	88.11 for C, 10.84 for H, 0.3 for N, 0.46 for S
Water, wt%	15–30	–	0.025	0.32 vol%
Density @15 °C, kg/L	1.1–1.3	0.72–0.76	0.89	0.95
Viscosity @10 °C, cSt	40–100 (cP) @500 °C	0.5 @20°C	3–7.5 @40 °C	130 @50 °C
Flash point,°C	40–110	−43	60	110
HHV, MJ/kg	16–19	45.7	–	42.93
LHV, MJ/kg	–	42.9	40.3	40.63
Ref.	[125]	[126]	[127], [128]	[129]

Based on Table 3, the chemical and physical properties of bio-oil differ significantly from those of well-known fossil fuels such as gasoline, light fuel oil (LFO), and heavy fuel oil (HFO). The composition of biomass-derived bio-oil differs significantly from that of gasoline, LFO, and HFO, which have high carbon contents of 86%, 86%, and 88.11%, respectively. It has 54–58% carbon, 5.5–7% hydrogen, and a

relatively high 35–40% oxygen concentration. The fact that bio-oil has a high oxygen content reduces the general energy content, resulting in HHV within 16–19 MJ/kg. This is way lower compared to gasoline HHV (45.7 MJ/kg), and HFO HHV (42.93 MJ/kg). Secondly, the high moisture content in bio-oil (15–30%) not only dilutes its energy potential but also gives practical challenges in storage and handling, probably causing corrosion and needing extra energy for water removal. The physical properties further complicate the direct substitution of bio-oil for fossil fuels. However, the density and viscosity of bio-oil are very variable, with values in the range of 1.1–1.3 kg/L and 40–100 cP at 500 °C, respectively. This contrasts significantly with the properties of gasoline, with a density of 0.72– 0.76 kg/L and a viscosity of 0.5 cSt at 20 °C; LFO, with a density of 0.89 kg/L and a viscosity of 3–7.5 cSt at 40°C; and HFO with a density of 0.95 kg/L and a viscosity of 130 cSt, which are more or less constant. This affects the efficiency and reliability of the delivery systems and combustion. In addition, even if the flash point (40–110 °C) of bio-oil is significantly higher than the flash point of gasoline (–43 °C), it is still much more unreliable than the flash point of LFO (60 °C) and HFO (110 °C). The low temperatures of the fluid lead, in any case to high viscosity; this condition could cause many difficulties in applying bio-oil to conventional engines and the related infrastructure without developing a particular system or even a completely new one to manage the flow and combustion capabilities of the fluid. This all points to the high and essential levels of technical and economic developments that have to be achieved for bio-oil to successfully replace conventional fossil fuels for energy applications.

Bio-oil, being of lower energy content with a high-water fraction, would require processing technologies for further development and improved fuel characteristics for better performance. On the other hand, developing compatible engine technologies and fuel systems to accept a liquid with variable viscosity and density is a necessity. How to deal with storage and handling challenges due to its high water and oxygen content poses another challenge, which would need material science innovations and fuel conditioning techniques. It is only with these comprehensive technological and infrastructural developments that bio-oil could move toward being a viable and sustainable alternative to fossil fuels. The primary reason for this is that bio-oil has a lower content of carbon and hydrogen, which are elements with higher HHV. Consequently, bio-oil would yield less heat in a combustion engine compared to HFO. In conclusion, bio-oil in its current state is an unsuitable fuel and necessitates substantial upgrading to be considered a drop-in fuel. This can be achieved through either biomass pre-treatment methods or downstream bio-oil upgrading processes.

6.3 *Syngas*

Syngas product from biomass pyrolysis is produced from the secondary cracking process of organic content [99]. Short-chain carbon gasses, such as H_2, CO, CO_2, CH_4, C_2H_4, C_2H_6, and O_2, are commonly produced through biomass pyrolysis (Table 4). Increased catalytic temperatures, residence times, and catalyst ratios can produce high hydrogen gas [96]. Elevated temperatures may lead to reduced H_2 and CH_4 gas because of oxidation and carbonization reactions while increasing CO_2, CO, C_2H_4, and C_2H_6 concentrations as well as the heat value instead. Degradation of cellulose and hemicelluloses can be indicated by a fairly high increase in CO_2 content, while CH_4 and CO are the results of volatile secondary cations released from pyrolysis [75]. The cracking and reforming of the compounds of carbonyl, ether, and carboxylic acids form CO and CO_2, while CH_4 comes from O-CH_3.

Related research expressed that biomass pyrolysis produces CO, CH_4 and CO_2 for the highest gas components [99]. The result of decarbonization is CO and CO_2, but CO_2 is also generated from interactions between oxygen and CO. Methane comes from disconnecting methyl groups on aromatic rings or aliphatic ring structures, and can result from radical reactions, such as the merger of methyl groups with H-H groups to form methane, where methyl groups are derived from the dissociation of the aliphatic chain of aromatic ring structures on lignin. Hydrogen comes from the disconnection of C-H or O-H.

Table 4: Analysis of syngas content of biomass pyrolysis results.

Biomass	H_2 (%)	CO (%)	CH_4 (%)	CO_2 (%)	C_2H_4 (%)	C_2H_6 (%)	O_2 (%)	Ref.
Coffee hulls	9 – 30	20 – 23	10.5 – 12	32 – 57	1 – 4	2 – 3	-	[113]
Grass	9.7 – 28	21.7 – 27.7	17.6 – 39.2	9.1 – 33.2	1.2 – 4.3	0.8 – 7.0	-	[75]
Neem seed cake	6.89 ± 1	0.46 ± 0.3	15.87 ± 2	7.16 ± 1	-	-	18.46 ± 2	[73]
Pigeon pea husk	4.66 ± 1	1.60 ± 1	21.57 ± 2	8.93 ± 1	-	-	14.58 ± 1	[73]
Yellow pea husk	0.15 ± 0.1	1.30 ± 1	24.77 ± 2	11.23 ± 1	-	-	15.56 ± 2	[73]
Groundnut shell	5.02 ± 1	10.16 ± 1	13.21 ± 1	6.97 ± 1	-	-	10.93 ± 1	[73]
Channa straw	4.36 ± 1	14.02 ± 1	19.93 ± 2	6.94 ± 1	-	-	10.58 ± 1	[73]
Wheat straw	7.05 ± 1	7.51 ± 1	18.70 ± 2	5.62 ±1	-	-	13.38 ± 1	[73]
Soybean straw	8.29 ± 1	13.85 ± 1	18.53 ± 2	7.80 ± 1	-	-	10.60 ± 1	[73]
Sawdust	7.11 ± 1	6.26 ± 1	22.25 ± 2	4.93 ± 0.5	-	-	15.40 ± 2	[73]
Sugarcane bagasse	8.7 – 45.3	13.9 – 60.1	6.9 – 31.1	11.7 – 58.1	0.6 – 2.2	0.6 – 2.2	-	[81]
Mixed wood chips	1.5 – 8	34 – 59	7 – 14	25 – 51	-	-	-	[32]

Elevating the temperature potentially diminished the CO_2 and H_2 levels, yet it does not have the same effect on CO and C_xH_y generation [32]. CO_2 dominates at low temperatures (150–350°C) due to degradation of hemicellulose and cellulose. In the meantime, at higher temperatures, the product is dominated by CH_4 and H_2 gases due to lignin degradation [67]. The use of catalysts also affects pyrolysis gasses, particularly in decreasing CO, CH_4, and CO_2 levels because of the catalyst's ability to catalyze the transformation of volatile structures and suppress further multiplied reactions [99]. In summary, the syngas generated will increase along with escalating the temperature in the pyrolysis process [81].

7 Potential Product from Biomass Pyrolysis

7.1 *Activated Carbon*

Activated carbon (AC) is an adsorbent material and catalyst buffer that has large porosity and surface area of 500–3000 m^2/g, characteristics of surface chemistry, and surface reactivity [19]. The method of making AC is a two-stage method (carbonization/ pyrolysis continued activation) and a single-stage method (carbonization and activation are done simultaneously). The single-stage method has advantages, in terms of simplicity process and the reduction of operating time, cost, energy consumption, and operator efforts [130].

The methods used for the synthesis of AC can be done physically, chemically as well as a combination of both [131]. Physical activation generally uses steam and CO_2 at high temperatures to obtain micropores [130], [132]. Activated carbon from biomass through CO_2 activation provides superior rate performance and lower charge transfer resistance compared to potassium hydroxide activation, making it an environmentally friendly alternative for supercapacitor electrodes [133]. This method requires a high temperature so it is more wasteful of energy, which makes it less applicable to industry. Chemical activation can be applied using chemicals [134], H_3PO_4 [135], and $ZnCl_2$ [136] (see Figure 6). This method generates good thermal stability characteristic of AC and forms a uniform mesoporous structure with a high specific surface area. AC derived through chemical activation is preferable to utilize for gas or water purification and sewage treatment [137].

Table 5 shows the comparison of AC from various biomasses. The use of a strong base (KOH) affects the formation of carbon [139]. The enhancement in surface area is influenced by the augmentation of the KOH/biochar ratio [138], raw material composition (higher cellulose), active carbon pore structure [139], and the decomposition of organic components of the carbon matrix that make up the pores resulted from chemical activation with KOH. Pore volume increases with the increasing temperature due to the loss of gas compounds caused by decomposition in materials [139], the formation of pore structures in internal molecules, and the formation of carbonaceous structures in pyrolysis processes. Chemical activation can develop and control the number of micropores with very similar pore size distributions [138]. Active species containing O in biomass react with KOH to remove most O-containing groups, resulting in a void forming a new O-containing group in the biochar. As a result, porosity develops widely on biochar [140].

Table 5: Comparison of AC from biomass.

Biomass	Activation	Activation Conditions	Method	Yield (wt%)	Surface Area (m^2/g)	Pore Volume (cm^3/g)	Application	Ref.
Pistachio shells	Steam	T = 830 °C, t = 2h, HR = 5 °C/min, FR = 3 cm^3/min	Physical Activation	12.80	821	0.68	Adsorbent methylene blue, basic brown 1, acid blue 74, 2,4-dichlorophenol,4 chlorophenol, and phenol	[138]
	KOH	T = 780 °C, t = 1h, HR = 10 °C/min, FR = 4 cm^3/min,	Chemical Activation	19.80–29.7	731–1687	0.4–1.68		
Palm kernel shell	CO_2	T = 850 °C, t = 1h, HR = 5 °C/min, FR = 150 cm^3/min and 450 cm^3/min,	Physical Activation	25.15	367.8	0.2199	Adsorption CO_2	[19]
Oleaster peel	$ZnCl_2$	T = 450 °C, t = 2h, HR = 10 °C/min	Chemical Activation	70.5	1719–2021	1.176–1.293	Adsorbent	[139]
	KOH	T = 800 °C, t = 2h, HR = 10 °C/min		48.3	1149–1816	0.609–0.978		

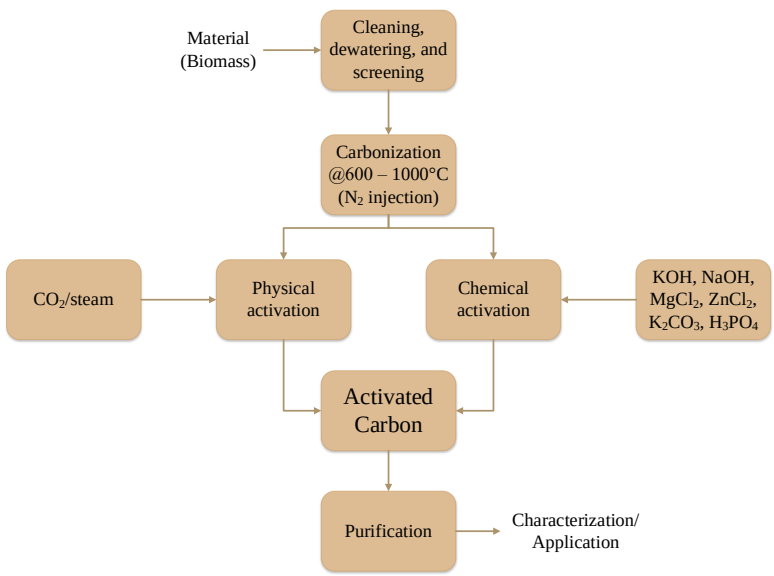

Figure 6: Biomass-based AC production path. Adapted from [141].

$ZnCl_2$ activators can break lateral bonds in cellulose molecules, resulting in AC with a higher surface area [136], [139]. The mesopore structure is seen in the activation of H_3PO_4 [132] with pores that can be used for the adsorption of large molecules such as wastewater treatment. The advantage of using H_3PO_4 as an activator is that it has a low corrosiveness level to equipment and does not leave metal residues, making it environmentally friendly, having good sedimentation performance as well as being cost-effective [135]. Activation of physics using CO_2 indicates a narrow micropore structure [132]. In addition, there is an increase in carbon and a decrease in hydrogen and oxygen. Decarboxylation of aromatization in heating CO_2 activation reduces H/C and O/C ratio [19].

Based on Table 5, yields vary between physical and chemical activation methods. Physical activation using steam or CO_2, generally results in lower yields (12.80% for steam-activated pistachio shells), as it primarily removes volatile compounds. In contrast, chemical activation (e.g., KOH, $ZnCl_2$) often yields higher percentages (70.5% for $ZnCl_2$-activated oleaster peel), as it promotes more efficient carbonization. Higher yields indicate more effective biomass conversion but may trade off certain material properties, such as surface area or pore structure. This balance is key for selecting AC based on application

needs. The main factors that affect the manufacture of AC are the types of precursors and activating substances [139]. Factors that affect the adsorption of organic materials are surface area, pore volume, and porosity [138].

AC finds diverse applications across various fields, showcasing its versatility and utility. Its wide-ranging uses include carbon adsorbent, water treatment, air purification, electro/magnetic shielding, electrochemical sensor development, energy storage systems (supercapacitor), and membrane capacitive deionization [19], [142]–[147] (see Figure 7(a)). Figure 7b illustrates the way to produce an electrochemical sensor from biomass (fruit peel). The unique properties of AC make it a valuable material in addressing challenges related to environmental remediation, sensing technologies, and sustainable energy solutions.

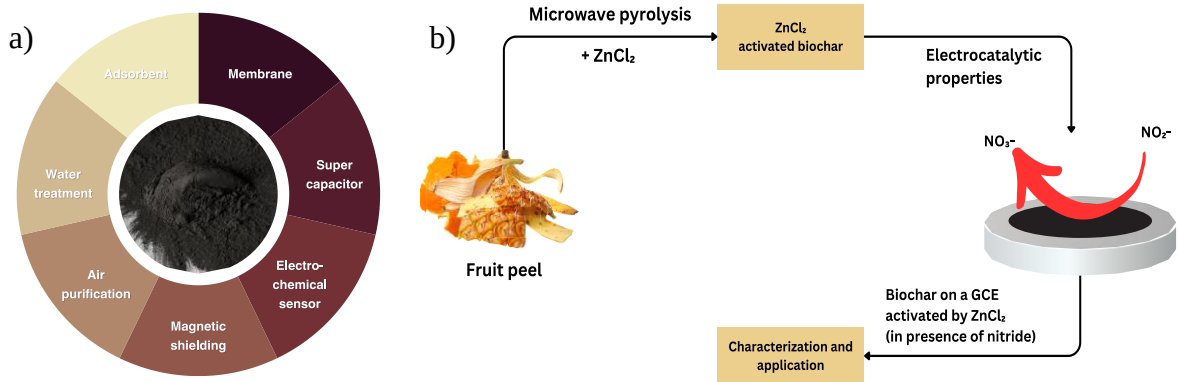

Figure 7: (a) Potential application of AC, (b) illustration of AC application on the electrochemical sensor from fruit peel through microwave-assisted pyrolysis. Adapted from [145].

7.2 *Magnetic activated carbon*

Magnetic activated carbon (MAC) is a solid material created by dispersing magnetic substrates onto AC [148]. It is attracting interest for its capability to eliminate heavy metals from wastewater, attributed to its advantageous physicochemical characteristics, including increased surface area and magnetic properties [149]. The production of MAC includes the integration of Fe_3O_4 into AC using two distinct iron sources: Fe_3O_4 derived from electric arc furnace slag and Fe_3O_4 from a solution of ferrous sulfate/ferric chloride. The magnetic biomass derived from the iron suspension exhibited superior Brunauer-Emmett-Teller surface area (S_{BET}) and a higher saturation of magnetic properties (Ms). Consequently, MAC emerges as a promising material for wastewater treatment, attributed to its elevated adsorption capacity and magnetic characteristics [150]. Ferrite substances are commonly regarded with considerable interest owing to their notable adsorption capabilities, lack of toxicity, and widespread accessibility [151]. Given the promising adsorptive potential of these materials, it is imperative to advance the synthesis of a composite MAC (CMAC) material based on activated carbon and assess its viability for application in wastewater treatment [152].

Magnetic properties of materials are frequently characterized using direct current (DC) magnetometry techniques, where a constant and uniform magnetic field is applied. Since the magnetic field remains steady during DC measurements, the sample must be moved physically to induce a detectable change in the field. One way to measure the moment by force is by using a vibrating-sample magnetometer (VSM) [153]. The samples' magnetic moment has to be more than 10^{-6} emu in order for the VSM analyzer to identify them accurately. In comparison to the baseline dimension of the detecting coils, it was found that utilizing a lower sample size with a vertical dimension produced more accurate findings. The samples should be positioned 35 mm apart, and the coil set's height should be kept at 40 mm, in order to maximize measurements. With this arrangement, the offset is guaranteed to be near the end of the sample holder, around 5 mm above the puck's surface [150]. Within the optical magneto-mechanical device, the sample was placed in a sample holder. The VSM technique is particularly valuable in the synthesis of MAC. This instrument allows for precise characterization of the magnetic properties of the material, which is essential

when synthesizing MAC with specific magnetic behaviors.

Typically, magnetic mesoporous carbon materials are prepared using a two-step method. Initially, mesoporous materials are crafted, followed by the infiltration of iron oxide nanoparticles [154]. The treatment of industrial wastewater through magnetic separation proves to be a promising technique, featuring convenient and rapid recovery, depending on the specific characteristics of the wastewater. The incorporation of magnetic adsorbents can augment the thermal stability and cross-linking density of these adsorbents. This method holds the potential to enhance the efficiency and processing times of urban and drinking water treatment plants [148]. The pathway of recovering and reusing MAC is shown in Figure 8.

There are several methods applied in order to produce the MAC, the co-precipitation is the most commonly used synthesis route because of its simplicity, consisting of mixing and heating [155], [156]. This approach holds significance in industry because of its cost-effectiveness and operation at temperatures below 100°C. Furthermore, it is environmentally friendly as it avoids the generation of toxic intermediates or solvents. Additionally, its reproducibility and ease of scalability contribute to its merits [157]. The primary drawback in the synthesis of Fe_3O_4 nanoparticles through co-precipitation lies in their inclination to aggregate, especially when they are extremely small. Additionally, precise control of reaction conditions is imperative to prevent the formation of non-magnetic compounds [157], [158]. The second larger method used is the thermochemical method, which requires specific equipment and an inert gas flow to gain a high carbon content (char). This approach was applied by several activists for specific needs, commonly for water treatment processes [159]–[166]. Pyrolysis often be employed because it effectively introduces magnetic properties while preserving the porous structure of activated carbon. This process involves high-temperature treatment in the presence of a magnetic precursor, resulting in a material with both magnetic and adsorbent characteristics, ideal for applications like environmental remediation and wastewater treatment. In the realm of wastewater treatment, powdered activated carbon (PAC) and granular activated carbon (GAC) stand out as the primary agents [167]. While GAC is commonly employed by researchers for its ease of separation from the bulk fluid through classification or screening, PAC offers advantages such as reduced contact time and lower capital costs. Consequently, the development of magnetic PAC (PMAC), a prospective composite material formed by blending PAC with magnetic iron oxide nanoparticles, allows for isolation from water through the application of an external magnetic field [167]. Therefore, it is a crucial technique for particular industries such as pharmaceuticals. Table S4 summarizes numerous overviews of the synthesis methods applied to obtain the MAC.

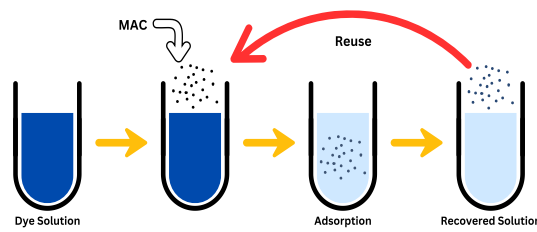

Figure 8: Schematic representation of the process for recovering and reusing magnetic activated carbon. Adapted from [148].

The absorption characteristics of AC can be attributed to its expansive surface area, well-established pore structure, and the functional groups formed during the manufacturing process [168]. Due to its cost-effectiveness and ease of regeneration compared to more sophisticated purification methods such as reverse osmosis membranes and ion exchange resins, activated carbon is a preferred treatment option. The properties of activated carbon, including surface chemistry, pore size, shape, and distribution, are influenced by the materials used, activation techniques, and activation conditions [169], [170]. Studies on the kinetics and thermodynamics of heavy metals using metal-doped metal oxide and ultrasonic synthesis methods have reported a relatively high adsorption capacity [171]–[173]. The resulting material composite exhibits promising features, including high adsorption capacity, reasonable reuse performance, cost-effectiveness, and eco-friendliness, making it an economically effective and hopeful adsorbent for purifying wastewater from heavy metal impurities.

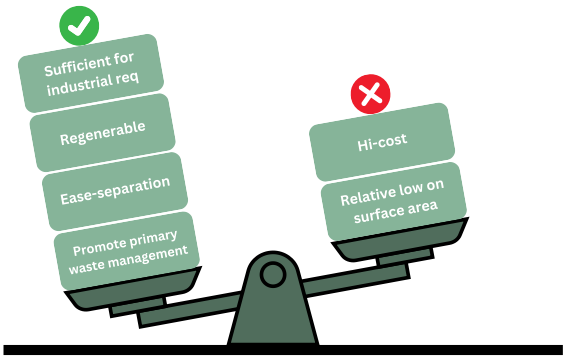

Figure 9: Benefits (check) and drawbacks (cross) of employing MAC in the elimination of contaminants from water. Adapted from [157].

Figure 9 outlines the advantages and disadvantages of using MAC in water treatment, particularly for contaminant removal. Given the undeniable benefits of these materials, they emerge as a sustainable option for water purification. However, a delicate balance must be struck between the magnetic properties of MAC and their potential impact on binding capacity towards target pollutants. The existing literature highlights a dearth of information on MAC's adsorption efficiency in multi-component systems and natural water matrices, emphasizing the need for further exploration in real treatment applications. Comprehensive study endeavors are imperative for understanding the intricate interplay between natural organic matter, inorganic and organic compounds, and various micropollutants present ubiquitously in aquatic environments and wastewater. These factors significantly influence the adsorption capacity of MAC towards pharmaceuticals. Moreover, there exists a critical necessity for thorough investigations about the regeneration protocols of MAC, emphasizing the identification of efficient and environmentally sustainable methodologies facilitating the reusability of MAC. Notably absent in extant literature are pilot-scale demonstrations elucidating the efficacy of MAC in pharmaceutical removal from water. Consequently, there is an urgent call to undertake such demonstrations in the imminent future to comprehensively evaluate the economic and technical feasibility of deploying these materials, thereby bridging the existing disparity between laboratory-based studies and real-world applications.

7.3 *Graphene*

Graphene has a high specific surface area (~2,630 m^2/g), high carrier mobility (~10,000 $cm^2/V.s$), high thermal conductivity (~5,000 W.M/K), and high Young modulus (~1.0 tPa) [174]. Graphene is the basic structural element of several carbon allotropes, such as graphite, CNT, and fullerenes that can be obtained chemically or mechanically from graphite powder. Graphene synthesis methods are generally known to have four types, namely chemically derived [175], graphite exfoliation [176], CVD [177], and organic synthesis [178]. Mechanical exfoliation and CVD can produce superior-quality graphene compared to other methods [174].

Due to its abundance and relatively inexpensive material, biomass is an attractive alternative precursor for preparing graphene [24]. The pyrolysis and thermal activation of precursors at high temperatures remain the most widely adopted methods to obtain single atomic metals supported on graphene with small domains of graphene surrounding the metal centers [179]. Graphene with high porosity can be prepared using pyrolysis from biomass with a well-defined carbonization method [174]. Synthesizing graphene from biomass consists of two stages: pyrolysis to obtain biochar [180] and activation to open and augment pores to graphene [25].

Existing study synthesized graphene from chitosan and alginate through pyrolysis at a temperature of 900–1200 °C. A temperature of 1100 °C is the optimum temperature for producing high-quality graphene in terms of electrical conductivity and better photoelectric catalytic activity. It is due to the presence of H_2, which serves as a chemical reduction and results in an additional decrease in oxygen content by forming H_2O or other volatile hydrogenation compounds. In addition, H_2 can reduce the density of defects in either undoped or doped graphene layers, resulting a slightly higher graphite content materials and a lower percentage of C-O/C-N and C=O bonds [181]. The synthesis techniques for producing graphene are shown in Figure 10.

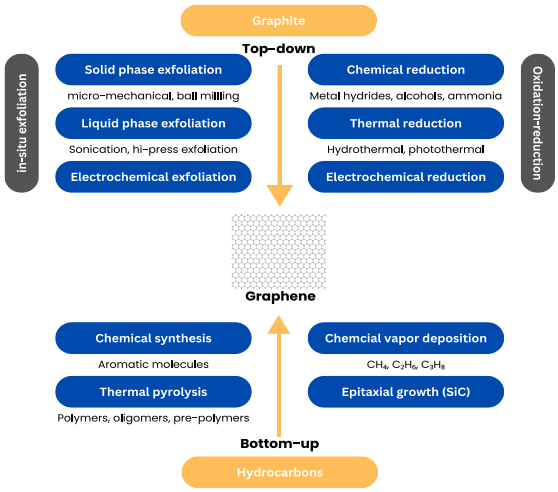

Figure 10: Schematic representation of the most frequently used synthesis techniques of graphene. Adapted from [183].

The two stages of pyrolysis in synthesizing graphene can increase the yield of graphene produced. $ZnCl_2$ activator is preferable because it encourages hydrolysis reactions by removing volatile compounds of O_2 and H_2 from the carbon matrix and it is also necessary in creating pores by penetrating the matrix [182]. This activator generates a large pore volume and high surface area for activated carbon, causing weight loss, increased elasticity, and enlarged yield products. The graphene produced is similar to nanosheets with graphite-like interlayer spacing (0.3380 nm), consisting of 2–4 atomic layers and a high crystalline degree (IG/ID = 9.35) [25]. Graphene has been widely adopted as an active material in a wide range of applications including metal ion detection, membrane applications, conversion CO_2, and gas sensors [183]. It can be concluded that graphene can be synthesized from biomass through pyrolysis, with physical and chemical activation influencing the final yield and quality of the produced graphene. Table 6 shows several researchers also surpassed their work to generate the graphene-related material (GRM) biomass-derived.

The practical uses of graphene are determined by numerous factors. The properties and potential applications of graphene can be significantly influenced by two crucial factors: the number of layers and the interlayer distance in the material produced [183]. Figure 11 provides a summary of the diverse synthesis methods and environmental applications of graphene. Graphene is currently under development for utilization in various environmental contexts, such as in water treatment membranes, as high-porosity adsorbents for decontamination purposes, as emerging technology, and as active materials in sensors for monitoring contamination [184].

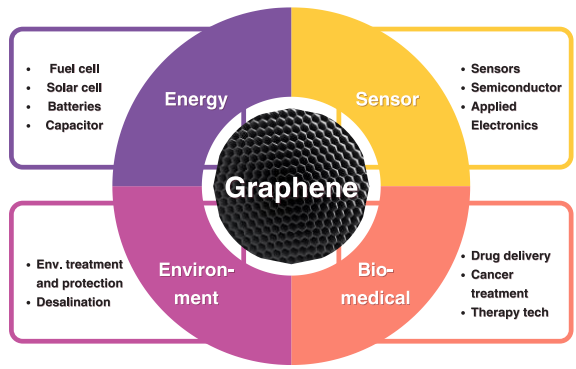

Figure 11: Graphical representation illustrating both the synthesis techniques and environmental applications of graphene. Adapted from [202].

Within the realm of optimizing energy storage technologies, graphene has emerged as a material of significant intrigue. This intrigue stems from its confluence of remarkable characteristics: exceptional mechanical flexibility, high specific surface area, an ultra-thin morphology, superior electrical conductivity, and a theoretically outstanding capacitance [185], [186]. Across a diverse range of energy storage systems, graphene has emerged as a material of significant interest. This includes applications in lithium-ion batteries, flexible and micro-supercapacitors, lithium-air batteries, lithium-sulfur batteries, fuel cell electrodes, and solar cells. Within these domains, graphene has been the subject of extensive research and development efforts, with a growing body of literature documenting its implementation [187], [188].

In the field of battery technology, the incorporation of functionalized graphene proves crucial for facilitating the attachment of other active species, thereby optimizing performance. Simultaneously, the ultra-high specific surface area of graphene assumes paramount importance in electric double-layer capacitors, ensuring substantial ion storage [189]. Furthermore, membranes composed of highly conductive graphene exhibit potential utility in lithium-sulfur batteries, serving as interlayers or current collectors [190]. In the catalytic growth/decomposition processes and accommodation

within lithium batteries, graphene's macro-porous structure emerges as a noteworthy catalyst [191].

Scientists are investigating the viability of employing graphene in the biomedical field. Reports indicate that graphene possesses exceptional qualities, making it well-suited for biological applications [192], [193]. Significantly, the heightened opacity, chemical reactivity, and unparalleled thermal conductivity are pivotal facts [2].

Table 6: Initial components, preparatory procedures, and GRM characterization from various sources.

Precursor	Pre-Treatment	Treatment	Product	Design	Elemental Analysis	Spectroscopy	BET (m^2/g)	Ref.
Kraft lignin	$Fe(NO_3)_3$, 1100 °C, 1h, Ar, CH_4	Modified Hummers'	Graphene oxide (GO)	Nanosheets 1–3 nm (1–3 layers) <1µm lateral size		I_D/I_G = 1.1–1.2		[194]
Medium-density fiberboard	$Ni(NO_3)_2$ impregnation, drying	300 °C–1000 °C, 30 min, N_2	Porous graphene-like carbon	Crumpled nanosheets	63%–86% C, 11%–29% O, 0%–1% Ni, 2%–7% N, C/O = 2.2–7.8	I_G/I_{DI} = 0.5–1.56	333–391	[195]
Coconut shell	Mix with $FeCl_3$, $ZnCl_2$, drying	900 °C, 1 h, N_2	Porous graphene-like nanosheets	Few and multilayer	O/C = 0.05812	I_D/I_G = 0.25	1,874	[196]
Coconut fibre	Washing, drying; KOH, 2 h, drying, heating 300 °C 1 h, 750 °C 3 h in Ar, HCl 12 h, washing, drying, HNO_3 12 h, washing, drying	300 °C 1 h, 750 °C, 3 h, Ar; HCl, 12 h; HNO_3,12 h S/N doping: mix with S/urea, 450 °C, 40 min, Ar; 750°C, 30 min, H_2	Porous, S/N-doped GO	0.91–4.19 nm thick	67%–85% C, 3.9% N, 0.9% S, O by dif	I_D/I_G = 0.98–1.18	1,083–1,114	[197]
Bituminous coal, coke, anthracite	Sonication in H_2SO_4 and HNO_3,2 h	100 °C–120 °C, 24 h	Graphene quantum dots	2.3–2.96 nm size, 1.5–3 nm thick		I_D/I_G = 1.28–1.90		[198]
Heavy fuel oil	H_2SO_4, 180 °C, 24 h; $Mn(NO_3)_2$, 900 °C, 3 h, N_2	Modified Hummers'; Chloro-sulfonic acid, 70 °C, 4 h	GO, Sulfonated GO	Few-layers	C/O = 0.79–0.90, 1.54%–7.58% S	I_D/I_G = 0.67–1.06	181.13–246.18	[199]

The energy source of biomass has the. In biomedical applications, graphene oxide and N-graphene, two notable functional groups of graphene, are preferred, yielding successful outcomes. Graphene has been widely incorporated into diverse biomedical applications, encompassing tissue engineering, delivery systems for drugs and genes, phototherapy modalities, facilitation of cellular proliferation and differentiation, biosensing technologies, bio-imaging methodologies, as well as detection and therapeutic interventions about cancerous or pathological conditions [200]. Its uniformity and ability to create a homogeneous structure make graphene widely utilized in biomedicine. The suitability of graphene for biological applications depends on factors like shape, size, morphology, thickness, and level of oxidation. An additional advantageous attribute is its minimal toxicity, as evidenced by its enduring stability within metabolic pathways and cellular uptake over an extended period [201]. Nonetheless, additional investigations are imperative concerning the in vivo utilization of graphene, particularly in the realm of drug conveyance. To expedite its integration into the market, biomedical enterprises ought to accord precedence to the aforementioned benchmarks. Consequently, preliminary research before commercialization assumes paramount importance, serving to lay the groundwork and furnish empirical

evidence elucidating the advantageous attributes of graphene for pivotal biomedical domains.

Graphene is also used as an electrocatalyst because it has a high cathodic current density, positive onset potential, low hydrogen peroxide formation, and an ideal transfer of electrons in an alkaline medium [203]. N-doped graphene can be used for the activation of heterogeneous peroxy-mono-sulfate (PMS) [204]. The increase in catalytic performance for PMS activation occurs due to an increase in the amount of nitrogen in graphene, which affects the increase in the oxidation rate of phenols, thus leading to high levels of doping [28].

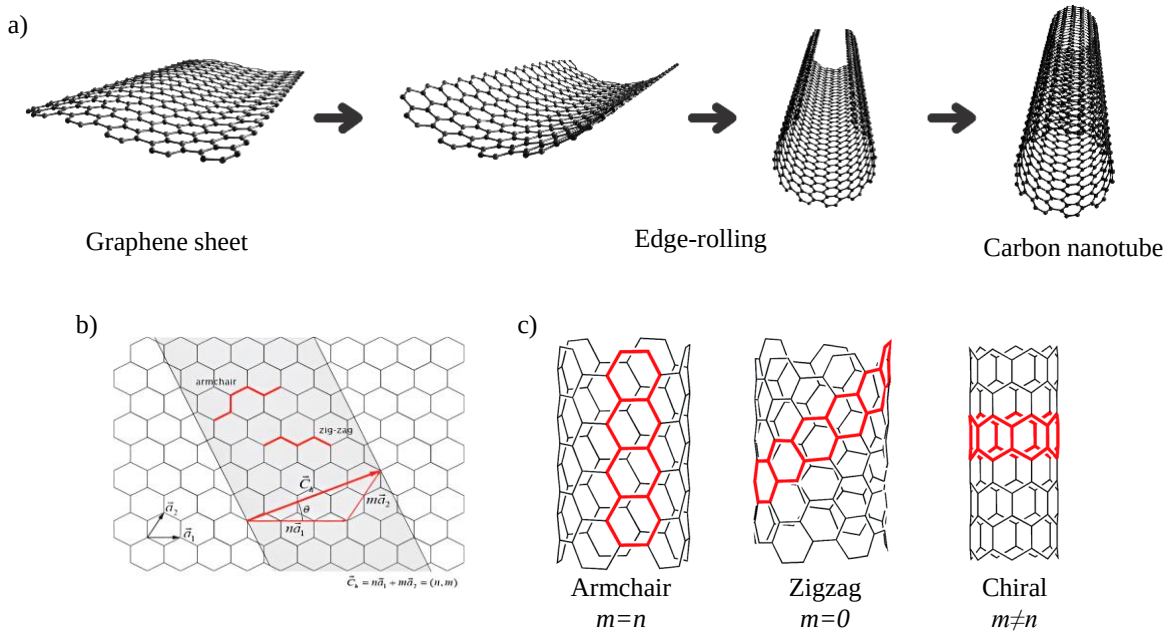

Figure 12: The way to obtain carbon nanotube. Licensed under CC-BY 4.0 [216] (a), Creating a carbon nanotube involves aligning the ends of the chiral vector C_h to form a nanotube with 1D lattice vector T and chiral angle Θ, using primitive lattice vectors a_1 and a_2 from 2D graphite. The illustration includes zigzag and armchair wrapping directions. Licensed under CC-BY 4.0 [217] (b), Various types of CNT are categorized by their chirality, i.e., armchair, zigzag and chiral. Licensed under CC-BY 3.0 [218] (c).

7.4 *Carbon nanotube*

Carbon nanotube (CNT) is elongated, hollow cylindrical structure composed of graphite sheets, commonly known as graphene, with diameters spanning from less than 1–10 nm (Figure 12(a)) [205]. The electronic properties of CNT are a consequence of their fascinating low-dimensional structure. This unique dimensionality confines the movement of charge carriers, resulting in specific electronic behavior. These properties, semiconducting or metallic, are dictated by two key factors: the diameter of the CNT and the orientation (chirality) of the graphene lattice relative to the tube axis [206]. The chirality is determined by basis vectors a_1 and a_2, which define the graphene lattice. The chiral vector (C), representing the eventual CNT circumference, is expressed as $C = na_1 + ma_2$, where n and m are integers. Different rolling of graphene sheets yields three classes of CNT: zigzag, armchair, and chiral (Figure 12(c)). The chirality of CNT is determined by their chiral indices (n, m) and is reflected in their electrical properties. Zigzag CNT is formed when m = 0, armchair CNT when n = m, and all other combinations of n, m result in chiral CNT ($n \neq m$) (Figure 12(b)). Notably, armchair CNTs consistently exhibit metallic behavior, while approximately two-thirds of zigzag CNTs are classified as semiconducting, with the remaining one-third being either metallic or possessing a narrow band gap [207]. Various techniques have been developed to produce high-quality CNT, including electric arc discharge [208],

laser ablation [209], sonochemical [210], diffusion flame [211] and catalytic chemical vapor deposition (CVD) [212]. Arc discharge and laser ablation yield superior quality and high purity of CNT, their extensive production costs render them impractical for large-scale industrial applications [97]. In contrast, the CVD method offers a viable alternative by producing CNT of comparable quality at reduced production expenses. This method operates on the principle of catalyzing the thermal decomposition of hydrocarbon compounds with metal particle catalysts to foster the growth of carbon nanotubes [213]. Notably, the fire synthesis technique stands out as a particularly effective and efficient means of CNT synthesis. By introducing oxygen into the system at controlled rates, the technique facilitates the autoignition of pyrolysis gasses, leading to the deposition of CO compounds on catalytic substrates [21]. Catalysts prepared via the impregnation method exhibit lower surface area and pore volume compared to those prepared using the sol-gel method, with respective values ranging from 81.06–90.71 m^2/g and 0.23 ml/g. Furthermore, the average pore size of impregnated catalysts measures approximately 7 nm, indicating a smaller dimensionality relative to sol-gel counterparts [214]. There is a large amount of carbon formed in the reacting catalyst, and most of it is multi-walled carbon nanotubes (MWCNT). Nickel catalysts produce the largest amount of valued carbon (about 93 wt%) compared to other catalysts [215].

Raman is one of the characteristic analyses of CNT to determine the effectiveness of CNT graphitization due to changes in the polarization of carbon atoms [215]. In Raman (ID/IG ratio) peak D shows defects in graphite lattice, while peak G indicates CNT purity. High CNT purity is indicated by a large D/G Ratio [219]. The CVD method works similarly to catalytic pyrolysis in producing CNT, that is pyrolysis gas settles onto the surface of the catalyst. CNT derived from pyrolysis are formed due to the decomposition of hydrocarbons on the surface of catalysts [219]. The working principle of the Pyrolysis-Flame Synthesis method to form CNT is pyrolysis gas mixed with oxygen gas so that there is a combustion reaction. The combustion gas goes to the synthesis reactor to form CNT [21].

The use of temperature for CNT synthesis can affect the characteristics of CNT obtained. Increased temperature leads to faster diffusion and deposition of carbon. In addition, CNT characteristics are also influenced by the ratio of raw materials to catalysts. Increasing the quantity of raw materials potentially enhances production. However, it may shrink the efficiency of raw material conversion into desired product [219]. CNT synthesis can use methane gas (commercial) because it has a high ratio of hydrogen and carbon. On the other hand, biomass is a promising material because its derivatives through pyrolysis are potentially the carbon source for CNT production demand such as volatiles, hydrocarbon, and biochar. Table 7 shows the comparison of CNT from several sources. Rising temperatures can form non-uniform carbon amorphous, soot, and CNT.

Catalyst support influences the yield, quality, and morphology of CNT. Ni-Mo/CaTiO3 catalysts can decompose catalytically resulting in high CNT yields and short CNT diameters because there are thermally stable species that can inhibit the agglomeration of particle metals. For higher temperature use it produces CNT with characteristics of diameters and lengths up to several micrometers and a lot of high-purity walls. CNT synthesis through Fe-Ni catalysts generates high thermal stability and graphitization characteristics [220].

Previous research synthesized CNT from palm kernel shells using microwave pyrolysis at 600 °C [20]. The CNTs are formed in volatile materials from cellulose that contain monosaccharides such as D-Glucopyranose and glucopyranose. Thermal decomposition produces volatiles with compositions that affect the type of carbon source for the formation of CNT. The formation of CNT can be assisted by Co and Fe catalysts that can increase the size of CNT so that CNTs are produced with an amorphous carbon matrix [222]. The method of heating and the use of Ni catalysts play a role in the formation and growth of CNT [99]. Synthesis of CNT with a mixture of Fe-Ni catalysts is efficient in forming thick CNT with better graphitization, and longer, and larger diameters than those with Fe catalysts [97]. Fe-Ni also plays a role in the reform reaction and formation of CNT [223]. Research conducted by Araga and Sharma synthesized MWCNT through the pyrolysis method continued with PECVD from coconut shells [221]. The growth of MWCNT is affected by the temperature and mineral catalysts (Ca, Mg, K, and Na) found in the coconut shell. Gasification or pyrolysis of CO and CH_4 gasses can be used for the CNT formation with longer and smoother characteristics than pure CO and CH_4 gasses [23]. Meanwhile, the synthesis of CNT through microwave pyrolysis has advantages such as low cost (does not require high duty, catalyst, or additional carbon source) and more environmentally friendly [20].

Table 7: Comparison between the properties of biomass-derived and commercial CNTs.

Sample	Synthesis Method	Diameter (nm)	Length (nm)	d-spacing (nm)	Raman ID/IG ratio	Morphology	Carbon Source	Ref.
Commercial CNT	CVD over a metal catalyst	25–100	200–1600	0.34	0.96	Ordered carbon structure with some defects	Methane gas	[20]
CNT synthesized from rice straw	CVD	22–66	100–500	-	0.753–0.942	straight, porous and rolled brous of cellulose microstructure	Hydrocarbons in the biomass	[97]
CNT synthesized from pine nutshell chars	microwave-assisted CVD	50±8	2600–3200	0.34	1.03–1.21	tubular and multiwall structure.	Hydrocarbons in the biomass	[99]
CNT synthesized from coconut shell derived charcoal	Pyrolysis and PECVD	25–30	few tens of micrometers	-	0.94	Ordered carbon structure with some defects	Charcoal	[221]
CNT synthesized from lignocellulosic biomass and sugarcane bagasse	Microwave pyrolysis with addition of catalyst Fe and Co	20±10 nm and 50±20 nm	30 nm, 86±26 nm, and 120± 40 nm	-	0.78–0.96	amorphous carbon matrix	Bio-Char	[222]
CNT synthesized from palm kernel shell	Microwave pyrolysis without external catalyst	50–100	600–1800	0.32	0.86	Ordered carbon structure with some defects	Volatiles in biomass	[20]

Table 8: The enhancement of concrete strength through the addition of carbon nanotubes.

Nanomaterial		Concrete Type	Tensile Strength (MPa)		Ref.
Type	Content		A week	4 weeks	
Ni-MWCNTs	(0.03–0.06)%vol	Portland cement	-	102.22–122.91	[228]
MWCNTs	(0–0.06)%wt.	Ordinary portland cement (expanded glass and silica)	-	5.4–7.6	[229]
Ni-CNTs	(0.02–0.08)%vol	Portland cement	-	83.5–109	[230]
CNTs	2.5–10%wt.	General purpose portland (hi-early strength) cement	34–46	40–55	[231]
CNTSS, CNTSL, CNTPL, CNTCOOH, CNTOH	(0.05–0.5)%wt.	Portland cement	35.6–78.3	44.5–84.9	[232]
CNTs, NS	(0–3.0)%wt.	Ordinary portland cement	-	6.32–10.42	[233]
Titania, MWCNTs-COOH	(0.5–1.5)%wt. (0.02–0.10)%wt.	Ordinary portland cement	-	30.17–39.98	[234]
MWCNTs-OH	(0–0.1)%wt.	Portland cement PCB40	-	3.5–9.0	[235]
COOH-MWCNTs	(0–0.125)%wt.	Portland Pozzolana cemen	21 – 30.5	32–39	[236]

CNT is a nanotechnology material that has strong mechanical strength and excellent electrical conductivity and can be used for many advanced applications, such as adsorbents, catalysts, composite materials, electronic devices, reactor layers, dyes, lubricants [21] and optics due to its excellent chemical structure [215]. Numerous research findings indicate a notable enhancement in the tensile strength of concrete with the integration of CNTs. This improvement is attributed to the ability of CNTs, with their shape and high tensile strength, to effectively serve as connectors for the matrix and bridge microcracks [224]. The stability and safety of a structure are significantly influenced by its compressive strength. Various studies have presented findings related to compressive strength for particular sample sizes and shapes, as indicated in Table 8. There was an enhancement in compressive strength, and an

increase in tensile strength after 4 weeks [225]. A related study also investigated tensile strength, examining split cylinder concrete samples at various curing ages (3 days, 7 days, 28 days, and 56 days) [226]. The results depicted in Figure 13(a) indicated that concrete containing MWCNTs exhibited heightened tensile strength. Analysis of the overall trend revealed that a minimal quantity of MWCNTs yielded the most substantial improvement, attributed to their effective dispersion at low concentrations. Other research corroborated these findings, demonstrating increased tensile strength with the addition of CNTs and other admixtures. For instance, a combination of fiber and CNT increased concrete's 28-day tensile strength by 15.52% [227].

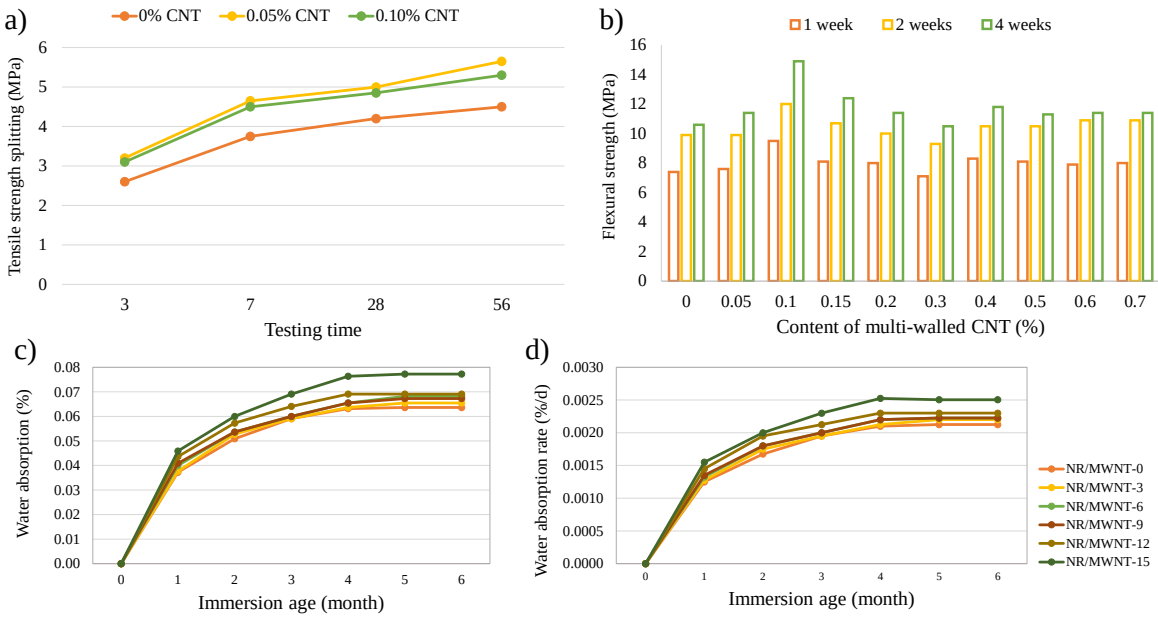

Figure 13: Tensile strength's splitting cylinder of CNT-Composite (a). Adopted from [226]; Cement/MWCNT's flexural strength (b). Adopted from [237]; Influence of MWNT on physical properties of natural rubber nanocomposite, water absorption (c); water absorption rate (d). Adopted from [238].

Various experiments have demonstrated that adding an appropriate amount of carbon nanotubes (CNTs) can enhance the flexural strength of concrete. Nevertheless, an excess of CNTs may lead to their accumulation in concrete, causing defects and weak areas that possibly diminish the flexural strength feature. Existing research conducted a systematic investigation into the impact of MWCNT content on the mechanical properties of cementitious composites. The test results involving hardening cement slurry with polycarboxylate superplasticizer revealed a 12.9, 15.8, and 2.0% increase in flexural strength at the age of 28 days when the MWCNTs content was 0.1, 0.3, and 0.5%, respectively. However, as the MWCNTs content increased from 0.3% to 0.5%, the strengthening effect diminished [239]. This trend aligns with the recent findings that investigated the flexural strength of MWCNTs-reinforced cement-based composites at three curing ages (Figure 13b) [237]. Notably, a 0.1% MWCNT concentration maximized the increase in flexural strength feature. Researchers explained that MWCNTs enhance concrete flexibility by bridging minuscule cracks and securely bonding hydration products. Consequently, employing lower concentrations of MWCNTs proves beneficial for improving flexural strength. Conversely, an excess of MWCNTs increases the likelihood of agglomeration, restricting sample uniformity and stress distribution, ultimately leading to a decline in flexural strength features [237], [240]–[242].

The subsequent examination, delineated in Table 9, encapsulates select scholarly contributions pertinent to this topic. An observable trend in recent scholarly discourse denotes a purposeful transition from natural to synthetic reinforcing fillers within the context of polymer matrix composites. This shift primarily stems

from the perceived mechanical advantages conferred by synthetic alternatives. Notably, natural rubber exhibits a comparatively diminished ecological footprint vis-à-vis thermoplastics and synthetic rubber. Moreover, natural rubber nanocomposites manifest exceptional physical, mechanical, thermal, and viscoelastic attributes, thereby holding substantial promise for contemporary biomedical applications. Specifically, its utility in prosthetic foot configurations, particularly when it is augmented with CNTs [243]–[245].

Table 9: Recap of the current studies on polymer nanocomposites CNTs-enhanced.

Matrix	Filler	Scope of Study	Findings	Application	Ref.
Natural rubber	MWCNTs	Creating a prosthetic foot using Compounding NR/MWCNT nanocomposite	A decrease in filler concentration enhances the geometric stability of natural rubber	Prosthetic foot	[238]
Silicone	Graphene, CNTs	Examining the strain-sensing characteristics of conductive polymer composites in silicone rubber (VMQ) composites through the incorporation of CNTs and Graphene	Composites of self-assembled CNTs-GR/VMQ exhibit a significantly reduced percolation threshold of 0.92wt% compared to CNTs/VMQ composites.	Varied	[246]
Natural rubber	CNTs	Analyzing the vibration and damping properties of a rotating laminated composite hybrid MR elastomer sandwich panel	Analyzing the vibration and damping properties of a rotating laminated composite hybrid MR elastomer sandwich panel	Transverse vibrations	[247]
Natural rubber	CNTs	Minimizing the clustering and settling of carbon nanotubes in polymer composites through the utilization of the slurry blending technique	Enhanced dispersion of carbon nanotubes in the natural rubber resulted in a 15.2% increase in the sample's tensile strength.	Rubber industry	[248]
Silicone rubber	Al_2O_3, CNTs	Employing carbon nanotubes as enhancers for the enhancement of thermal and mechanical properties in alumina-filled silicone rubber	A greater proportion of alumina powder leads to increased thermal conductivity in composites.	Varied	[249]
Natural rubber	MWCNTs & carbon black	Improving the mechanical characteristics of rubber containing carbon nanotubes	Multi-walled carbon nanotubes (MWCNTs) played a substantial role in improving the mechanical characteristics of natural rubber.	Varied	[250]
Polyurethane	CNTs	Creating a CNT-TPUNC with exceptional conductivity for smart clothing applications	Modulating the carbon nanotube concentration in thermoplastic polyurethane enables the manipulation of stress and strain characteristics within the fibers	Smart clothing applications	[251]
Thermoplastics	CNTs	Thermoplastics reinforced by CNTs	Carbon nanotubes were effectively distributed within the high-density polyethene matrix, leading to enhanced mechanical properties.	Varied	[252]

Moreover, the requirement for materials with enhanced environmental stability led to the execution of a physical test aligned with nanocomposite principles. The water absorption patterns are depicted in Figure 3(c), while the absorption rate is detailed in Figure 13(c) and (d). Notably, steady water uptake is observed in the initial 30 days, succeeded by a gradual decline and eventual cessation, ascribed to the diffusion phenomenon wherein water molecules infiltrate the composite material. During the amalgamation process of filler and matrix phases, hydrophilic fillers are enveloped by the rubber phase, resulting in their isolation from neighboring fillers. Consequently, the ingress of water molecules into the enclosed interstices becomes arduous, a consequence of the manufacturing technique, particularly compression molding in this context. Enhancing the interfacial adhesion between MWCNTs and natural rubber matrix involves surface treatments that promote a more consistent interaction between the filler and matrix. This, in turn, facilitates the transfer of load from the NR matrix to the filler, fostering stress flow throughout the composite and yielding favorable viscoelastic properties [253].

8 Sustainability view

Based on various manufacturing processes, Table 10 presents a comprehensive assessment of the global warming potential (GWP) and energy consumption of various materials, such as biochar, AC, MAC, graphene, and CNT to indicate the sustainability impact. Because of the differences in these materials' production methods, the results show considerable differences in energy usage and CO_2 emissions. For instance, pyrolysis produces biochar that uses much less energy (between 0.18 and 4.90 GJ/t) and occasionally emits less CO_2. Given that the pyrolysis process can stabilize carbon that would otherwise be released into the atmosphere, this suggests a carbon sequestration effect.

On the other hand, a greater range of energy requirements and emissions are seen in the manufacturing of activated carbon and magnetic activated carbon, which is mostly achieved by the pyrolysis of different feedstocks. There are related emissions of 1.70 to 47.15 t CO_2eq/t and energy requirements for AC generation ranging from 11.27 to 208.00 GJ/t. These numbers greatly rely on the kind of feedstock utilized and the presence or absence of energy recovery techniques. For instance, the intense energy needs and high carbon intensity of coal and woody biomass feedstocks result in considerable CO_2 emissions and significant energy inputs during the production of AC. The environmental advantages of utilizing waste-derived and renewable feedstocks are highlighted by the fact that using agricultural wastes or waste materials, such as pomace for MAC, may dramatically lower energy use and emissions.

Techniques like CVD and flash joule heating (FJH) demand large energy inputs and produce a significant amount of CO_2 emissions when producing graphene and CNTs. For example, the CVD process on substrates may yield up to 28,550.00 t CO_2eq/t and demand up to 408,710.00 GJ/t. These numbers highlight how energy-intensive the production of sophisticated nanomaterials is. The intricacy and high technological demands of these materials' production processes account for a major portion of the noticeable variations in energy and emission scales between them. Because CVD procedures require high temperatures and regulated conditions to assure material purity and structural integrity, they have substantial energy demands and emissions.

Table 10: Energy demand and emission of several pyrolyzed biomass-derived products.

Material	Method	Energy (GJ/t)	Emission (t CO_2eq/t)	Ref.
Biochar				
Corn Stover	Pyrolysis	0.84	–0.80 to –0.70	[254], [255]
Miscanthus	Pyrolysis	0.18	–0.74	[256]
Switchgrass	Pyrolysis	4.90	–442.00	[257]
Late stover	Pyrolysis	4.12	-864.00	[257]
Yard waste	Pyrolysis	4.04	36.00	[257]
Activated Carbon				
Olive-waste cake	Pyrolysis	11.27	11.09	[258]
Soybean shell	Pyrolysis	17.00–51.00	5.86–47.15	[259]
Woody biomass	Pyrolysis	158.33	8.60	[260]
Coal	Pyrolysis	241.62	18.28	[260]
Softwood, (energy recovery)	Pyrolysis	25.00–155.00	1.70–9.30	[261]
Hardwood, (energy recovery)	Pyrolysis	23.00–208.00	1.50–12.00	[261]
Poplar	Pyrolysis	13.72	1.85	[262]
Magnetic Activated Carbon				
Pomace leaves/plastic waste	Pyrolysis	7.17	0.63	[263]
Graphene				
Sawdust, commercial	FJH	68.40	8.88	[264]
Wheat straw, commercial	FJH	32.40	2.73	[264]
Corn straw, commercial	FJH	61.20	8.45	[264]
Rice straw, commercial	FJH	64.80	11.50	[264]
Graphite, commercial	CVD[#]	7,710.00	10^6	[265]
	EE[a]	1,850.00	280.00	[265]
	rGO2C[b]	8.00	81.00	[265]
	rGO2T[c]	11.00	46.00	[265]
Carbon Nanotube				
$C_2H_2/H_2/H_2O/CO_2/C_2H_4$, lab scale	CVD (fluidized bed)	6,550.00	480.00	[266]
	CVD (on substrates)	408,710.00	28,550.00	[266]

[#]Continious; a=electrochemical exfoliation; b=chemical oxidation and subsequent chemical reduction; c=chemical oxidation and subsequent thermal reduction.

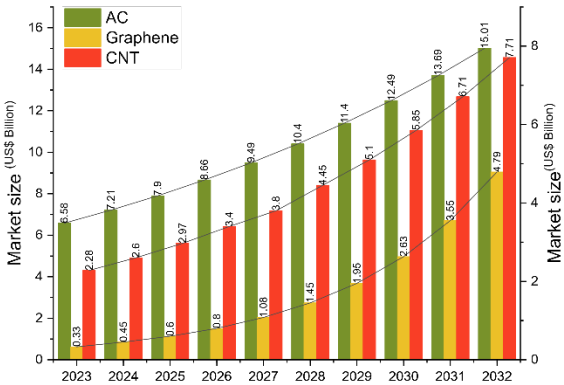

Figure 14: Activated carbon, graphene, and carbon nanotubes market size forecast (2023–2032). Data adapted from [267]–[269].

Comparative analysis between commercially manufactured and biomass-derived pyrolysis derivative product counterparts presents a compelling avenue for advancing sustainability within academic discourse. Initially, directing attention towards sourcing biomass from renewable and locally available reservoirs holds promise for mitigating the ecological footprint associated with transportation logistics while concurrently diminishing reliance on finite resources. Moreover, refining manufacturing protocols to optimize energy efficiency and minimize waste generation stands as a pivotal strategy for mitigating environmental impacts. The integration of carbon capture and utilization technologies within biomass conversion processes emerges as a potent means to augment carbon sequestration capabilities, thereby amplifying the carbon-negative attributes of biomass-based material. Finally, advocacy for transparency and certification schemes to uphold responsible sourcing and production practices carries significant weight in fostering consumer trust and support for biomass-based materials as a viable sustainable alternative to commercially produced counterparts within academic circles.

Between 2023 and 2032, the market sizes for AC, graphene, and CNT show a steady rise, indicating a robust increasing trend in demand (Figure 14). Several economic elements contribute to this ongoing expansion. First and foremost, the need for these cutting-edge materials is being driven by developments in technology and novel applications, especially in energy storage, environmental remediation, and electronics. Energy storage solutions that are efficient are becoming increasingly important due to the growing use of electric cars and renewable energy sources, such as graphene and CNTs. In addition, increased environmental concerns brought about by global industrialization and urbanization drive the need for sophisticated filtration and adsorption technologies, which raises the need for AC.

According to the supply-demand law, economies of scale and improvements in production technology should lead to a gradual decline in the price of graphene over time [270], making it more widely available and reasonably priced for a range of applications. Positive feedback loops are created when manufacturing costs decrease, leading to a rise in supply and a subsequent increase in demand due to decreased pricing. This pattern matches the graphene market's observed growth, indicating that the use of the technology will increase as it develops and becomes more affordable. Strategic government initiatives and funding for nanotechnology research also support the growth of this material's market. Therefore, the strong market development predicted by the graph is supported by the interaction of economic scalability, technical advancement, and strategic policy assistance.

Activated carbon, graphene, carbon nanotubes, biochar, and other carbon-based compounds sourced from diverse countries are all included in Table 11 along with a thorough unit pricing. Because biochar is produced by pyrolyzing organic matter, its price varies a great deal depending on the area and kind of feedstock. In the United States, for instance, pinewood biochar from Missouri costs $0.9 per kilogram, whereas bamboo biochar from Alabama costs $7. The costliest biochar is notably virgin wood from Massachusetts, USA, which costs $17.8 per kilogram. This shows how the cost of processing and the availability of raw materials affect the price of biochar.

Due to its adsorption qualities, activated carbon is valued differently depending on the source material and the processing techniques used. Commercial varieties, including Filtrasorb–400 from Pennsylvania, cost $20 to $22 per kilogram, while activated carbon from Idaho, USA, is available for $2 per kilogram, which is a far lower price. It is made from corn, manure, and forestry debris. Whereas other types, such as bamboo and coal-derived granules and pellets, range in price from $0.6 to $1.95 per kilogram, granular coconut-derived activated carbon from Illinois, USA, costs $9.2 per kilogram. These variations demonstrate how economically viable various sources of activated carbon and their production processes are.

Table 11: Comparative of pyrolyzed biomass-derived products unit prices

Material	Origin	US$/kg	Ref.
Biochar			
Bamboo	Alabama, USA	7	[255]
Corn debris, manure, and forestry debris	Idaho, USA	1.5	
Hardwood	Australia	2.3	
Pinewood	Missouri, USA	0.9	
Pinewood – organic conifer biomass	Oregon, USA	8.3	
Softwood chips	California, USA	3.5	
Tree branches	Kansas, USA	11	
Virgin wood	Massachusetts, USA	17.8	
Activated Carbon			
Commercial type Filtrasorb–400	Pennsylvania, USA	20–22	[255]
Corn debris, manure, and forestry debris	Idaho, USA	2	
Granular, Coconut	Illinois, USA	9.2	
Powder, Coconut	Henan, China	0.87–1.13	[271]
Granule, Bamboo		0.6–1.5	
Pellet, Coal		0.95–1.95	
Bulk, Wood	Henan, China	0.9–1.2	[272]
Granule, Palm kernel shell		0.86–1.58	
Graphene (CVD)			
Monolayer graphene film (1in^2, on Si-SiO_2)	Vermont, USA	299*	[273]
Bilayer graphene film (1cm^2, on Si-SiO_2)		606*	
Trilayer graphene film (1cm^2, on Si-SiO_2)		857*	
Carbon Nanotube			
Masterbatches	Vermont, USA	85–95	[273]
OH Functionalized SW-DWCNT (1-2 nm)		77.8–130	
COOH Functionalized SW-DWCNT (1-4 nm)		77.8–125	
MWCNT (8-15 nm)		0.9–15	
MWCNT (10-20 nm)		0.9–15	
MWCNT (20-30 nm)		0.7–10	
MWCNT (30-50 nm)		0.7–10	

* Price per unit area

Since they need advanced technology to produce and have remarkable mechanical and electrical qualities, advanced materials like graphene and carbon nanotubes are substantially more expensive. More sophisticated bilayer and trilayer graphene films cost \$606 and \$857 per cm^2, respectively, whereas monolayer graphene film costs \$299 per cm^2 in Vermont, USA. Depending on their size and functionalization, carbon nanotubes can range in price from \$0.7 to \$130 per kilogram. For example, depending on their diameter, OH-functionalized single-walled carbon nanotubes (SW-DWCNT) range in price from \$77.8 to \$130 per kilogram, whereas multi-walled carbon nanotubes (MWCNT) cost between \$0.7 and \$15 per kilogram. Because of their substantial benefits for a range of high-tech applications and their sophisticated manufacturing methods, graphene and carbon nanotubes are expensive materials.

9 Conclusions

Biomass, as a renewable source, shows promise in generating valuable materials such as AC, MAC, graphene, and CNTs via catalytic and non-catalytic pyrolysis. Commonly, biomass pyrolysis generates 3 types of products, biochar, bio-oil, and gas. These derivatives have wide applications to several downstream, including serving as adsorbents, catalysts, composite materials, electronic devices, reactor coatings, dyes, energy storage, sensors, fuel cells and many more through certain processes. The pyrolysis process is influenced by several factors, including the type of raw material, operating conditions, catalyst selection, and the specific pyrolysis method employed. Lignocellulosic materials, in particular, exhibit unique characteristics that result in varying product distributions under specific conditions. Four widely applied pyrolysis methods each have distinct objectives in optimizing product yields. Additionally, the use of catalysts can selectively enhance the production of desired compounds, further tailoring the output to meet

specific goals. The results highlight the potential of pyrolysis technology to efficiently convert biomass into valuable carbon-based products. The AC and MAC can be synthesized from pyrolyzed biochar following certain activation process, while graphene and carbon nanotubes (CNTs) can be produced either from the hydrocarbon fraction of pyrolyzed biomass (bottom-up procedure) or through *in situ* exfoliation and oxidation-reduction reactions of graphite (top-down procedure). AC, known for its high surface area and porous structure, is widely used for adsorption applications due to its ability to effectively capture a variety of contaminants. MAC further enhances this by demonstrating selective adsorption of metals from liquid mediums, aided by an external magnetic field for easy extraction. Additionally, several techniques exist for developing composites reinforced with CNTs and graphene, allowing for customization according to the specific properties required for the final application.

The development of sustainable opportunities for biomass-based graphene and CNT synthesis is a crucial area of focus. These environmentally friendly products have potential applications across various sectors, supporting sustainability goals. CNT exhibited the highest emission on climate change, up to 28,550 kg CO_2eq/kg because it requires such a big of energy for heating purposes. Compared to biochar, it can stabilize carbon that would otherwise be released into the atmosphere (carbon sequestration) up to –864 kg CO_2eq/kg although it also needs the energy for heating purposes that reach up to 4.12 MJ/kg. Currently, graphene is the most expensive material up to US\$857/cm^2 for commercial because of its great properties in several applications. Optimization of production processes, integration of carbon capture technologies, and promotion of transparent certification schemes can further enhance the role of biomass-derived activated carbon in mitigating environmental impacts and advancing sustainability objectives in academic and industrial domains. Further research and development efforts are necessary to improve its properties and market competitiveness.

Acknowledgments

Financial backing for this project was provided through Domestic Cooperation Grants from the Ministry of Education, Culture, Research, and Technology in Indonesia, under the reference numbers 160/E5/PG.02.00.PL/2023 and 1280.1/UN27.22/PT. 01.03/2023.

Author Contribution

J.K.: conceptualization, funding acquisition, supervision; I.P.: formal analysis, resources, visualization, writing—original draft; Z.L.: investigation, methodology, project administration, resources; M.M.: investigation, methodology, resources; E.K.: data curation, writing—review and editing; M.Y.: data curation, writing—review and editing; D.H.: data curation, writing—review and editing. All authors have read and agreed to the published version of the manuscript.

Conflicts of Interest

The authors declare that they have no known competing financial interests or personal relationships that could have appeared to influence the work reported in this study.

References

[1] N. Rouhi, A. Akhgari, N. Orouji, A. Nezami, M. Rahimzadegan, and H. Kamali, "Recent progress in the graphene-based biosensing approaches for the detection of Alzheimer's biomarkers," *Journal of Pharmaceutical and Biomedical Analysis*, vol. 222, Jan. 2023, Art. no. 115084.

[2] S. Legino, R. Hidayawanti, and I. Wirantika, "Waste as fastest cycle of renewable energy sources through TOSS Model," *Journal of Physics: Conference Series*, vol. 1282, no. 1, Jul. 2019, Art. no. 012041.

[3] K. Ridhuan, D. Irawan, and R. Setiawan, "Comparison of Types and Size of Biomass on Pirolysis Combustion Toward the Results of Bio-Charcoal and Liquid Smoke," *Journal of Engineering and Scientific Research*, vol. 2, no. 1, pp. 10–15, Dec. 2020.

[4] E. Singh, A. Kumar, R. Mishra, S. You, L. Singh, S. Kumar, and R. Kumar, "Pyrolysis of waste biomass and plastics for production of biochar and its use for removal of heavy metals from aqueous solution," *Bioresource Technology*, vol. 320, Jan. 2021, Art. no. 124278.

[5] C. Gopu, L. Gao, M. Volpe, L. Fiori, and J. L. Goldfarb, "Valorizing municipal solid waste: Waste to energy and activated carbons for water treatment via pyrolysis," *Journal of Analytical and Applied Pyrolysis*, vol. 133, pp. 48–58, Aug. 2018.

[6] J. S. Lu, Y. Chang, C. S. Poon, and D. J. Lee, "Slow pyrolysis of municipal solid waste (MSW): A review," *Bioresource Technology*, vol. 312, Sep. 2020, Art. no. 123615.

[7] P. Das, C. V.P., T. Mathimani, and A. Pugazhendhi, "Recent advances in thermochemical methods for the conversion of algal biomass to energy," *Science of The Total Environment*, vol. 766, Apr. 2021, Art. no. 144608.

[8] Y. Uemura, "Gasification/pyrolysis/torrefaction," in *A-Z of Biorefinery: A Comprehensive View*. Amsterdam, Netherlands: Elsevier, pp. 389–419, Jan. 2022.

[9] L. Matsakas, Q. Gao, S. Jansson, U. Rova, and P. Christakopoulos, "Green conversion of municipal solid wastes into fuels and chemicals," *Electronic Journal of Biotechnology*, vol. 26, pp. 69–83, Mar. 2017.

[10] S. Wang, S. Wang, T. Song, S. Yin, E. U. Hartge, T. Dymala, L. Shen, S. Heinrich, and J. Werther, "Syngas, tar and char behavior in chemical looping gasification of sawdust pellet in fluidized bed," *Fuel*, vol. 270, Jun. 2020, Art. no. 117464.

[11] M. R. Zakaria, M. A. Ahmad Farid, Y. Andou, I. Ramli, and M. A. Hassan, "Production of biochar and activated carbon from oil palm biomass: Current status, prospects, and challenges," *Industrial Crops and Products*, vol. 199, Sep. 2023, Art. no. 116767.

[12] J. González-Arias, X. Gómez, M. González-Castaño, M. E. Sánchez, J. G. Rosas, and J. Cara-Jiménez, "Insights into the product quality and energy requirements for solid biofuel production: A comparison of hydrothermal carbonization, pyrolysis and torrefaction of olive tree pruning," *Energy*, vol. 238, Jan. 2022, Art. no. 122022.

[13] B. Charmas, B. Wawrzaszek, and K. Jedynak, "Effect of pyrolysis temperature and hydrothermal activation on structure, physicochemical, thermal and dye adsorption characteristics of the biocarbons," *ChemPhysChem*, vol. 25, no. 4, Feb. 2024, Art. no. e202300773.

[14] D. Aboelela, H. Saleh, A. M. Attia, Y. Elhenawy, T. Majozi, and M. Bassyouni, "Recent advances in biomass pyrolysis processes for bioenergy production: Optimization of operating conditions," *Sustainability*, vol. 15, no. 14, Jul. 2023, Art. no. 11238.

[15] A. A. Bianasari, M. S. Khaled, T. D. Hoang, M. S. Reza, M. S. A. Bakar, and A. K. Azad, "Influence of combined catalysts on the catalytic pyrolysis process of biomass: A systematic literature review," *Energy Conversion and Management*, vol. 309, Jun. 2024, Art. no. 118437.

[16] M. Tawalbeh, A. Al-Othman, T. Salamah, M. Alkasrawi, R. Martis, and Z. A. El-Rub, "A critical review on metal-based catalysts used in the pyrolysis of lignocellulosic biomass materials," *Journal of Environmental Management*, vol. 299, Dec. 2021, Art. no. 113597.

[17] F. Mo, H. Ullah, N. Zada, and A. Shahab, "A review on catalytic co-pyrolysis of biomass and plastics waste as a thermochemical conversion to produce valuable products," *Energies*, vol. 16, no. 14, Jul. 2023, Art. no. 5403.

[18] M. S. Reza, S. Afroze, K. Kuterbekov, A. Kabyshev, K. Zh. Bekmyrza, J. Taweekun, F. Ja'afar, M. Saifullah Abu Bakar, A. K. Azad, H. Roy, and M. S. Islam, "Ex situ catalytic pyrolysis of invasive pennisetum purpureum grass with activated carbon for upgrading bio-oil," *Sustainability*, vol. 15, no. 9, May 2023, Art. no. 7628.

[19] N. A. Rashidi and S. Yusup, "Potential of palm kernel shell as activated carbon precursors through single stage activation technique for carbon dioxide adsorption," *Journal of Cleaner Production*, vol. 168, pp. 474–486, Dec. 2017.

[20] J. E. Omoriyekomwan, A. Tahmasebi, J. Zhang, and J. Yu, "Mechanistic study on direct synthesis of carbon nanotubes from cellulose by means of microwave pyrolysis," *Energy Conversion and Management*, vol. 192, pp. 88–99, Jul. 2019.

[21] P. P. D. K. Wulan, J. O. D. Sidauruk, and J. A. Ningtyas, "The effect of pyrolysis temperature and time of polypropylene on quality of carbon nanotube with flame synthesis method," *E3S Web of Conferences*, vol. 67, Nov. 2018, Art. no. 03030.

[22] J. E. Omoriyekomwan, A. Tahmasebi, J. Dou, R. Wang, and J. Yu, "A review on the recent advances in the production of carbon nanotubes and carbon nanofibers via microwave-assisted pyrolysis of biomass," *Fuel Processing Technology*, vol. 214, Apr. 2021, Art. no. 106686.

[23] B. Zhang, G. Piao, J. Zhang, C. Bu, H. Xie, B. Wu, and N. Kobayashi, "Synthesis of carbon nanotubes from conventional biomass-based gasification gas," *Fuel Processing Technology*, vol. 180, pp. 105–113, Nov. 2018.

[24] D. Ouyang, L. Hu, G. Wang, B. Dai, F. Yu, and L. Zhang, "A review of biomass-derived graphene and graphene-like carbons for electrochemical

energy storage and conversion," *New Carbon Materials*, vol. 36, no. 2, pp. 350–372, Apr. 2021.

[25] I. F. Sukmana, P. Widiatmoko, I. Nurdin, Devianto, and T. Prakoso, "Effect of $ZnCl_2$ on properties of graphene produced from palm empty fruit bunch," *IOP Conference Series: Materials Science and Engineering*, vol. 778, no. 1, Apr. 2020, Art. no. 012011.

[26] M. Trandafir, M. Florea, F. Neaţu, A. Primo, V. I. Parvulescu, and H. García, "Graphene from alginate pyrolysis as a metal-free catalyst for hydrogenation of nitro compounds," *ChemSusChem*, vol. 9, no. 13, pp. 1565–1569, Jul. 2016.

[27] D. Mondal, M. Sharma, C.-H. Wang, Y.-C. Lin, H.-C. Huang, A. Saha, S. K. Nataraj, and K. Prasad, "Deep eutectic solvent promoted one step sustainable conversion of fresh seaweed biomass to functionalized graphene as a potential electrocatalyst," *Green Chemistry*, vol. 18, no. 9, pp. 2819–2826, 2016.

[28] D. Li, X. Duan, H. Sun, J. Kang, H. Zhang, M. O. Tade, and S. Wang, "Facile synthesis of nitrogen-doped graphene via low-temperature pyrolysis: The effects of precursors and annealing ambience on metal-free catalytic oxidation," *Carbon*, vol. 115, pp. 649–658, May 2017.

[29] R. K. Rathour, M. Devi, P. Dahiya, N. Sharma, N. Kaushik, D. Kumari, P. Kumar, R. R. Baadhe, A. Walia, A. K. Bhatt, and R. K. Bhatia, "Recent trends, opportunities and challenges in sustainable management of rice straw waste biomass for green biorefinery," *Energies*, vol. 16, no. 3, Feb. 2023, Art. no. 1429.

[30] P. Khongphakdi, A. Palamanit, N. Phusunti, Y. Tirawanichakul, and P. Shrivastava, "Evaluation of oil palm biomass potential for bio-oil production via pyrolysis processes," *International Journal of Integrated Engineering*, vol. 12, no. 2, pp. 226–233, 2020.

[31] J. Wei, Q. Guo, L. Ding, Y. Gong, J. Yu, and G. Yu, "Understanding the effect of different biomass ash additions on pyrolysis product distribution, char physicochemical characteristics, and char gasification reactivity of bituminous coal," *Energy and Fuels*, vol. 33, no. 4, pp. 3068–3076, Apr. 2019.

[32] M. Buffi, A. M. Rizzo, L. Pari, and D. Chiaramonti, "Intermediate pyrolysis campaign to assess products yield and quality varying biomass particle size, temperatures and composition," *International Journal of Oil, Gas and Coal Technology*, vol. 17, no. 3, Mar. 2018, Art. no. 355.

[33] F. Abnisa, A. Arami-Niya, W. M. A. W. Daud, and J. N. Sahu, "Characterization of bio-oil and bio-char from pyrolysis of palm oil wastes," *BioEnergy Research*, vol. 6, no. 2, pp. 830–840, Jun. 2013.

[34] A. İşçen, K. Öznacar, K. M. M. Tunç, and M. E. Günay, "Exploring the critical factors of biomass pyrolysis for sustainable fuel production by machine learning," *Sustainability*, vol. 15, no. 20, Oct. 2023, Art. no. 14884.

[35] W. Wang, Y. Gu, C. Zhou, and C. Hu, "Current challenges and perspectives for the catalytic pyrolysis of lignocellulosic biomass to high-value products," *Catalyst*, vol. 12, no. 12, Dec. 2022, Art. no. 1524.

[36] Z. Chaula, G. John, M. Said, S. Manyele, and C. Mhilu, "Non-Isothermal Degradation and Thermodynamic Properties of Pine Sawdust," *Smart Grid and Renewable Energy*, vol. 9, no. 12, pp. 272–284, Dec. 2018.

[37] X. Gu, X. Ma, L. Li, C. Liu, K. Cheng, and Z. Li, "Pyrolysis of poplar wood sawdust by TG-FTIR and Py-GC/MS," *Journal of Analytical and Applied Pyrolysis*, vol. 102, pp. 16–23, Jul. 2013.

[38] T. Sun, L. Zhang, Y. Yang, Y. Li, S. Ren, L. Dong, and T. Lei, "Fast pyrolysis of cellulose and the effect of a catalyst on product distribution," *International Journal of Environmental Research and Public Health*, vol. 19, no. 24, Dec. 2022, Art. no. 16788.

[39] X. Zhou, W. Li, R. Mabon, and L. J. Broadbelt, "A critical review on hemicellulose pyrolysis," *Energy Technology*, vol. 5, no. 1, pp. 52–79, Jan. 2017.

[40] E. Leng, Y. Guo, J. Chen, S. Liu, J. E, and Y. Xue, "A comprehensive review on lignin pyrolysis: Mechanism, modeling and the effects of inherent metals in biomass," *Fuel*, vol 309, Feb. 2022, Art. no. 122102.

[41] F.-X. Collard and J. Blin, "A review on pyrolysis of biomass constituents: Mechanisms and composition of the products obtained from the conversion of cellulose, hemicelluloses and lignin," *Renewable and Sustainable Energy Reviews*, vol. 38, pp. 594–608, Oct. 2014.

[42] A. Funke, M. Tomasi Morgano, N. Dahmen, and H. Leibold, "Experimental comparison of two bench scale units for fast and intermediate pyrolysis," *Journal of Analytical and Applied Pyrolysis*, vol. 124, pp. 504–514, Mar. 2017.

[43] N. H. Nam, V. N. Linh, L. D. Dung, and V. T. T. Ha, "Physico-chemical characterization of forest and agricultural residues for energy conversion processes," *Vietnam Journal of Chemistry*, vol. 58, no. 6, pp. 735–741, Dec. 2020.

[44] A. Karimah, I. K. Hani, R. P. B. Laksana, M. Ismayati, N. N. Solihat, F. P. Sari, I. Budiman, M. Ghozali, O. Farobie, D. S. Nawawi, M. A. R. Lubis, M. H. Hussin, T. Watanabe, and W. Fatriasari, "Extraction of lignin from sugarcane trash and its potency as biosurfactant," *Bioresource Technology Reports*, vol. 24, Dec. 2023, Art. no. 105540.

[45] G. Tiwari, A. Sharma, A. Kumar, and S. Sharma, "Assessment of microwave-assisted alkali pretreatment for the production of sugars from banana fruit peel waste," *Biofuels*, vol. 10, no. 1, pp. 3–10, Jan. 2019.

[46] S. Aninda Dhar, T. Us Sakib, and L. Naher Hilary, "Effects of pyrolysis temperature on production and physicochemical characterization of biochar derived from coconut fiber biomass through slow pyrolysis process," *Biomass Conversion and Biorefinery*, vol. 12, pp. 2631–2647, Jul. 2022.

[47] N. H. Jabarullah, A. S. Kamal, and R. Othman, "A modification of palm waste lignocellulosic materials into biographite using iron and nickel catalyst," *Processes*, vol. 9, no. 6, Jun. 2021, Art. no. 1079.

[48] L. N. Megashah, H. Ariffin, M. R. Zakaria, and Y. Ando, "Characteristics of cellulose from oil palm mesocarp fibres extracted by multi-step pretreatment methods," in *IOP Conference Series: Materials Science and Engineering*, vol. 368, Jun. 2018, Art. no. 012001.

[49] M. Muryanto, Y. Sudiyani, M. A. Darmawan, E. M. Handayani, and M. Gozan, "Simultaneous delignification and furfural production of palm oil empty fruit bunch by novel ternary deep eutectic solvent," *Arabian Journal for Science and Engineering*, vol. 48, pp. 16359–16371. Dec. 2023.

[50] S. Kumar, K. Paritosh, N. Pareek, A. Chawade, and V. Vivekanand, "De-construction of major Indian cereal crop residues through chemical pretreatment for improved biogas production: An overview," *Renewable and Sustainable Energy Reviews*, vol. 90, pp. 160–170, Jul. 2018.

[51] H. V. Lee, S. B. A. Hamid, and S. K. Zain, "Conversion of lignocellulosic biomass to nanocellulose: Structure and chemical process," *The Scientific World Journal*, vol. 2014, Aug. 2014, Art. no. 631013.

[52] S. L. Lo, Y. F. Huang, P. Te Chiueh, and W. H. Kuan, "Microwave pyrolysis of lignocellulosic biomass," *Energy Procedia*, vol.107, pp. 41–46, May 2017.

[53] A. S. Hozman-Manrique, A. J. Garcia-Brand, M. Hernández-Carrión, and A. Porras, "Isolation and characterization of cellulose microfibers from colombian cocoa pod husk via chemical treatment with pressure effects," *Polymers*, vol. 15, no. 3, Feb. 2023, Art. no. 0664.

[54] M. Stöcker, "Perspectives for thermochemical conversions of lignocellulosic biomass," *Small*, vol. 20, Sep. 2023, Art. no. 2302495.

[55] D. Czajczyńska, L. Anguilano, H. Ghazal, R. Krzyżyńska, A. J. Reynolds, N. Spencer, and H. Jouhara, "Potential of pyrolysis processes in the waste management sector," *Thermal Science and Engineering Progress*, vol. 3, pp. 171–197, Sep. 2017.

[56] H. Durak, "Comprehensive assessment of thermochemical processes for sustainable waste management and resource recovery," *Processes*, vol. 11, no. 7. Jul. 2023, Art. no. 2092.

[57] T. Kan, V. Strezov, and T. J. Evans, "Lignocellulosic biomass pyrolysis: A review of product properties and effects of pyrolysis parameters," *Renewable and Sustainable Energy Reviews*, vol. 57, pp. 1126–1140, May 2016.

[58] D. Aboelela, H. Saleh, A. M. Attia, Y. Elhenawy, T. Majozi, and M. Bassyouni, "Recent advances in biomass pyrolysis processes for bioenergy production: Optimization of operating conditions," *Sustainability*, vol. 15, no. 14, Jul. 2023, Art. no. 11238.

[59] J. Wakatuntu, P. W. Olupot, J. Jjagwe, E. Menya, and M. Okure, "Optimization of pyrolysis conditions for production of rice husk-based bio-oil as an energy carrier," *Results in Engineering*, vol. 17, Mar. 2023, Art. no. 100947.

[60] T. Steiner, K. Schulze, R. Scharler, and A. Anca-Couce, "Extension of the layer particle model for volumetric conversion reactions during char gasification," *Combustion and Flame*, vol. 256, Oct. 2023, Art. no. 112940.

[61] R. Junga, J. Pospolita, and P. Niemiec, "Combustion and grindability characteristics of palm kernel shells torrefied in a pilot-scale installation," *Renewable Energy*, vol. 147, pp. 1239–1250, Mar. 2020.

[62] A. V. Bridgwater, "Review of fast pyrolysis of biomass and product upgrading," *Biomass and Bioenergy*, vol. 38, pp. 68–94, Mar. 2012.

[63] İ. Demiral and S. Şensöz, "Fixed-bed pyrolysis of Hazelnut (*Corylus Avellana L.*) bagasse: Influence of pyrolysis parameters on product yields," *Energy Sources, Part A: Recovery, Utilization, and Environmental Effects*, vol. 28, no. 12, pp. 1149–1158, Sep. 2006.

[64] A. Dewangan, D. Pradhan, and R. K. Singh, "Co-pyrolysis of sugarcane bagasse and low-density polyethylene: Influence of plastic on pyrolysis product yield," *Fuel*, vol. 185, pp. 508–516, Dec. 2016.

[65] X. J. Lee, L. Y. Lee, B. Y. Z. Hiew, S. Gan, S. Thangalazhy-Gopakumar, and H. K. Ng, "Valorisation of oil palm wastes into high yield and energy content biochars via slow pyrolysis: Multivariate process optimisation and combustion kinetic studies," *Materials Science for Energy Technologies*, vol. 3, pp. 601–610, Jul. 2020.

[66] M. Tripathi, J. N. Sahu, and P. Ganesan, "Effect of process parameters on production of biochar from biomass waste through pyrolysis: A review," *Renewable and Sustainable Energy Reviews*, vol. 55, pp. 467–481, Mar. 2016.

[67] J. Waluyo, I. G. B. N. Makertihartha, and H. Susanto, "Pyrolysis with intermediate heating rate of palm kernel shells: Effect temperature and catalyst on product distribution," *AIP Conference Proceedings*, vol. 1977, Jun. 2018, Art. no. 020026.

[68] Y. Zhang, Z. Ma, Q. Zhang, J. Wang, Q. Ma, Y. Yang, X. Luo, and W. Zhang, "Comparison of the physicochemical characteristics of bio-char pyrolyzed from moso bamboo and rice husk with different pyrolysis temperatures," *BioResources*, vol. 12, no. 3, May 2017.

[69] P. R. Bhoi, A. S. Ouedraogo, V. Soloiu, and R. Quirino, "Recent advances on catalysts for improving hydrocarbon compounds in bio-oil of biomass catalytic pyrolysis," *Renewable and Sustainable Energy Reviews*, vol. 121, Apr. 2020, Art. no. 109676.

[70] A. Sattar, G. A. Leeke, A. Hornung, and J. Wood, "Steam gasification of rapeseed, wood, sewage sludge and miscanthus biochars for the production of a hydrogen-rich syngas," *Biomass and Bioenergy*, vol. 69, pp. 276–286, Oct. 2014.

[71] Z. Ma, Y. Yang, Q. Ma, H. Zhou, X. Luo, X. Liu, S. Wang, "Evolution of the chemical composition, functional group, pore structure and crystallographic structure of bio-char from palm kernel shell pyrolysis under different temperatures," *Journal of Analytical and Applied Pyrolysis*, vol. 127, pp. 350–359, Sep. 2017.

[72] T. Bridgwater, "Challenges and opportunities in fast pyrolysis of biomass: Part II," *Johnson Matthey Technology Review*, vol. 62, no. 2, pp. 150–160, Apr. 2018.

[73] F. Tinwala, P. Mohanty, S. Parmar, A. Patel, and K. K. Pant, "Intermediate pyrolysis of agro-industrial biomasses in bench-scale pyrolyser: Product yields and its characterization," *Bioresource Technology*, vol. 188, pp. 258–264, Jul. 2015.

[74] L. Hu, X. Y. Wei, X. H. Guo, H. P. Lv, and G. H. Wang, "Investigation on the kinetic behavior, thermodynamic and volatile products analysis of chili straw waste pyrolysis," *Journal of Environmental Chemical Engineering*, vol. 9, no. 5, Oct. 2021, Art. no. 105859.

[75] T. Imam and S. Capareda, "Characterization of bio-oil, syn-gas and bio-char from switchgrass pyrolysis at various temperatures," *Journal of Analytical and Applied Pyrolysis*, vol. 93, pp. 170–177, Jan. 2012.

[76] L. E. Hernandez-Mena, A. A. B. Pécora, and A. L. Beraldo, "Slow pyrolysis of bamboo biomass: Analysis of biochar properties," *Chemical Engineering Transactions*, vol. 37, pp. 115–120, May 2014.

[77] D. Chen, Y. Li, K. Cen, M. Luo, H. Li, and B. Lu, "Pyrolysis polygeneration of poplar wood: Effect of heating rate and pyrolysis temperature," *Bioresource Technology*, vol. 218, pp. 780–788, Oct. 2016.

[78] P. Roy and G. Dias, "Prospects for pyrolysis technologies in the bioenergy sector: A review," *Renewable and Sustainable Energy Reviews*, vol. 77, pp. 59–69, Sep. 2017.

[79] A. S. Nugraha, Setiadi, and T. S. Utami, "The Effect of pyrolysis conditions to produce levoglucosan from rice straw," *E3S Web of Conferences*, vol. 67, Nov. 2018, Art. no. 03026.

[80] C. E. Efika, J. A. Onwudili, and P. T. Williams, "Influence of heating rates on the products of high-temperature pyrolysis of waste wood pellets and biomass model compounds," *Waste Management*, vol. 76, pp. 497–506, Jun. 2018.

[81] S. A. Arni, "Comparison of slow and fast pyrolysis for converting biomass into fuel," *Renewable Energy*, vol. 124, pp. 197–201, Aug. 2018.

[82] C. T. Primaz, A. Ribes-Greus, and R. A. Jacques, "Valorization of cotton residues for production of bio-oil and engineered biochar," *Energy*, vol. 235, Nov. 2021, Art. no. 121363.

[83] W. Jerzak, M. Reinmöller, and A. Magdziarz, "Estimation of the heat required for intermediate pyrolysis of biomass," *Clean Technologies and Environmental Policy*, vol. 24, no. 10, pp. 3061–3075, Dec. 2022.

[84] I. D. V. Torri, V. Paasikallio, C. S. Faccini, R. Huff, E. B. Caramão, V. Sacon, A. Oasmaa, and C. A. Zini, "Bio-oil production of softwood and hardwood forest industry residues through fast and intermediate pyrolysis and its chromatographic characterization," *Bioresource Technology*, vol. 200, pp. 680–690, Jan. 2016.

[85] M. Pahnila, A. Koskela, P. Sulasalmi, and T. Fabritius, "A review of pyrolysis technologies and the effect of process parameters on biocarbon properties," *Energies*, vol. 16, no. 19, Oct. 2023, Art. no. 6936.

[86] T. Y. A. Fahmy, Y. Fahmy, F. Mobarak, M. El-Sakhawy, and R. E. Abou-Zeid, "Biomass pyrolysis: past, present, and future," *Environment, Development and Sustainability*, vol. 22, no. 1, pp. 17–32, Jan. 2020.

[87] S. Nanda, J. Mohammad, S. N. Reddy, J. A. Kozinski, and A. K. Dalai, "Pathways of lignocellulosic biomass conversion to renewable fuels," *Biomass Conversion and Biorefinery*, vol. 4, no. 2, pp. 157–191, Sep. 2014.

[88] K. Maliutina, A. Tahmasebi, J. Yu, and S. N. Saltykov, "Comparative study on flash pyrolysis characteristics of microalgal and lignocellulosic biomass in entrained-flow reactor," *Energy Conversion and Management*, vol. 151, pp. 426–438, Nov. 2017.

[89] R. Pardo, L. Taboada-Ruiz, E. Fuente, B. Ruiz, M. Díaz-Somoano, L. F. Calvo, and S. Paniagua, "Exploring the potential of conventional and flash pyrolysis methods for the valorisation of grape seed and chestnut shell biomass from agri-food industry waste," *Biomass and Bioenergy*, vol. 177, Oct. 2023, Art. no. 106942.

[90] T. Sun, Z. Chen, R. Wang, Y. Yang, L. Zhang, Y. Li, P. Liu, and T. Lei, "Influences of the reaction temperature and catalysts on the pyrolysis product distribution of lignocellulosic biomass (Aspen wood and rice husk)," *Polymers*, vol. 15, no. 14, Jul. 2023, Art. no. 3104.

[91] Y. Zhang, H. Lei, Z. Yang, D. Duan, E. Villota, and R. Ruan, "From glucose-based carbohydrates to phenol-rich bio-oils integrated with syngas production via catalytic pyrolysis over an activated carbon catalyst," *Green Chemistry*, vol. 20, no. 14, pp. 3346–3358, Jul. 2018.

[92] Q. Bu, H. Lei, L. Wang, Y. Wei, L. Zhu, Y. Liu, J. Liang, J. Tang, "Renewable phenols production by catalytic microwave pyrolysis of Douglas fir sawdust pellets with activated carbon catalysts," *Bioresource Technology*, vol. 142, pp. 546–552, Aug. 2013.

[93] Q. Bu, H. Lei, L. Wang, G. Yadavalli, Y. Wei, X. Zhang, L. Zhu, and Y. Liu, "Biofuel production from catalytic microwave pyrolysis of Douglas fir pellets over ferrum-modified activated carbon catalyst," *Journal of Analytical and Applied Pyrolysis*, vol. 112, pp. 74–79, Mar. 2015.

[94] D. Duan, Y. Zhang, H. Lei, E. Villota, and R. Ruan, "Renewable jet-fuel range hydrocarbons production from co-pyrolysis of lignin and soapstock with the activated carbon catalyst," *Waste Management*, vol. 88, pp. 1–9, Apr. 2019.

[95] S. Eibner, F. Broust, J. Blin, and A. Julbe, "Catalytic effect of metal nitrate salts during pyrolysis of impregnated biomass," *Journal of Analytical and Applied Pyrolysis*, vol. 113, pp. 143–152, May 2015.

[96] S. Liu, J. Zhu, M. Chen, W. Xin, Z. Yang, and L. Kong, "Hydrogen production via catalytic pyrolysis of biomass in a two-stage fixed bed reactor system," *International Journal of Hydrogen Energy*, vol. 39, no. 25, pp. 13128–13135, Aug. 2014.

[97] N. A. Fathy, "Carbon nanotubes synthesis using carbonization of pretreated rice straw through chemical vapor deposition of camphor," *RSC Advances*, vol. 7, no. 45, pp. 28535–28541, May 2017.

[98] C. T. Zhang, L. Zhang, Q. Li, Y. Wang, Q. Liu, T. Wei, D. Dong, S. Salavati, M. Gholizadeh, and X. Hu, "Catalytic pyrolysis of poplar wood over transition metal oxides: Correlation of catalytic behaviors with physiochemical properties of the oxides," *Biomass and Bioenergy*, vol. 124, pp. 125–141, May 2019.

[99] J. Zhang, A. Tahmasebi, J. E. Omoriyekomwan, and J. Yu, "Production of carbon nanotubes on bio-char at low temperature via microwave-assisted CVD using Ni catalyst," *Diamond and Related Materials*, vol. 91, pp. 98–106, Jan. 2019.

[100] J. G. Speight, *Upgrading by Hydrocracking*. Amsterdam: Elsevier, 2019.
[101] T. Liu, Y. Li, Y. Zhou, S. Deng, and H. Zhang, "Efficient pyrolysis of low-density polyethylene for regulatable oil and gas products by ZSM-5, HY and MCM-41 catalysts," *Catalysts*, vol. 13, no. 2, Feb. 2023, Art. no. 0382.
[102] D. K. Maharani, Y. Kusumawati, W. N. Safitri, R. E. Nugraha, H. Holilah, N. A. Sholeha, A. A. Jalil, H. Bahruji, and D. Prasetyoko, "Optimization of hierarchical ZSM-5 structure from kaolin as catalysts for biofuel production," *RSC Advances*, vol. 13, no. 21, pp. 14236–14248, May 2023.
[103] Y. Zhang, J. Huang, and P. T. Williams, "Fe-Ni-MCM-41 catalysts for hydrogen-rich syngas production from waste plastics by pyrolysis-catalytic steam reforming," *Energy and Fuels*, vol. 31, no. 8, pp. 8497–8504, Aug. 2017.
[104] Y. Chi, J. Xue, J. Zhuo, D. Zhang, M. Liu, and Q. Yao, "Catalytic co-pyrolysis of cellulose and polypropylene over all-silica mesoporous catalyst MCM-41 and Al-MCM-41," *Science of the Total Environment*, vol. 633, pp. 1105–1113, Aug. 2018.
[105] B. Wei, L. Jin, D. Wang, H. Shi, and H. Hu, "Catalytic upgrading of lignite pyrolysis volatiles over modified HY zeolites," *Fuel*, vol. 259, Jan. 2020, Art. no. 116234.
[106] K. Ding S. Liu, Y. Huang a, S. Liu, N. Zhou, P.Peng, Y. Wang, P. Chen, and R. Ruan, "Catalytic microwave-assisted pyrolysis of plastic waste over NiO and HY for gasoline-range hydrocarbons production," *Energy Conversion and Management*, vol. 196, pp. 1316–1325, Sep. 2019.
[107] S. Zhang, M. Yang, J. Shao, H. Yang, K. Zeng, Y. Chen, J. Luo, F. A. Agblevor, and H. Chen, "The conversion of biomass to light olefins on Fe-modified ZSM-5 catalyst: Effect of pyrolysis parameters," *Science of the Total Environment*, vol. 628–629, pp. 350–357, Jul. 2018.
[108] S. L. Wong, N. Ngadi, T. A. T. Abdullah, and I. M. Inuwa, "Conversion of low density polyethylene (LDPE) over ZSM-5 zeolite to liquid fuel," *Fuel*, vol. 192, pp. 71–82, Mar. 2017.
[109] B. Roozbehani, S. A. Sakaki, M. Shishesaz, N. Abdollahkhani, and S. Hamedifar, "Taguchi method approach on catalytic degradation of polyethylene and polypropylene into gasoline," *Clean Technologies and Environmental Policy*, vol. 17, no. 7, pp. 1873–1882, Oct. 2015.
[110] Y. Mo, L. Zhao, Z. Wang, C. L. Chen, G. Y. A. Tan, and J. Y. Wang, "Enhanced styrene recovery from waste polystyrene pyrolysis using response surface methodology coupled with Box–Behnken design," *Waste Management*, vol. 34, no. 4, pp. 763–769, Apr. 2014.
[111] J. P. Chakraborty and D. K. Shrivastava, "Pretreatment of biomass for efficient pyrolysis," in *Bioenergy Research: Integrative Solution for Existing Roadblock*, M. Srivastava, N. Srivastava, and R. Singh, Eds. Singapore: Springer, 2021, pp. 23–36.
[112] Y. Li, B. Xing, Y. Ding, X. Han, and S. Wang, "A critical review of the production and advanced utilization of biochar via selective pyrolysis of lignocellulosic biomass," *Bioresource Technology*, vol. 312, Sep. 2020, Art. no. 123614.
[113] J. A. Menéndez, A. Domínguez, Y. Fernández, and J. J. Pis, "Evidence of self-gasification during the microwave-induced pyrolysis of coffee hulls," *Energy and Fuels*, vol. 21, no. 1, pp. 373–378, Jan. 2007.
[114] W. Chen, S. Shi, J. Zhang, M. Chen, and X. Zhou, "Co-pyrolysis of waste newspaper with high-density polyethylene: Synergistic effect and oil characterization," *Energy Conversion and Management*, vol. 112, pp. 41–48, Mar. 2016.
[115] P. Basu, *Biomass Gasification, Pyrolysis and Torrefaction*, 3rd ed. Amsterdam, Netherlands: Elsevier, 2013.
[116] W. Gu, Y. Wang, Z. Feng, D. Wu, H. Zhang, H. Yuan, Y. Sun, L. Xiu, W. Chen, and W. Zhang, "Long-term effects of biochar application with reduced chemical fertilizer on paddy soil properties and japonica rice production system," *Frontiers in Environmental Science*, vol. 10, Jun. 2022, Art. no. 902752.
[117] Y. Chen, M. Xu, L. Yang, H. Jing, W. Mao, J. Liu, Y. Zou, Y. Wu, H. Zhou, W. Yang, and P. Wu, "A critical review of biochar application for the remediation of greenhouse gas emissions and nutrient loss in rice paddies: Characteristics, mechanisms, and future recommendations," *Agronomy*, vol. 13, no. 3, Mar. 2023, Art. no. 0893.
[118] J. M. Lee, H. C. Jeong, H. S. Gwon, H. S. Lee, H. R. Park, G. S. Kim, D. G. Park, and S. I. Lee, "Effects of biochar on methane emissions and crop yields in east asian paddy fields: A regional scale meta-analysis," *Sustainability*, vol. 15, no. 12, Jun. 2023, Art. no. 9200.

[119] A. N. A. Haque, Md. K. Uddin, M. F. Sulaiman, A. M. Amin, M. Hossain, Z. M. Solaiman, and M. Mosharrof, "Rice growth performance, nutrient use efficiency and changes in soil properties influenced by biochar under alternate wetting and drying irrigation," *Sustainability*, vol. 14, no. 13, Jun. 2022, Art. no. 7977.

[120] A. N. A. Haque Md. K. Uddin, M. F. Sulaiman, A. M. Amin, M. Hossain, Z. M. Solaiman, A. A. Aziz, and M. Mosharrof, "Combined use of biochar with 15Nitrogen labelled urea increases rice yield, N use efficiency and fertilizer N recovery under water-saving irrigation," *Sustainability*, vol. 14, no. 13, Jul. 2022, Art. no. 7622.

[121] Y. Zhao, X. Wang, G. Yao, Z. Lin, L. Xu, Y. Jiang, Z. Jin, S. Shan, and L. Ping, "Advances in the effects of biochar on microbial ecological function in soil and crop quality," *Sustainability*, vol. 14, no. 16, Aug. 2022, Art. no. 10411.

[122] Y. Feng and D. Meier, "Extraction of value-added chemicals from pyrolysis liquids with supercritical carbon dioxide," *Journal of Analytical and Applied Pyrolysis*, vol. 113, pp. 174–185, May 2015.

[123] G. Lyu, S. Wu, and H. Zhang, "Estimation and comparison of bio-oil components from different pyrolysis conditions," *Frontiers in Energy Research*, vol. 3, Jun. 2015, Art. no. 00028.

[124] T. Aysu, H. Durak, S. Güner, A. Ş. Bengü, and N. Esim, "Bio-oil production via catalytic pyrolysis of *Anchusa azurea*: Effects of operating conditions on product yields and chromatographic characterization," *Bioresource Technology*, vol. 205, pp. 7–14, Apr. 2016.

[125] X. Hu and M. Gholizadeh, "Biomass pyrolysis: A review of the process development and challenges from initial researches up to the commercialisation stage," *Journal of Energy Chemistry*, vol. 39, pp. 109–143, Dec. 2019.

[126] X. Hu and M. Gholizadeh, "Progress of the applications of bio-oil," *Renewable and Sustainable Energy Reviews*, vol. 134, Dec. 2020, Art. no. 110124.

[127] T. Tzanetakis, S. Moloodi, N. Farra, B. Nguyen, A. McGrath, and M. J. Thomson, "Comparison of the spray combustion characteristics and emissions of a wood-derived fast pyrolysis liquid-ethanol blend with number 2 and number 4 fuel oils in a pilot-stabilized swirl burner," *Energy and Fuels*, vol. 25, no. 10, pp. 4305–4321, Oct. 2011.

[128] A. Oasmaa, E. Kuoppala, and D. C. Elliott, "Development of the basis for an analytical protocol for feeds and products of bio-oil hydrotreatment," *Energy and Fuels*, vol. 26, no. 4, pp. 2454–2460, Apr. 2012.

[129] S. S. Hou, W. C. Huang, F. M. Rizal, and T. H. Lin, "Co-firing of fast pyrolysis bio-oil and heavy fuel oil in a 300-kWth furnace," *Applied Sciences*, vol. 6, no. 11, Oct. 2016, Art. no. 0326.

[130] A. Zubrik, M. Matik, S. Hredzák, M. Lovás, Z. Danková, M. Kováčová, and J. Briančin, "Preparation of chemically activated carbon from waste biomass by single-stage and two-stage pyrolysis," *Journal of Cleaner Production*, vol. 143, pp. 643–653, Feb. 2017.

[131] B. Yang, Y. Liu, Q. Liang, M. Chen, L. Ma, L. Li, Q. Liu, W. Tu, D. Lan, and Y. Chen, "Evaluation of activated carbon synthesized by one-stage and two-stage co-pyrolysis from sludge and coconut shell," *Ecotoxicology and Environmental Safety*, vol. 170, pp. 722–731, Apr. 2019.

[132] Z. Wang, J. Wu, T. He, and J. Wu, "Corn stalks char from fast pyrolysis as precursor material for preparation of activated carbon in fluidized bed reactor," *Bioresource Technology*, vol. 167, pp. 551–554, Sep. 2014.

[133] A. Taurbekov, A. Abdisattar, M. Atamanov, M. Yeleuov, C. Daulbayev, K. Askaruly, B. Kaidar, Z. Mansurov, J. Castro-Gutierrez, A. Celzard, V. Fierro, and T. Atamanova, "Biomass derived high porous carbon via CO_2 activation for supercapacitor electrodes," *Journal of Composites Science*, vol. 7, no. 10, Oct. 2023, Art. no. 0444.

[134] Md. A. Islam, M. J. Ahmed, W. A. Khanday, M. Asif, and B. H. Hameed, "Mesoporous activated carbon prepared from NaOH activation of rattan (*Lacosperma secundiflorum*) hydrochar for methylene blue removal," *Ecotoxicology and Environmental Safety*, vol. 138, pp. 279–285, Apr. 2017.

[135] Y. Sun, H. Li, G. Li, B. Gao, Q. Yue, and X. Li, "Characterization and ciprofloxacin adsorption properties of activated carbons prepared from biomass wastes by H_3PO_4 activation," *Bioresource Technology*, vol. 217, pp. 239–244, Oct. 2016.

[136] K. Ö. Köse, B. Pişkin, and M. K. Aydınol, "Chemical and structural optimization of $ZnCl_2$ activated carbons via high temperature CO_2 treatment for EDLC applications," *International*

Journal of Hydrogen Energy, vol. 43, no. 40, pp. 18607–18616, Oct. 2018.

[137] R. Rajamani, B. V. Kumar, A. Sujith, and E. Karthick, "Activated carbon production from waste biomass," *International Journal of Engineering and Technology*, vol. 7, no. 3, pp. 345–348, Sep. 2018.

[138] F.-C. Wu, R.-L. Tseng, and C.-C. Hu, "Comparisons of pore properties and adsorption performance of KOH-activated and steam-activated carbons," *Microporous and Mesoporous Materials*, vol. 80, no. 1–3, pp. 95–106, May 2005.

[139] E. Yagmur, Y. Gokce, S. Tekin, N. I. Semerci, and Z. Aktas, "Characteristics and comparison of activated carbons prepared from oleaster (*Elaeagnus angustifolia* L.) fruit using KOH and $ZnCl_2$," *Fuel*, vol. 267, May 2020, Art. no. 117232.

[140] W. Chen, M. Gong, K. Li, M. Xia, Z. Chen, H. Xiao, Y. Fang, Y. Chen, H. Yang, and H. Chen, "Insight into KOH activation mechanism during biomass pyrolysis: Chemical reactions between O-containing groups and KOH," *Applied Energy*, vol. 278, Nov. 2020, Art. no. 115730.

[141] P. Ndagijimana, H. Rong, P. Ndokoye, J. P. Mwizerwa, F. Nkinahamira, S. Luo, D. Guo, and B. Cui, "A review on activated carbon/graphene composite-based materials: Synthesis and applications," *Journal of Cleaner Production*, vol. 417, Sep. 2023, Art. no. 138006.

[142] P. Schumann M. Muschket, D. Dittmann, L. Rabe, T. Reemtsma, M. Jekel, and A. S. Ruhl, "Is adsorption onto activated carbon a feasible drinking water treatment option for persistent and mobile substances?" *Water Research*, vol. 235, May 2023, Art. no. 119861.

[143] S. N. Maximoff, R. Mittal, A. Kaushik, and J. S. Dhau, "Performance evaluation of activated carbon sorbents for indoor air purification during normal and wildfire events," *Chemosphere*, vol. 304, Oct. 2022, Art. no. 135314.

[144] K. S. Anu, K. A. Vishnumurthy, A. Mahesh, and K. Natarajan, "Effect of carbon fiber reinforcement on the mechanical and electromagnetic shielding properties of the Fe_3O_4-carbonaceous/epoxy composites," *Polymers for Advanced Technologies*, vol. 34, no. 9, pp. 2946–2960, Sep. 2023.

[145] S. Allende, Y. Liu, M. A. Zafar, and M. V. Jacob, "Nitrite sensor using activated biochar synthesised by microwave-assisted pyrolysis," *Waste Disposal and Sustainable Energy*, vol. 5, no. 1, pp. 1–11, Mar. 2023.

[146] T. Wang, R. Pan, M. L. Martins, J. Cui, Z. Huang, B. P. Thapaliya, C. L. Do-Thanh, M. Zhou, J. Fan, Z. Yang, M. Chi, T. Kobayashi, J. Wu, E. Mamontov, and S. Dai, "Machine-learning-assisted material discovery of oxygen-rich highly porous carbon active materials for aqueous supercapacitors," *Nature Communications*, vol. 14, no. 1, Dec. 2023, Art. no. 4607.

[147] H. Yoon, T. Min, S. H. Kim, G. Lee, D. Oh, D. C. Choi, and S. Kim, "Effect of activated carbon electrode material characteristics on hardness control performance of membrane capacitive deionization," *RSC Advances*, vol. 13, no. 45, pp. 31480–31486, Oct. 2023.

[148] S. Moosavi, C. W. Lai, S. Gan, G. Zamiri, O. Akbarzadeh Pivehzhani, and M. R. Johan, "Application of efficient magnetic particles and activated carbon for dye removal from wastewater," *ACS Omega*, vol. 5, no. 33, pp. 20684–20697, Aug. 2020.

[149] M. Z. A. Zaimee, M. S. Sarjadi, and M. L. Rahman, "Heavy metals removal from water by efficient adsorbents," *Water*, vol. 13, no. 19, Oct. 2021, Art. no. 2659.

[150] C. Anyika, N. A. M. Asri, Z. A. Majid, A. Yahya, and J. Jaafar, "Synthesis and characterization of magnetic activated carbon developed from palm kernel shells," *Nanotechnology for Environmental Engineering*, vol. 2, no. 1, Dec. 2017.

[151] J. Heo, Y. Yoon, G. Lee, Y. Kim, J. Han, and C. M. Park, "Enhanced adsorption of bisphenol A and sulfamethoxazole by a novel magnetic $CuZnFe_2O_4$–biochar composite," *Bioresource Technology*, vol. 281, pp. 179–187, Jun. 2019.

[152] E. Allahkarami, A. Dehghan Monfared, L. F. O. Silva, and G. L. Dotto, "Lead ferrite-activated carbon magnetic composite for efficient removal of phenol from aqueous solutions: Synthesis, characterization, and adsorption studies," *Scientific Reports*, vol. 12, no. 1, Dec. 2022, Art. no. 10718.

[153] S. E. Sandler, B. Fellows, and O. Thompson Mefford, "Best practices for characterization of magnetic nanoparticles for biomedical applications," *Analytical Chemistry*, vol. 91, no. 22, pp. 14159–14169, Nov. 2019.

[154] F. Wang, J. Zhang, and D. M. Jia, "Facile synthesis of shell-core structured Fe_3O_4@ACS as recyclable magnetic adsorbent for methylene

blue removal," *Journal of Dispersion Science and Technology*, vol. 40, no. 12, pp. 1736–1743, Dec. 2019.

[155] M. T. H. Siddiqui, S. Nizamuddin, H. A. Baloch, N. M. Mubarak, M. Al-Ali, S. A. Mazari, A. W. Bhutto, R. Abro, M. Srinivasan, and G. Griffin, "Fabrication of advance magnetic carbon nano-materials and their potential applications: A review," *Journal of Environmental Chemical Engineering*, vol. 7, no. 1, Feb. 2019, Art. no. 102812.

[156] K. R. Thines, E. C. Abdullah, N. M. Mubarak, and M. Ruthiraan, "Synthesis of magnetic biochar from agricultural waste biomass to enhancing route for waste water and polymer application: A review," *Renewable and Sustainable Energy Reviews*, vol. 67, pp. 257-276, Jan. 2017.

[157] L. S. Rocha, D. Pereira, É. Sousa, M. Otero, V. I. Esteves, and V. Calisto, "Recent advances on the development and application of magnetic activated carbon and char for the removal of pharmaceutical compounds from waters: A review," *Science of The Total Environment*, vol. 718, May 2020, Art. no. 137272.

[158] T. Ahn, J. H. Kim, H. M. Yang, J. W. Lee, and J. D. Kim, "Formation pathways of magnetite nanoparticles by coprecipitation method," *Journal of Physical Chemistry C*, vol. 116, no. 10, pp. 6069–6076, Mar. 2012.

[159] O. Kazak, "Fabrication of in situ magnetic activated carbon by co-pyrolysis of sucrose with waste red mud for removal of Cr(VI) from waters," *Environmental Technology and Innovation*, vol. 24, Nov. 2021, Art. no. 101856.

[160] P. S. Thue, C. S. Umpierres, E. C. Lima, D. R. Lima, F. M. Machado, G. S. dos Reis, R. S. da Silva, F. A. Pavan, and H. N. Tran, "Single-step pyrolysis for producing magnetic activated carbon from tucumã (*Astrocaryum aculeatum*) seed and nickel(II) chloride and zinc(II) chloride. Application for removal of nicotinamide and propanolol," *Journal of Hazardous Materials*, vol. 398, Nov. 2020, Art. no. 122903.

[161] X. Zhang, Y. Li, Y. He, D. Kong, B. Klein, S. Yin, and H. Zhao, "Preparation of magnetic activated carbon by activation and modification of char derived from co-pyrolysis of lignite and biomass and its adsorption of heavy-metal-containing wastewater," *Minerals*, vol. 12, no. 6, Jun. 2022, Art. no. 0665

[162] K. M. Lompe, D. Menard, and B. Barbeau, "Performance of biological magnetic powdered activated carbon for drinking water purification," *Water Research*, vol. 96, pp. 42–51, Jun. 2016.

[163] S. Cheng, L. Zhang, A. Ma, H. Xia, J. Peng, C. Li, and J. Shu, "Comparison of activated carbon and iron/cerium modified activated carbon to remove methylene blue from wastewater," *Journal of Environmental Sciences*, vol. 65, pp. 92–102, Mar. 2018.

[164] C. Zhang, S. Jiang, and W. Zhang, "Adsorptive performance of coal-based magnetic activated carbon for cyclic volatile methylsiloxanes from landfill leachate," *Environmental Science and Pollution Research*, vol. 25, no. 5, pp. 4803–4810, Feb. 2018.

[165] Z. Wu, H. Zhang, E. Ali, A. Shahab, H. Huang, H. Ullah, and H. Zeng, "Synthesis of novel magnetic activated carbon for effective Cr(VI) removal via synergistic adsorption and chemical reduction," *Environmental Technology and Innovation*, vol. 30, May 2023, Art. no. 103092.

[166] C.-H. Shih, J. Kim, S.-H. Yang, O. Soker, T. J. Strathmann, and K.-H. Chu, "Remediation of PFAS-impacted soils using magnetic activated carbon (MAC) and hydrothermal alkaline treatment (HALT)," *Science of The Total Environment*, vol. 912, Feb. 2024, Art. no. 168931.

[167] A. Khalil, M. Salem, S. Ragab, M. Sillanpää, and A. El Nemr, "Orange peels magnetic activate carbon (MG-OPAC) composite formation for toxic chromium absorption from wastewater," *Scientific Reports*, vol. 13, no. 1, Dec. 2023, Art. no. 3402.

[168] A. M. El-Shamy, H. K. Farag, and W. M. Saad, "Comparative study of removal of heavy metals from industrial wastewater using clay and activated carbon in batch and continuous flow systems," *Egyptian Journal of Chemistry*, vol. 60, no. 6, pp. 1165–1175, 2017.

[169] R. E. Guedes, A. S. Luna, and A. R. Torres, "Operating parameters for bio-oil production in biomass pyrolysis: A review," *Journal of Analytical and Applied Pyrolysis*, vol. 129, pp. 134–149, Jan. 2018.

[170] Z. Wang, H. Yang, Y. Li, and X. Zheng, "Robust silk fibroin/graphene oxide aerogel fiber for radiative heating textiles," *ACS Applied Materials and Interfaces*, vol. 12, no. 13, pp. 15726–15736, Apr. 2020.

[171] M. Tuzen, A. Sarı, and T. A. Saleh, "Response surface optimization, kinetic and thermodynamic studies for effective removal of rhodamine B by magnetic AC/CeO_2 nanocomposite," *Journal of Environmental Management*, vol. 206, pp. 170–177, Jan. 2018.

[172] Z. Ali, R. Ullah, M. Tuzen, S. Ullah, A. Rahim, and T. A. Saleh, "Colorimetric sensing of heavy metals on metal doped metal oxide nanocomposites: A review," *Trends in Environmental Analytical Chemistry*, vol. 37, Mar. 2023, Art. no. e00187.

[173] E. Altıntıg, M. Yenigun, A. Sarı, H. Altundag, M. Tuzen, and T. A. Saleh, "Facile synthesis of zinc oxide nanoparticles loaded activated carbon as an eco-friendly adsorbent for ultra-removal of malachite green from water," *Environmental Technology and Innovation*, vol. 21, Feb. 2021, Art. no. 101305.

[174] X. Kong, Y. Zhu, H. Lei, C. Wang, Y. Zhao, E. Huo, X. Lin, Q. Zhang, M. Qian, W. Mateo, R. Zou, Z. Fang, and R. Ruan, "Synthesis of graphene-like carbon from biomass pyrolysis and its applications," *Chemical Engineering Journal*, vol. 399, Nov. 2020, Art. no. 125808.

[175] P. Kumar, N. Divya, and J. K. Ratan, "Synthesis and characterization of chemically derived graphene oxide from graphite," *Lecture Notes in Civil Engineering*, vol. 30, pp. 85–94, Apr. 2019.

[176] R. Jin, N. Brljak, J. M. Slocik, R. Rao, M. R. Knecht, T. R. Walsh, and M. R. Knecht, "Graphene exfoliation using multidomain peptides," *Journal of Materials Chemistry B*, vol. 12, no. 20, pp. 4824–4832, May 2024.

[177] B. Liu and S. Ma, "Precise synthesis of graphene by chemical vapor deposition," *Nanoscale*, vol. 16, no. 9, pp. 4407–4433, Feb. 2024.

[178] J. I. Paredes, S. Villar-Rodil, A. Martínez-Alonso, and J. M. D. Tascón, "Graphene oxide dispersions in organic solvents," *Langmuir*, vol. 24, no. 19, pp. 10560–10564, Oct. 2008.

[179] H. Fei, J. Dong, D. Chen, T. Hu, X. Duan, I. Shakir, Y. Huang, and X. Duan, "Single atom electrocatalysts supported on graphene or graphene-like carbons," *Chemical Society Reviews*, vol. 48, no. 20, pp. 5207–5241, Oct. 2019.

[180] J. K. Saha and A. Dutta, "A review of graphene: Material synthesis from biomass sources," *Waste and Biomass Valorization*, vol. 13, no. 3, pp. 1385–1429, Mar. 2022.

[181] J. He, A. Anouar, A. Primo, and H. García, "Quality improvement of few-layers defective graphene from biomass and application for H_2 generation," *Nanomaterials*, vol. 9, no. 6, Jun. 2019, Art. no. 0895.

[182] M. H. M. Zubir and M. A. A. Zaini, "Twigs-derived activated carbons via H_3PO_4/$ZnCl_2$ composite activation for methylene blue and congo red dyes removal," *Scientific Reports*, vol. 10, no. 1, pp. 1–17, Aug. 2020.

[183] Q. Abbas, P. A. Shinde, M. A. Abdelkareem, A. H. Alami, M. Mirzaeian, A. Yadav, and A. G. Olabi, "Graphene synthesis techniques and environmental applications," *Materials*, vol. 15, no. 21, Nov. 2022, Art. no. 7804.

[184] L. Feng, Z. Qin, Y. Huang, K. Peng, F. Wang, Y. Yan, and Y. Chen, "Boron-, sulfur-, and phosphorus-doped graphene for environmental applications," *Science of the Total Environment*, vol. 698, Jan. 2020, Art. no. 134239.

[185] L. Huang, J. Pei, H. Jiang, C. Li, and X. Hu, "Electricity generation across graphene oxide membranes," *Materials Research Bulletin*, vol. 97, pp. 96–100, Jan. 2018.

[186] A. K. Worku, D. W. Ayele, and N. G. Habtu, "Recent advances and future perspectives in engineering of bifunctional electrocatalysts for rechargeable zinc–air batteries," *Materials Today Advances*, vol. 9, Mar. 2021, Art. no. 100116.

[187] A. K. Worku, D. W. Ayele, N. G. Habtu, B. T. Admasu, G. Alemayehu, B. Z. Taye, and T. A. Yemata, "Energy storage technologies; Recent advances, challenges, and prospectives," in *Energy Systems in Electrical Engineering Planning of Hybrid Renewable Energy Systems, Electric Vehicles and Microgrid*, pp. 125–150, 2022.

[188] A. K. Worku, D. W. Ayele, N. G. Habtu, and M. D. Ambaw, "Engineering nanostructured Ag doped α-MnO_2 electrocatalyst for highly efficient rechargeable zinc-air batteries," *Heliyon*, vol. 8, no. 10, Oct. 2022 Art. no. e10960.

[189] A. K. Worku, D. W. Ayele, N. G. Habtu, and T. A. Yemata, "Engineering Co_3O_4/MnO_2 nanocomposite materials for oxygen reduction electrocatalysis," *Heliyon*, vol. 7, no. 9, Sep. 2021, Art. no. e08076.

[190] N. G. Habtu, A. K. Worku, D. W. Ayele, M. A. Teshager, and Z. G. Workineh, "Facile preparation and electrochemical investigations

of copper-ion doped α-MnO_2 nanoparticles," *Advances of Science and Technology*, pp. 543–553, Jan. 2022.

[191] M. Velický and P. S. Toth, "From two-dimensional materials to their heterostructures: An electrochemist's perspective," *Applied Materials Today*, vol. 8, pp. 68–103, Sep. 2017.

[192] N. Bellier, P. Baipaywad, N. Ryu, J. Y. Lee, and H. Park, "Recent biomedical advancements in graphene oxide- and reduced graphene oxide-based nanocomposite nanocarriers," *Biomaterials Research*, vol. 26, Dec. 2022, Art. no. 65.

[193] K. Alam, Y. Y. Jo, C.-K. Park, and H. Cho, "Synthesis of graphene oxide using atmospheric plasma for prospective biological applications," *International Journal of Nanomedicine*, vol. 15, pp. 5813–5824, Aug. 2020.

[194] J. Li, Q. Yan, X. Zhang, J. Zhang, and Z. Cai, "Efficient conversion of lignin waste to high value bio-graphene oxide nanomaterials," *Polymers*, vol. 11, no. 4, Apr. 2019, Art. no. 0623.

[195] A. Gomez-Martin, J. Martinez-Fernandez, M. Ruttert, M. Winter, T. Placke, and J. Ramirez-Rico, "Porous graphene-like carbon from fast catalytic decomposition of biomass for energy storage applications," *ACS Omega*, vol. 4, no. 25, pp. 21446–21458, Dec. 2019.

[196] L. Sun, C. Tian, M. Li, X. Meng, L. Wang, R. Wang, J. Yin, and H. Fu, "From coconut shell to porous graphene-like nanosheets for high-power supercapacitors," *Journal of Materials Chemistry A*, vol. 1, no. 21, pp. 6462–6470, May 2013.

[197] K. K. Yadav, H. Singh, S. Rana, Sunaina, H. Sammi, S. T. Nishanthi, R. Wadhwa, N. Khan, and M. Jha, "Utilization of waste coir fibre architecture to synthesize porous graphene oxide and their derivatives: An efficient energy storage material," *Journal of Cleaner Production*, vol. 276, Dec. 2020, Art. no. 124240.

[198] R. Ye, C. Xiang, J. Lin, Z. Peng, K. Huang, Z. Yan, N. P. Cook, E. L. G. Samuel, C. C. Hwang, G. Ruan, G. Ceriotti, A. R. O. Raji, A. A. Martí, and J. M. Tour, "Coal as an abundant source of graphene quantum dots," *Nature Communications*, vol. 4, no. 1, pp. 1–7, Dec. 2013.

[199] C. P. Lawagon, K. Faungnawakij, S. Srinives, S. Thongratkaew, K. Chaipojjana, A. Smuthkochorn, P. Srisrattha, and T. Charinpanitkul, "Sulfonated graphene oxide from petrochemical waste oil for efficient conversion of fructose into levulinic acid," *Catalysis Today*, vol. 375, pp. 197–203, Sep. 2021.

[200] Y. Qu, F. He, C. Yu, X. Liang, D. Liang, L. Ma, Q. Zhang, J. Lv, and J. Wu, "Advances on graphene-based nanomaterials for biomedical applications," *Materials Science and Engineering: C*, vol. 90, pp. 764–780, Sep. 2018.

[201] A. K. Worku and D. W. Ayele, "Recent advances of graphene-based materials for emerging technologies," *Results in Chemistry*, vol. 5, Jan. 2023, Art. no. 100971.

[202] K. A. Madurani, S. Suprapto, N. I. Machrita, S. L. Bahar, W. Illiya, and F. Kurniawan, "Progress in graphene synthesis and its application: history, challenge and the future outlook for research and industry," *ECS Journal of Solid State Science and Technology*, vol. 9, no. 9, Oct. 2020, Art. no. 093013.

[203] B. W. Zhang, T. Zheng, Y. X. Wang, Y. Du, S. Q. Chu, Z. Xia, R. Amal, S. X. Dou, and L. Dai, "Highly efficient and selective electrocatalytic hydrogen peroxide production on Co-O-C active centers on graphene oxide," *Communications Chemistry*, vol. 5, no. 1, Dec. 2022, Art. no. 43.

[204] G. Wang, S. Chen, X. Quan, H. Yu, and Y. Zhang, "Enhanced activation of peroxymonosulfate by nitrogen doped porous carbon for effective removal of organic pollutants," *Carbon*, vol. 115, pp. 730–739, May 2017.

[205] R. Suresh and S. Rajendran, "Carbon-based adsorbents for remediation of noxious pollutants from water and wastewater," in *Sustainable Materials for Sensing and Remediation of Noxious Pollutants*, Eds. I. Tyagi, J. Goscianska, M. H. Dehghani, and R. R. Karri, Amsterdam, Netherlands: Elsevier, 2022, pp. 177–194.

[206] Q. Yang, E. P. Nguyen, C. de C. C. Silva, G. Rosati, and A. Merkoçi, "Signal enhancement strategies," in *Wearable Physical, Chemical and Biological Sensors*, E. Morales-Narvaez and C. Dincer, Amsterdam, Netherlands: Elsevier, 2022, pp. 123–168.

[207] M. V. Kharlamova, M. G. Burdanova, M. I. Paukov, and C. Kramberger, "Synthesis, sorting, and applications of single-chirality single-walled carbon nanotubes," *Materials*, vol. 15, no. 17, Sep. 2022, Art. no. 5898.

[208] K. Truus, O. Volobujeva, R. Kaupmees, A. Tamm, M. Rähn, R. Raid, K. Koppel, and R. Tuvikene, "Recent advances of carbon nanotubes synthesis by the electric arc technique using atomized platinum-group metal catalysts,"

Materials Science and Engineering: B, vol. 300, Feb. 2024, Art. no. 117121.

[209] A. Al Baroot, K. A. Elsayed, F. A. Khan, S. A. Haladu, F. Ercan, E. Çevik, Q. A. Drmosh, and M. A. Almessiere, "Anticancer activity of Au/CNT nanocomposite fabricated by nanosecond pulsed laser ablation method on colon and cervical cancer," *Micromachines*, vol. 14, no. 7, Jul. 2023, Art. no. 1455.

[210] S. Zhao, A. J. Gillen, Y. Li, and A. Noy, "Sonochemical synthesis and ion transport properties of surfactant-stabilized carbon nanotube porins," *Journal of Physical Chemistry Letters*, vol. 14, no. 41, pp. 9372–9376, Oct. 2023.

[211] H. Cheng How, Y. Leong Chow, H. Yee Wong, J. Hou Ho, and C. Lim Law, "Synthesising copper-carbon nanotube composites through methane diffusion flame," *Materials Today: Proceedings*, vol. 66, pp. 2655–2659, Jan. 2022.

[212] I. V. Novikov, D. V. Krasnikov, E. M. Khabushev, V. S. Shestakova, Y. E. Matyushkin, and A. G. Nasibulin, "A new method for evaluation of nanotube growth kinetics in aerosol CVD," *Carbon*, vol. 217, Jan. 2024, Art. no. 118589.

[213] D. Yao and C.-H. Wang, "Pyrolysis and in-line catalytic decomposition of polypropylene to carbon nanomaterials and hydrogen over Fe- and Ni-based catalysts," *Applied Energy*, vol. 265, May 2020, Art. no. 114819.

[214] D. Yao, H. Li, Y. Dai, and C. H. Wang, "Impact of temperature on the activity of Fe-Ni catalysts for pyrolysis and decomposition processing of plastic waste," *Chemical Engineering Journal*, vol. 408, Mar. 2021, Art. no. 127268.

[215] J. Wang, B. Shen, M. Lan, D. Kang, and C. Wu, "Carbon nanotubes (CNTs) production from catalytic pyrolysis of waste plastics: The influence of catalyst and reaction pressure," *Catalysis Today*, vol. 351, pp. 50–57, Jul. 2020.

[216] H. M. Nmnarioglu, K. Mercari, and Civalek, "Finite element model and size dependent stability analysis of boron nitride and silicon carbide nanowires/nanotubes," *Scientia Iranica*, vol. 26, no. 4, pp. 2079–2099, Aug. 2019.

[217] A. Venkataraman, E. V. Amadi, Y. Chen, and C. Papadopoulos, "Carbon nanotube assembly and integration for applications," *Nanoscale Research Letters*, vol. 14, no. 20, Dec. 2019.

[218] T.J. Sisto, L. N. Zakharov, B. M. White, and R. Jasti, "Towards pi-extended cycloparaphenylenes as seeds for CNT growth: Investigating strain relieving ring-openings and rearrangements," *Chemical Science*, vol. 7, no. 6, pp. 3681–3688, Feb. 2016.

[219] J. C. Acomb, C. Wu, and P. T. Williams, "Effect of growth temperature and feedstock ratio on the production of carbon nanotubes and hydrogen from the pyrolysis of waste plastics," *Journal of Analytical and Applied Pyrolysis*, vol. 113, pp. 231–238, May 2015.

[220] D. Yao, C. Wu, H. Yang, Y. Zhang, M. A. Nahil, Y. Chen, P. T. Williams, and H. Chen, "Co-production of hydrogen and carbon nanotubes from catalytic pyrolysis of waste plastics on Ni-Fe bimetallic catalyst," *Energy Conversion and Management*, vol. 148, pp. 692–700, Sep. 2017.

[221] R. Araga and C. S. Sharma, "One step direct synthesis of multiwalled carbon nanotubes from coconut shell derived charcoal," *Materials Letters*, vol. 188, pp. 205–207, Feb. 2017.

[222] B. Debalina, R. B. Reddy, and R. Vinu, "Production of carbon nanostructures in biochar, bio-oil and gases from bagasse via microwave assisted pyrolysis using Fe and Co as susceptors," *Journal of Analytical and Applied Pyrolysis*, vol. 124, pp. 310–318, Mar. 2017.

[223] L. He, S. Hu, X. Yin, J. Xu, H. Han, H. Li, Q. Ren, S. Su, Y. Wang, and J. Xiang, "Promoting effects of Fe-Ni alloy on co-production of H_2 and carbon nanotubes during steam reforming of biomass tar over Ni-Fe/α-Al_2O_3," *Fuel*, vol. 276, Sep. 2020, Art. no. 118116.

[224] L. Silvestro and P. Jean Paul Gleize, "Effect of carbon nanotubes on compressive, flexural and tensile strengths of Portland cement-based materials: A systematic literature review," *Construction and Building Materials*, vol. 264, Dec. 2020, Art. no. 120237.

[225] S. Jalali Mosallam, H. Pesaran Behbahani, M. Shahpari, and R. Abaeian, "The effect of carbon nanotubes on mechanical properties of structural lightweight concrete using LECA aggregates," *Structures*, vol. 35, pp. 1204–1218, Jan. 2022.

[226] S. S. U. H. Gillani, A. Khitab, S. Ahmad, R. A. Khushnood, G. A. Ferro, S. M. Saleem Kazmi, L. A. Qureshi, and L. Restuccia, "Improving the mechanical performance of cement composites by carbon nanotubes addition," *Procedia Structural Integrity*, vol. 3, pp. 11–17, 2017.

[227] S. E. Mohammadyan-Yasouj and A. Ghaderi, "Experimental investigation of waste glass powder, basalt fibre, and carbon nanotube on the mechanical properties of concrete," *Construction*

and Building Materials, vol. 252, Aug. 2020, Art. no. 119115.

[228] D. Wang, X. Wang, A. Ashour, L. Qiu, and B. Han, "Compressive properties and underlying mechanisms of nickel coated carbon nanotubes modified concrete," *Construction and Building Materials*, vol. 319, Feb. 2022, Art. no. 126133.

[229] A. Adhikary, M. Mahbubul, A. Bhuiyan, and M. Hoque, "Comparison of reproductive performance of Brahman crossbred females with other available cattle genotypes in Mymensingh District," *Journal of Bangladesh Agricultural University*, vol. 19, no. 1, pp. 61–66, Mar. 2021.

[230] S. Dong, D. Wang, A. Ashour, B. Han, and J. Ou, "Nickel plated carbon nanotubes reinforcing concrete composites: From nano/micro structures to macro mechanical properties," *Composites Part A: Applied Science and Manufacturing*, vol. 141, Feb. 2021, Art. no. 106228.

[231] A. J. N. MacLeod, A. Fehervari, W. P. Gates, E. O. Garcez, L. P. Aldridge, and F. Collins, "Enhancing fresh properties and strength of concrete with a pre-dispersed carbon nanotube liquid admixture," *Construction and Building Materials*, vol. 247, Jun. 2020, Art. no. 118524.

[232] A. Hawreen and J. A. Bogas, "Influence of carbon nanotubes on steel–concrete bond strength," *Materials and Structures*, vol. 51, no. 6, Dec. 2018.

[233] K. Narasimman, T. M. Jassam, T. S. Velayutham, M. M. M. Yaseer, and R. Ruzaimah, "The synergic influence of carbon nanotube and nanosilica on the compressive strength of lightweight concrete," *Journal of Building Engineering*, vol. 32, Nov. 2020, Art. no. 101719.

[234] M. A. Mousavi, A. Sadeghi-Nik, A. Bahari, C. Jin, R. Ahmed, T. Ozbakkaloglu, and J. de Brito, "Strength optimization of cementitious composites reinforced by carbon nanotubes and Titania nanoparticles," *Construction and Building Materials*, vol. 303, Oct. 2021, Art. no. 124510.

[235] N. Cong Thang and H. Ngoc Duc, "Effect of Carbon Nanotube on properties of lightweight concrete using recycled Expanded Polystyrene (EPS)," *IOP Conference Series: Materials Science and Engineering*, vol. 869, Jul. 2020, Art. no. 032049.

[236] M. Kaur, K. Murari, and G. Singh, "Influence of multi-walled carbon nanotubes on mechanical properties of cement concrete," *IOP Conference Series: Materials Science and Engineering*, vol. 814, Jun. 2020, Art. no. 012001.

[237] J. Huang, D. Rodrigue, and P. Guo, "Flexural and compressive strengths of carbon nanotube reinforced cementitious composites as a function of curing time," *Construction and Building Materials*, vol. 318, Feb. 2022 Art. no. 125996.

[238] R. O. Medupin, O. K. Abubakre, A. S. Abdulkareem, R. A. Muriana, and A. S. Abdulrahman, "Carbon nanotube reinforced natural rubber nanocomposite for anthropomorphic prosthetic foot purpose," *Scientific Reports*, vol. 9, no. 1, Dec. 2019, Art. no. 20146.

[239] J. Zhang, Y. Ke, J. Zhang, Q. Han, and B. Dong, "Cement paste with well-dispersed multi-walled carbon nanotubes: Mechanism and performance," *Construction and Building Materials*, vol. 262, Nov. 2020, Art. no. 120746.

[240] M. Mansouri Sarvandani, M. Mahdikhani, H. Aghabarati, and M. Haghparast Fatmehsari, "Effect of functionalized multi-walled carbon nanotubes on mechanical properties and durability of cement mortars," *Journal of Building Engineering*, vol. 41, Sep. 2021, Art. no. 102407.

[241] A. M. Rashad, "Effect of carbon nanotubes (CNTs) on the properties of traditional cementitious materials," *Construction and Building Materials*, vol. 153, pp. 81–101, Oct. 2017.

[242] P. Zhang, J. Su, J. Guo, and S. Hu, "Influence of carbon nanotube on properties of concrete: A review," *Construction and Building Materials*, vol. 369, Mar. 2023, Art. no. 130338.

[243] B. Oldfrey, A. Tchorzewska, R. Jackson, M. Croysdale, R. Loureiro, C. Holloway, and M. Miodownik, "Additive manufacturing techniques for smart prosthetic liners," *Medical Engineering and Physics*, vol. 87, pp. 45–55, Jan. 2021.

[244] B. Mensah, H. G. Kim, J. H. Lee, S. Arepalli, and C. Nah, "Carbon nanotube-reinforced elastomeric nanocomposites: A review," *International Journal of Smart and Nano Materials*, vol. 6, no. 4, pp.211–238, Oct. 2015.

[245] S. Frackowiak, J. Ludwiczak, and K. Leluk, "Man-made and natural fibres as a reinforcement in fully biodegradable polymer composites: A concise study," *Journal of Polymers and the Environment*, vol. 26, no. 12, pp. 4360–4368, Dec. 2018.

[246] H. Yang, L. Yuan, X. F. Yao, Z. Zheng, and D. N. Fang, "Monotonic strain sensing behavior of self-assembled carbon nanotubes/graphene silicone rubber composites under cyclic loading,"

Composites Science and Technology, vol. 200, Nov. 2020, Art. no. 108474.

[247] R. Selvaraj, M. Ramamoorthy, and A. B. Arumugam, "Experimental and numerical studies on dynamic performance of the rotating composite sandwich panel with CNT reinforced MR elastomer core," *Composite Structures*, vol. 277, Dec. 2021, Art. no. 114560.

[248] J. S. Gao, Z. Liu, Z. Yan, and Y. He, "A novel slurry blending method for a uniform dispersion of carbon nanotubes in natural rubber composites," *Results in Physics*, vol. 15, Dec. 2019, Art. no. 102720.

[249] J.-L. Lin, S.-M. Su, Y.-B. He, and F.-Y. Kang, "Improving thermal and mechanical properties of the alumina filled silicone rubber composite by incorporating carbon nanotubes," *New Carbon Materials*, vol. 35, no. 1, pp. 66–72, Feb. 2020.

[250] P. Jawahar, V. Payak, J. Chandradass, and P. Prabhu, "Optimization of mechanical properties of CNT-rubber nanocomposites," *Materials Today: Proceedings*, vol. 45, part 7, pp. 7183–7189, 2021.

[251] S. Lepak-Kuc, B. Podsiadły, A. Skalski, D. Janczak, M. Jakubowska, and A. Lekawa-Raus, "Highly conductive carbon nanotube-thermoplastic polyurethane nanocomposite for smart clothing applications and beyond," *Nanomaterials*, vol. 9, no. 9, Sep. 2019, Art. no. 1287.

[252] N. Salah, A. M. Alfawzan, A. Saeed, A. Alshahrie, and W. Allafi, "Effective reinforcements for thermoplastics based on carbon nanotubes of oil fly ash," *Scientific Reports*, vol. 9, Dec. 2019, Art. no. 20288.

[253] Y. Li, G. Liu, L. Wang, J. Zhang, M. Xu, and S. Q. Shi, "Multifunctional conductive graphite/cellulosic microfiber-natural rubber composite sponge with ultrasensitive collision-warning and fire-warning," *Chemical Engineering Journal*, vol. 431, Mar. 2022, Art. no. 134046.

[254] Q. Dang, M. Mba Wright, and R. C. Brown, "Ultra-low carbon emissions from coal-fired power plants through bio-oil co-firing and biochar sequestration," *Environmental Science and Technology*, vol. 49, no. 24, pp. 14688–14695, Dec. 2015.

[255] H. A. Alhashimi and C. B. Aktas, "Life cycle environmental and economic performance of biochar compared with activated carbon: A meta-analysis," *Resources, Conservation and Recycling*, vol. 118, pp. 13–26, Mar. 2017.

[256] P. Bartocci, G. Bidini, P. Saputo, and F. Fantozzi, "Biochar pellet carbon footprint," *Chemical Engineering Transactions*, vol. 50, pp. 217–222, Jun. 2016.

[257] K. G. Roberts, B. A. Gloy, S. Joseph, N. R. Scott, and J. Lehmann, "Life cycle assessment of biochar systems: Estimating the energetic, economic, and climate change potential," *Environmental Science and Technology*, vol. 44, no. 2, pp. 827–833, Jan. 2010.

[258] K. Hjaila, R. Baccar, M. Sarrà, C. M. Gasol, and P. Blánquez, "Environmental impact associated with activated carbon preparation from olive-waste cake via life cycle assessment," *Journal of Environmental Management*, vol. 130, pp. 242–247, Nov. 2013.

[259] C. V Sepúlveda-Cervantes, E. Soto-Regalado, P. Rivas-García, M. Loredo-Cancino, F. dJ Cerino-Córdova, and R. B. García Reyes, "Technical-environmental optimisation of the activated carbon production of an agroindustrial waste by means response surface and life cycle assessment," *Waste Management & Research: The Journal for a Sustainable Circular Economy*, vol. 36, no. 2, pp. 121–130, Feb. 2018.

[260] H. Gu, R. Bergman, N. Anderson, and S. Alanya-Rosenbaum, "Life-cycle assessment of activated carbon from woody biomass," *Wood and Fiber Science*, vol. 50, no. 3, pp. 229–243, Jul. 2018.

[261] M. Liao, S. Kelley, and Y. Yao, "Generating energy and greenhouse gas inventory data of activated carbon production using machine learning and kinetic based process simulation," *ACS Sustainable Chemistry and Engineering*, vol. 8, no. 2, pp. 1252–1261, Jan. 2020.

[262] M. Kim, G. Kim, M. Kim, and G. Kim, "Life cycle assessment of activated carbon production system by using poplar," *Journal of Korean Society of Environmental Engineers*, vol. 36, no. 11, pp. 725–732, Nov. 2014.

[263] A. I. Osman, A. M. Elgarahy, N. Mehta, A. H. Al-Muhtaseb, A. S. Al-Fatesh, and D. W. Rooney, "Facile synthesis and life cycle assessment of highly active magnetic sorbent composite derived from mixed plastic and biomass waste for water remediation," *ACS Sustainable Chemistry and Engineering*, vol. 10, no. 37, pp. 12433–12447, Sep. 2022.

[264] C. Jia, M. Pang, Y. Lu, Y. Liu, M. Zhuang, B. Liu, J. Lu, T. Wei, L. Wang, T. Bian, M. Wang,

F. Yu, L. Sun, L. Lin, T. Teng, X. Wu, Z. He, J. Gao, J. Luo, S. Zhang, L. Feng, X. Yin, F. You, G. Li, L. Zhang, Y. G. Zhu, X. Zhu, and Y. Yang, "Graphene environmental footprint greatly reduced when derived from biomass waste via flash joule heating," *One Earth*, vol. 5, no. 12, pp. 1394–1403, Dec. 2022.

[265] M. Cossutta, J. McKechnie, and S. J. Pickering, "A comparative LCA of different graphene production routes," *Green Chemistry*, vol. 19, no. 24, pp. 5874–5884, Nov. 2017.

[266] H. Y. Teah, T. Sato, K. Namiki, M. Asaka, K. Feng, and S. Noda, "Life cycle greenhouse gas emissions of long and pure carbon nanotubes synthesized via on-substrate and fluidized-bed chemical vapor deposition," *ACS Sustainable Chemistry and Engineering*, vol. 8, no. 4, pp. 1730–1740, Feb. 2020.

[267] Precedence Research. "Activated Carbon Market Size – 1961." PrecedenceResearch.com. https://www.precedenceresearch.com/activated-carbon-market (accessed Jul. 2, 2024).

[268] Precedence Research. "Graphene Market Size - 3576." PrecedenceResearch.com. https://www.precedenceresearch.com/graphene-market (accessed Jul. 2, 2024).

[269] Precedence Research. "Carbon Nanotubes Market Size." PrecedenceResearch.com. https://www.precedenceresearch.com/carbon-nanotubes-market (accessed Jul. 2, 2024).

[270] T. Schmaltz, L. Wormer, U. Schmoch, and H. Döscher, "Graphene Roadmap Briefs (No. 3): meta-market analysis 2023," *2D Materials*, vol. 11, no. 2, Jan. 2024, Art. no. 022002.

[271] Kelincarbon. "Our Products." Kelincarbon.com. https://www.kelincarbon.com/products/Powder-activated-carbon (accessed Jul. 1, 2024).

[272] Zhulincarbon. "Our Products." Kelincarbon.com. https://www.zhulincarbon.com/products/granular-activated-carbon/ (accessed Jul. 1, 2024).

[273] Cheaptubes. "Product Categories." Kelincarbon.com. https://www.cheaptubes.com/cheap-tubes-inc-online-shop/ (accessed Jul. 1, 2024).

Supporting Information

Table S1: Proximate and ultimate analysis of biomass.

Biomass	Proximate Analysis				Ultimate Analysis					Ref.
	VM (%)	FC (%)	Moisture (%)	Ash (%)	C (%)	H (%)	N (%)	S (%)	O (%)	
Coffee husk	66.85	14.00	12.75	6.40	42.68	6.10	1.92	0.42	48.88	[1]
Rubber wood chip	80.21	17.88	32.19#	1.91	51.44	6.32	0.17	0.08	41.99	[2]
Rice husk	66.17	17.62	9.53#	16.21	48.89	6.22	0.09	0.08	44.72	[2]
Rice straw	71.02	15.47	10.01#	13.51	47.56	6.55	0.01	0.16	45.72	[2]
Corn cob	80.01	18.07	10.01#	1.92	43.61	6.55	0.01	0.09	49.74	[2]
Corn stalks	81.42	6.36	5.54	6.74	51.12	6.30	0.86	0.12	42.41	[3]
Candlenut shell	81.90	12.60	2.40	3.10	53.78	4.37	0.37	nd	41.50	[4]
Coconut coir	82.13	13.82	1.73	4.05	49.36	6.57	1.23	0.14	42.70	[5]
Empty fruit bunch*	78.34	18.46	-	3.20	46.77	6.84	0.71	0.29	45.39	[6]
Mesocarp fiber	69.2 ± 0.24	14.2 ± 2.60	12.5 ± 0.24	4.1 ± 1.20	43.94	5.51	0.71	0.05	38.74	[7]
Bamboo	76.61	21.68	44.51#	1.71	51.11	6.22	0.09	0.06	42.52	[2]
Wheat straw	59.4 ± 0.03	27.3 ± 0.02	5.0 ± 0.10	7.9 ± 0.04	44.00	5.80	0.40	0.30	42.40	[8]
Sawdust	77.65	18.54	33.91#	3.81	51.11	6.13	0.19	0.05	42.52	[2]
Paper waste*	72.80	9.50	-	11.20	39.78	5.50	0.10	nd	54.62	[9]
Sugarcane bagasse	74.98	17.11	10.21#	7.91	48.89	6.22	0.02	0.25	43.88	[2]
Sugarcane pulp*	74.00	16.46	-	1.06	45.70	5.24	0.14	nd	48.92	[10]
Cassava pulp	85.12	13.76	15.13#	1.12	45.53	7.11	0.03	0.04	47.29	[2]
Pine wood*	65.11	12.79	-	2.10	43.28	5.10	0.35	nd	51.27	[11]
Cow dung*	15.13	15.46	-	21.41	38.00	3.94	1.21	nd	56.85	[11]
Corn stover*	82.58	12.48	-	4.94	49.38	6.52	0.63	nd	43.47	[12]
Sugarcane peel*	80.04	15.42	-	4.54	46.47	6.23	0.92	nd	46.38	[12]
Waste coffee grounds*	78.69	14.25	-	7.06	44.89	6.14	0.35	nd	48.62	[12]
Bamboo leaves*	71.59	16.57	-	11.84	39.98	5.81	1.12	nd	53.09	[12]
Palm kernel shell*	70.45	18.89	-	2.47	48.25	6.41	0.15	nd	42.69	[13]
Olive kernel residues*	71.30	20.40	-	0.40	47.20	5.50	0.30	nd	38.70	[14]
Mixed wood chips*	75.20	18.00	-	0.80	48.10	5.80	0.10	nd	39.30	[14]
Waste wood*	76.00	15.00	-	2.00	46.60	5.80	0.40	nd	38.20	[15]
Cellulose*	82.00	13.00	-	nd	41.70	5.90	0.41	nd	52.00	[15]
Xylan*	73.00	17.00	-	4.00	40.30	5.50	0.41	nd	49.80	[15]
Lignin*	56.00	36.00	-	4.00	61.30	5.10	1.10	0.70	27.70	[15]

*Dry-based analysis and the moisture content are scrutinized by ASTM E1756-08 standard
nd: not detected

Table S2: Ultimate and proximate analysis of pyrolyzed biochar.

Biomass	Ultimate Analysis					HHV (MJ/kg)	Surface Area (m^2/g)	Pores Volume (cm^3/g)	Proximate Analysis			Ref.
	C (%)	O (%)	H (%)	S (%)	N (%)				VM (wt%)	FC (wt%)	Ash (wt%)	
Coffee hulls	64–69.3	3.7–9.7	0.7–2.4	0.3	1.6–2.8	-	1.4	0.005	12.3–22	57.2–63.3	20.8–24.4	[16]
Grass	75.2–82	14.1–17.7	2.4–4.9	0.3	1.2–1.9	28.9–29.4	0.1–1	0.6–0.7	8–20	70–79	10–14	[17]
Palm shell	79.4	16.61	3.18	0	0.82	28.85	-	-	18	72.5	2	[18]
EFB	64.93	31.41	2.55	0	1.12	21.34	-	-	40.1	41.7	12.8	[18]
Mesocarp fiber	67.7	29.23	2.43	0	0.65	29.06	-	-	52	30.6	4.3	[18]
Corn stalks	72.28	22.47	3.14	0.9	1.09		-	-	23.79	55.12	16.73	[19]
Ferula orientalis L.	59.74–70.32	25.22–34.87	3.07–3.71	0	0.82–1.68	19.27–24.34	-	-	-	-	-	[20]
Neem seed cake	68.83	13.29	2.53	0.11	1.77	25.84	-	-	-	-	-	[21]
Pigeon pea husk	73.88	10.87	2.46	0.03	1.05	28.03	-	-	-	-	-	[21]
Yellow pea husk	68.97	14.65	2.34	0.05	1.13	26.04	-	-	-	-	-	[21]
Ground nut shell	68.04	15.95	1.5	0.14	1.17	24.22	-	-	-	-	-	[21]
Channa straw	63.44	23.1	1.24	0.15	0.75	20.09	-	-	-	-	-	[21]
Wheat straw	64.22	24.12	1.03	0.31	0.53	20.01	-	-	-	-	-	[21]
Soybean straw	65.42	21.57	1.41	0.07	0.61	23.28	-	-	-	-	-	[21]
Bamboo	82.1±0.6	14.6±0.6	2.72 ±0.02	0.0012 ±0.00004	0.54 ±0.05	30.86 ±0.187	4.52–331.2	0.01–0.4	8.10±1.7	81.5±0.4	3.9±0.4	[22], [23]
Mixed wood chips	71.6	5.95	3.09	0.1	0.8	26.08	-	-	26.4	55.2	18.2	[14]
Olive kernel residues	79.4	9.7	3.76	0.1	0.6	30.93	-	-	28.8	65	6.2	[14]
Pine nut shell	81.43	12.71	2.86	0	0.65	-	-	-	27.95	69.62	2.35	[24]

Table S3: Yield of pyrolysis through several catalysts and ratio variations.

Biomass	HR (°C/min)	FR (mL/min)	Temp (°C)	Cat. Type	Cat. Ratio	Bio-oil (wt%)	Biochar (wt%)	Gas (wt%)	Ref.
Cotton Seeds	70	200	550	MgO	5%	42	20	23	[25]
					10%	36	21.5	24	
					15%	35	22.5	28	
					20%	30	25	30	
Ferula Orientalis L.	50	100	350	Al_2O_3	5%	41.42	33.75	24.83	[20]
					10%	40.83	31.18	27.99	
					15%	40.11	30.55	29.34	
			400	Al_2O_3	5%	42.38	29.41	28.21	
					10%	41.66	27.93	30.41	
					15%	40.87	26.64	32.49	
			450	Al_2O_3	5%	43.18	25.78	31.04	
					10%	42.78	24.85	32.37	
					15%	41.59	23.11	35.3	
			500	Al_2O_3	5%	44.67	23.12	32.21	
					10%	42.21	22.74	35.05	
					15%	41.64	21.93	36.43	
			550	Al_2O_3	5%	41.73	22.47	35.8	
					10%	40.95	21.36	37.69	
					15%	39.72	21.39	38.89	
			600	Al_2O_3	5%	40.86	21.84	37.3	
					10%	39.68	21.23	39.09	
					15%	39.13	20.76	40.11	
Ferula orientalis L.	50	100	350	ZnO	5%	42.56	35.78	21.66	[20]
					10%	42.58	33.83	23.59	
					15%	43.08	33.07	23.85	
			400	ZnO	5%	43.23	32.06	24.71	
					10%	43.01	31.44	25.55	
					15%	43.56	30.82	25.62	
			450	ZnO	5%	44.65	28.18	27.17	
					10%	44.62	26.39	28.99	
					15%	45.03	25.61	29.36	
			500	ZnO	5%	44.97	25.86	29.17	
					10%	44.96	24.42	30.62	
					15%	45.22	24.32	30.46	
			550	ZnO	5%	42.58	24.97	32.45	
					10%	42.47	24.23	33.3	
					15%	41.85	23.08	35.07	
			600	ZnO	5%	41.54	23.18	35.28	
					10%	40.89	23.05	36.06	
					15%	40.34	22.86	36.8	

Biomass	HR (°C/min)	FR (mL/min)	Temp (°C)	Cat. Type	Cat. Ratio	Bio-oil (wt%)	Biochar (wt%)	Gas (wt%)	Ref.
Ferula orientalis L.	50	100	350	ZnO	5%	42.56	35.78	21.66	[20]
					10%	42.58	33.83	23.59	
					15%	43.08	33.07	23.85	
			400	ZnO	5%	43.23	32.06	24.71	
					10%	43.01	31.44	25.55	
					15%	43.56	30.82	25.62	
			450	ZnO	5%	44.65	28.18	27.17	
					10%	44.62	26.39	28.99	
					15%	45.03	25.61	29.36	
			500	ZnO	5%	44.97	25.86	29.17	
					10%	44.96	24.42	30.62	
					15%	45.22	24.32	30.46	
			550	ZnO	5%	42.58	24.97	32.45	
					10%	42.47	24.23	33.3	
					15%	41.85	23.08	35.07	
			600	ZnO	5%	41.54	23.18	35.28	
					10%	40.89	23.05	36.06	
					15%	40.34	22.86	36.8	
Verbascum thapsus L.	50	100	400	ZnO	10%	37.85	31.58	30.57	[26]
				Al_2O_3		34.26	27.72	38.02	
			450	ZnO		38.77	26.76	34.47	
				Al_2O_3		36.91	24.37	38.72	
			500	ZnO		40.43	23.48	36.09	
				Al_2O_3		37.38	22.84	39.78	
			550	ZnO		38.67	22.04	39.29	
				Al_2O_3		35.41	20.65	43.94	
Eucalyptus	-	0.0025	500	Mn	-	26	34	19	[27]
				Fe	-	28	31	19	
				Co	-	27	31	19	
				Ni	-	22	29	22	
				Cu	-	27	29	19	
				Zn	-	25	33	18	
				Ce	-	24	34	20	
Lignin	-	100	600	HY 5.1	-	27.75	48.25	24	
				HY 30	-	28	49.5	22.5	
Poplar wood	-	120	500	CeO_2	-	14.5	29.7	23.2	
				CoO	-	19.2	29.7	22.5	
				Cr_2O_3	-	14.5	29.7	22	
				CuO	-	16	29.7	21	
				Fe_2O_3	-	17	29.7	21.5	
				Mn_2O_3	-	18.8	29.7	22.5	
				NiO	-	18	29.7	18	
				TiO_2	-	23	29.7	19.5	
				V_2O_5	-	18.5	29.7	20.5	

Table S4: The techniques employed for generating MAC focus on eliminating pharmaceuticals from water and wastewater.

AC Source	Preparation	Experimental Conditions			S_{BET} (m^2/g)	M, (emu/g)	Ref.
		Impregnation	Minerals/Oxides (CP)	Finishing Step			
Co-precipitation							
Commercial PAC (coal-based)	Washing with DW* and drying	•$FeCl_3 . 6H_2O$ •$FeSO_4 . 7H_2O$	CP:Fe minerals, with a Fe_2O_3 (%wt.): •MAC_1: 10% •MAC_2: 38% •MAC_3: 54%	-	•CP: 1256 •MAC_1: 783 •MAC_2: 748 •MAC_3: 433 •γ-Fe_2O_3: 6	•Fe_2O_3: 57.8 •MAC_1: 5.2 •MAC_2: 20.1 •MAC_3: 30.3	[28]
Commercial PAC	Nitric acid treatment, DW* washing and drying	•$FeCl_3 . 6H_2O$ •$FeCl_2 . 4H_2O$	CP:Fe_3O_4 (ex-situ) •MAC_1: 2:1 w/w •MAC_2: 4:1 w/w •MAC_3: 8:1 w/w	•Magnetic separation and drying •Washing with IICl 0.2M and DW* •Drying at room temperature	•CP: 1378 •MAC_3: 1241	•Fe_3O_4: 60 •MAC_3: 5.06	[29]
Polyethylene terephthalate waste	•Pyrolysis at 400 °C and 725 °C, with N_2 •Calcination at 925 °C with N_2 and 925 °C with CO_2	$FeCl_3$	CP (4g) and $FeCl_3$ (0.5M in DW and ethanol)	•Filtration •Washing with ethanol •Drying at 80 °C	•CP: 659.6 •MAC: 288.8	•MAC: 35.4	[30]
Commercial AC	-	•$FeCl_3 . 6H_2O$ •$NiSO_4 . 6H_2O$	CP:$NiFe_2O_4$ 1:1w/w	•Washing •Drying at 100 °C	•CP: 731.3 •MAC: 564.4 •$NiFe_2O_4$: 90.3	•MAC: 18.58 •$NiFe_2O_4$: 47.36	[30]
Thermochemical methods							
Brown marine macroalgae	•Sieved <1.0 mm •Pyrolysis N_2 addition at 400 °C	$FeCl_3 . 6H_2O$	CP:$FeCl_3$ 1:2.61w/w	•Filtration •Washing with DW* •Drying at 150 °C	•CP: 0.861 (inactivated) •MAC: 420.810	MAC: 24.09	[31]
Agricultural wastes: Cornstalks, reed stalks, willow	Washing with DW*, drying and sizing (<100 mesh)	$FeCl_3$	PS:$FeCl_3$:$ZnCl_2$ 10:2:1 w/w	•Washing with DW* •Drying at 105 °C	•MAC_1: 760.7 •MAC_2: 777.5 •MAC_3: 856	-	[32]
Mycelial pellets	-	•$(NH_4)_3[Fe(C_6H_5O_7)_2]$	$(NH_4)_3[Fe(C_6H_5O_7)_2]$ 0–0.5g/L	•Washing with 0.1M HCl and dW* •Drying at 70 °C	CMΔC: 1986.0	CMΔC: 21.6	[33]
Oxidative hydrolysis in alkaline conditions							
Pine sawdust	Pyrolysis at 650 °C, sieving (75–300μm) and washing with 0.01M NaOH	$FeCl_2 . 4H_2O$	CP saturated in $FeCl_2 . 4H_2O$ 0.3M	•Centrifugation •Washing with DW* •Drying at 40 °C	•CP: 297.8 •MAC: 125.8	•CP: 297.8 •MAC: 125.8	[34]
Pine sawdust	Pyrolysis at 650 °C, sieving (75–300μm) and washing with 0.01M NaOH	$FeCl_2 . 4H_2O$	CP:Fe minerals with a Fe_3O_4 (%wt.) •MAC_1: 25% •MAC_2: 50% •MAC_3: 75%	•Centrifugation •Washing with DW* •Drying at 40 °C	•CP: 297.8 •Fe_3O_4: 19.4 •MAC_1: 252.1 •MAC_2: 154.9 •MAC_3: 97.4	•CP: 0.3 •Fe_3O_4: 89.9 •MAC_1: 16.2 •MAC_2: 42.1 •MAC_3: 59.4	[35]

*DW: deionized water; dW: distilled water.

References

[1] S. Poyilil, A. Palatel, and M. Chandrasekharan, "Physico-chemical characterization study of coffee husk for feasibility assessment in fluidized bed gasification process," *Environmental Science and Pollution Research*, vol. 29, no. 34, pp. 51041–51053, Jul. 2022.

[2] N. H. Nam, V. N. Linh, L. D. Dung, and V. T. T. Ha, "Physico-chemical characterization of forest and agricultural residues for energy conversion processes," *Vietnam Journal of Chemistry*, vol. 58, no. 6, pp. 735–741, Dec. 2020.

[3] S. Nizamuddin, H. A. Baloch, N. M. Mubarak, S. Riaz, M. T. H. Siddiqui, P. Takkalkar, M. M. Tunio, S. Mazari, and A. W. Bhutto, "Solvothermal Liquefaction of Corn Stalk: Physico-chemical properties of bio-oil and biochar," *Waste and Biomass Valorization*, vol. 10, no. 7, pp. 1957–1968, Jul. 2019.

[4] M. Makaborang, S. S. Kabeko, J. J. S. Dethan, and M. L. Lano, "Biomass gasification of candlenut shell and coconut coir with the updraft gasifier method being alternative fuel," *IOP Conference Series: Materials Science and Engineering*, vol. 823, May 2020, Art. no. 012017.

[5] S. A. Dhar, T. U. Sakib, and L. N. Hilary, "Effects of pyrolysis temperature on production and physicochemical characterization of biochar derived from coconut fiber biomass through slow pyrolysis process," *Biomass Conversion and Biorefinery*, vol. 12, pp. 2631–2647, Nov. 2020.

[6] D. Hantoko, M. Yan, B. Prabowo, and H. Susanto, "Preparation of empty fruit bunch as a feedstock for gasification process by employing hydrothermal treatment," *Energy Procedia*, vol. 100, pp. 1003–1008, Oct. 2018.

[7] C. Mueanmas and N. Rakmak, "Enhancing the fuel properties of oil palm Mesocarp Fiber using screw conveyor reactor torrefaction," *Energy Conversion and Management*, vol. 298, Dec. 2023, Art. no. 117772.

[8] S. L. Majamo and T. A. Amibo, "Modeling and optimization of chemical-treated torrefaction of wheat straw to improve energy density by response surface methodology," *Biomass Conversion and Biorefinery*, Apr. 2023.

[9] W. Chen, S. Shi, J. Zhang, M. Chen, and X. Zhou, "Co-pyrolysis of waste newspaper with high-density polyethylene: Synergistic effect and oil characterization," *Energy Conversion and Management*, vol. 112, pp. 41–48, Mar. 2016.

[10] B. Debalina, R. B. Reddy, and R. Vinu, "Production of carbon nanostructures in biochar, bio-oil and gases from bagasse via microwave assisted pyrolysis using Fe and Co as susceptors," *Journal of Analytical and Applied Pyrolysis*, vol. 124, pp. 310–318, Mar. 2017.

[11] G. Pahla, T. A. Mamvura, F. Ntuli, and E. Muzenda, "Energy densification of animal waste

lignocellulose biomass and raw biomass," *South African Journal of Chemical Engineering*, vol. 24, no. 12, pp. 168–175, Dec. 2017.

[12] S. L. Lo, Y. F. Huang, P. Te Chiueh, and W. H. Kuan, "Microwave pyrolysis of lignocellulosic biomass," *Energy Procedia*, vol. 24, no. 5, pp. 41–46, May 2017.

[13] J. Waluyo, I. G. B. N. Makertihartha, and H. Susanto, "Pyrolysis with intermediate heating rate of palm kernel shells: Effect temperature and catalyst on product distribution," *AIP Conference Proceedings*, vol. 1977, Jun. 2018, Art. no. 020026.

[14] M. Buffi, A. M. Rizzo, L. Pari, and D. Chiaramonti, "Intermediate pyrolysis campaign to assess products yield and quality varying biomass particles size, temperatures and composition," *International Journal of Oil, Gas and Coal Technology*, vol. 17, no. 3, pp. 355–373, Mar. 2018.

[15] C. E. Efika, J. A. Onwudili, and P. T. Williams, "Influence of heating rates on the products of high-temperature pyrolysis of waste wood pellets and biomass model compounds," *Waste Management*, vol. 76, no. 6, pp. 497–506, Jun. 2018.

[16] J. A. Menéndez, A. Domínguez, Y. Fernández, and J. J. Pis, "Evidence of self-gasification during the microwave-induced pyrolysis of coffee hulls," *Energy & Fuels*, vol. 21, no. 1, pp. 373–378, Dec. 2007.

[17] T. Imam and S. Capareda, "Characterization of bio-oil, syn-gas and bio-char from switchgrass pyrolysis at various temperatures," *Journal of Analytical and Applied Pyrolysis*, vol. 93, pp. 170–177, Jan. 2012.

[18] F. Abnisa, A. Arami-Niya, W. M. A. W. Daud, and J. N. Sahu, "Characterization of bio-oil and bio-char from pyrolysis of palm oil wastes," *Bioenergy Research*, vol. 6, pp. 830–840, Feb. 2013.

[19] Z. Wang, J. Wu, T. He, and J. Wu, "Corn stalks char from fast pyrolysis as precursor material for preparation of activated carbon in fluidized bed reactor," *Bioresource Technology*, vol. 167, pp. 551–554, Sep. 2014.

[20] T. Aysu and M. M. Küçük, "Biomass pyrolysis in a fixed-bed reactor: Effects of pyrolysis parameters on product yields and characterization of products," *Energy*, vol. 64, pp. 1002–1025, Jan. 2014.

[21] F. Tinwala, P. Mohanty, S. Parmar, A. Patel, and K. K. Pant, "Intermediate pyrolysis of agro-industrial biomasses in bench-scale pyrolyser: Product yields and its characterization," *Bioresource Technology*, vol. 188, pp. 258–264, Jul. 2015.

[22] L. E. Hernandez-Mena, A. A. B. Pécora, and A. L. Beraldo, "Slow Pyrolysis of bamboo biomass: Analysis of biochar properties," *Chemical Engineering Transactions*, vol. 37, pp. 115–120, May 2014.

[23] Y. Zhang, Z. Ma, Q. Zhang, J. Wang, Q. Ma, Y. Yang, X. Luo, and W. Zhang, "Comparison of the physicochemical characteristics of bio-char pyrolyzed from moso bamboo and rice husk with different pyrolysis temperatures," *BioResources*, vol. 12, no. 3, May 2017, Art. no. 4652.

[24] J. Zhang, A. Tahmasebi, J. E. Omoriyekomwan, and J. Yu, "Production of carbon nanotubes on bio-char at low temperature via microwave-assisted CVD using Ni catalyst," *Diamond and Related Materials*, vol. 91, pp. 98–106, Jan. 2019.

[25] E. Pütün, "Catalytic pyrolysis of biomass: Effects of pyrolysis temperature, sweeping gas flow rate and MgO catalyst," *Energy*, vol. 35, no. 7, pp. 2761–2766, Jul. 2010.

[26] T. Aysu and H. Durak, "Pyrolysis of giant mullein (*Verbascum thapsus* L.) in a fixed-bed reactor: Effects of pyrolysis parameters on product yields and character," *Energy Sources, Part A: Recovery, Utilization, and Environmental Effects*, vol. 38, no. 5, pp. 661–669, Apr. 2016.

[27] S. Eibner, F. Broust, J. Blin, and A. Julbe, "Catalytic effect of metal nitrate salts during pyrolysis of impregnated biomass," *Journal of Analytical and Applied Pyrolysis*, vol. 113, pp. 143–152, May 2015.

[28] K. M. Lompe, S. Vo Duy, S. Peldszus, S. Sauvé, and B. Barbeau, "Removal of micropollutants by fresh and colonized magnetic powdered activated carbon," *Journal of Hazardous Materials*, vol. 360, pp. 349–355, Oct. 2018.

[29] M. Baghdadi, E. Ghaffari, and B. Aminzadeh, "Removal of carbamazepine from municipal wastewater effluent using optimally synthesized magnetic activated carbon: Adsorption and sedimentation kinetic studies," *Journal of Environmental Chemical Engineering*, vol. 4, no. 3, pp. 3309–3321, Sep. 2016.

[30] A. C. Fröhlich, E. L. Foletto, and G. L. Dotto, "Preparation and characterization of $NiFe_2O_4$/

activated carbon composite as potential magnetic adsorbent for removal of ibuprofen and ketoprofen pharmaceuticals from aqueous solutions," *Journal of Cleaner Production*, vol. 229, pp. 828–837, Aug. 2019.

[31] K.W. Jung, B.H. Choi, K.G. Song, and J.W. Choi, "Statistical optimization of preparing marine macroalgae derived activated carbon/iron oxide magnetic composites for sequestering acetylsalicylic acid from aqueous media using response surface methodology," *Chemosphere*, vol. 215, Jan. 2019, pp. 432–443.

[32] B. Wang, Y. Song Jiang, F. Yun Li, and D. Yue Yang, "Preparation of biochar by simultaneous carbonization, magnetization and activation for norfloxacin removal in water," *Bioresource Technology*, vol. 233, pp. 159–165, Jun. 2017.

[33] H. Luo, Y. Zhang, Y. Xie, Y. Li, M. Qi, R. Ma, S. Yang, and Y. Wang, "Iron-rich microorganism-enabled synthesis of magnetic biocarbon for efficient adsorption of diclofenac from aqueous solution," *Bioresource Technology*, vol. 282, pp. 310–317, Jun. 2019.

[34] F. Reguyal and A. K. Sarmah, "Adsorption of sulfamethoxazole by magnetic biochar: Effects of pH, ionic strength, natural organic matter and 17α-ethinylestradiol," *Science of the Total Environment*, vol. 628–629, pp. 722–730, Jul. 2018.

[35] F. Reguyal and A. K. Sarmah, "Site energy distribution analysis and influence of Fe_3O_4 nanoparticles on sulfamethoxazole sorption in aqueous solution by magnetic pine sawdust biochar," *Environmental Pollution*, vol. 233, pp. 510–519, Feb. 2018.